Unoffical notes: Search for boosted top+Higgs resonance in the all hadronic decay mode

Lucas Corcodilos

May 9, 2021

Contents

1 Analysis strategy and selection

Dijet search for boosted $X \to tH$. The benchmark, X, is a VLQ T' produced in association with a bottom quark. The interaction with an associated top quark is currently ignored since the simulation samples are inconsistent with the UL versions available for all other simulation. The associated quark will have much lower transverse momentum than the T' decay products and so the affect on the analysis is expected to be small (ie. quark will be along beamline).

1.1 Selection

Signal region (SR)	QCD control for SR	Validation region (VR)	QCD control for VR
Two AK8 jets separated by $\Delta\phi > \pi/2$ $p_T > 350$ GeV for each jet $\lvert\eta\rvert < 2.4$ for each jet $m_{\text{jet}} > 50$ for each jet			
At least one jet top tagged		No jet top tagged	
Higgs tag pass	Higgs tag fail	Higgs tag pass	Higgs tag fail

Table 1: Analysis selection for four selection regions. The definitions of the "top tag" and "Higgs tag" can be found in 2.

	DeepAK8	Particle Net	Mass
Top quark	0.94	0.94	[105,210] GeV
Higgs boson	0.96 (mass-decorrelated)	0.98 (mass-decorrelated)	-

Table 2: Selections for top and Higgs jet tagging. The analysis considers using either DeepAK8 or ParticleNet so the working points for both are provided. Note that the Higgs tag uses the mass-decorrelated version of each tagger and does not use a jet mass selection because of the nature of the background estimate. The choice of NN-scores is based off of $S/\sqrt{B}$ optimization of the four different variables with N-1 cuts, as shown in Figs.6 and 7.

2 Initial studies on jet tagging

Two neural network based taggers are considered for jet tagging - DeepAK8 and ParticleNet. Several aspects of these taggers can affect this analysis and are considered when choosing between the taggers.

First and most importantly, the tagger must be decorrelated from the jet mass so as not to sculpt the jet mass distribution. The two dimensional background estimation method uses the jet mass as one of the axis in which to measure data. If the taggers sculpt the jet mass so as to create a signal-like peak, the background will be harder to discriminant from potential signal.

Additionally, the data-driven estimate of the QCD multijet background relies on a smooth ratio of the distributions of those events passing and failing the tagger. If the "pass" is sculpted and the "fail" is not, we cannot hope to use our transfer function method without introducing method for potential signal bias.

Second, the tagger should be good at distinguishing between top and Higgs jets so the tagger can be used to easily identify which side of the event is which physics object. In particular, the analysis would benefit from a tagger that correctly identifes that real Higgs jets are not top jets.

Finally, the tagger should be efficient at removing background without requiring a MC-to-data scale factor that is large or has large uncertainties that could dominant the total systematic uncertainty for the analysis.

With these three items in mind, we examined two variables - the difference in mass between the two jets and the difference in top tagging scores between the two jets - and plotted them against each other. In addition to considering the two taggers, we also considered four scenarios based on the simulation truth.

From left to right in Figs. 1 and 2:

- The first scenario does nothing with simulation truth.
- The second scenario examines when neither the top nor Higgs jet identified by the tagger were able to be matched to their respective generator particle ("Bad match").
- The third scenario examines when both the top and Higgs jets identified by the tagger were matched successfully to their respective generator particle ("Good match").
- The fourth scenario identifies the top and Higgs jets based on the generator particle information and then the variables plotted are calculated based on this information.

In other words, the fourth scenario flips the order of operations of the third scenario. The distributions for both taggers and the four scenarios are shown in Figs. 1 and 2 where a 2016 $T' \to tH$ signal with a T' mass of 1200 GeV is examined.

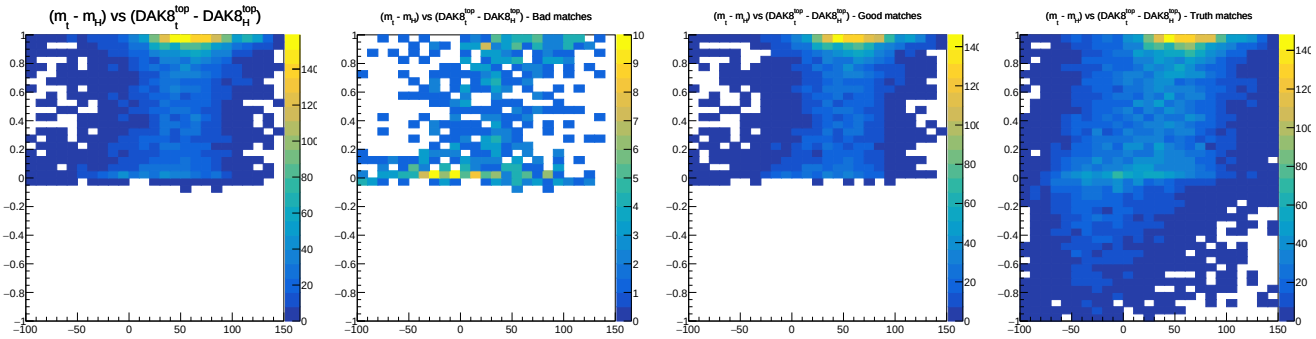

Figure 1: DeepAK8 studies

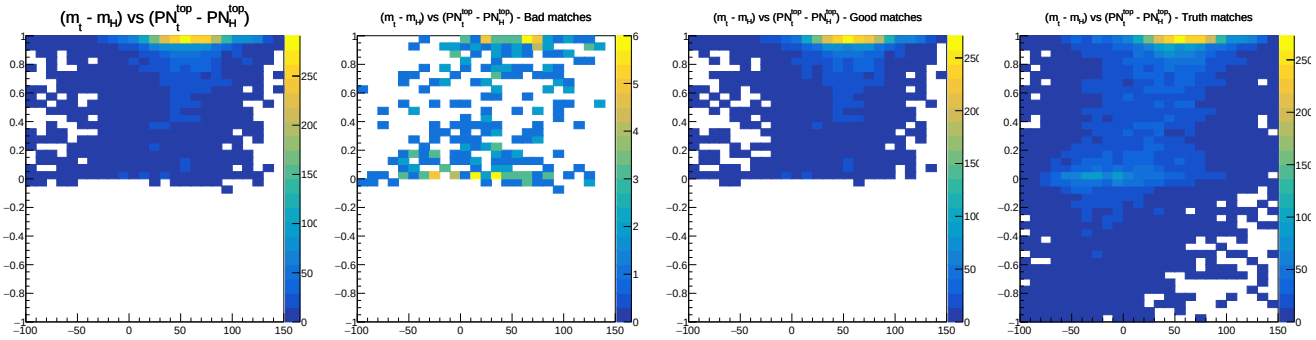

Figure 2: ParticleNet studies

3 Kinematic distributions

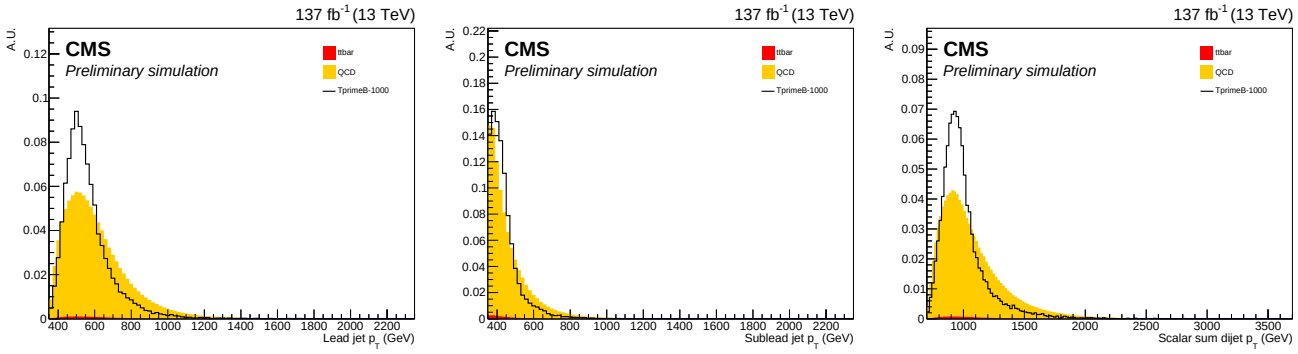

Figure 3: The p_T of the leading (left) and subleading (middle) jet in the event and the scalar sum of the two (right). The total background is represented as a stack of QCD (yellow) and ttbar (red) MC and the total is normalized to unity. The signal (black line) is separately normalized to unity.

4 Jet tagging variables

Two variables are used to tag a canidate jet - the tagger score and the jet mass. In order to inspect these variables, a series of N-1 plots are made - one for each the top jet mass, top jet tagger score, Higgs jet mass, and Higgs jet tagger score. When one variable is plotted, the other three are cut on.

Since this means a Higgs and top cannot be identified without impacting the distributions, the top quark is assumed to be the leading jet in p_T. The MC truth shows this is true 50% of the time. The other N-1 cuts in a given

plot should kill most of the mis-matched events (where the top jet is actually a Higgs and vice versa) with some fraction remaining. As can be seen in 1, that fraction is decently large when tagging a real Higgs with the DeepAK8 top tagger. This effect explains the Higgs peak in Figure 4.

Figures 4, 5, 6, and 7 compare simulation for all of Run 2.

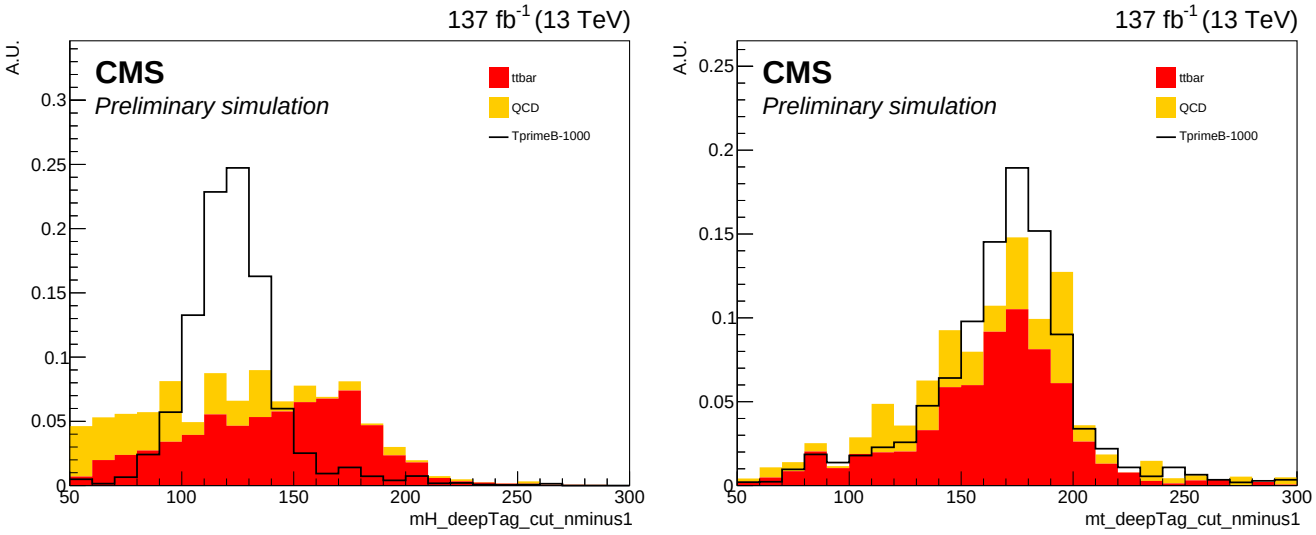

Figure 4: Shape comparison of the jet mass distributions for the Higgs (left) and top (right) jets when using the mass decorrelated DeepAK8 tagger. The total background is represented as a stack of QCD (yellow) and ttbar (red) MC and the total is normalized to the expected number of background events. The signal (black line) is separately normalized to the expected number of signal events assuming the cross section is 1pb.

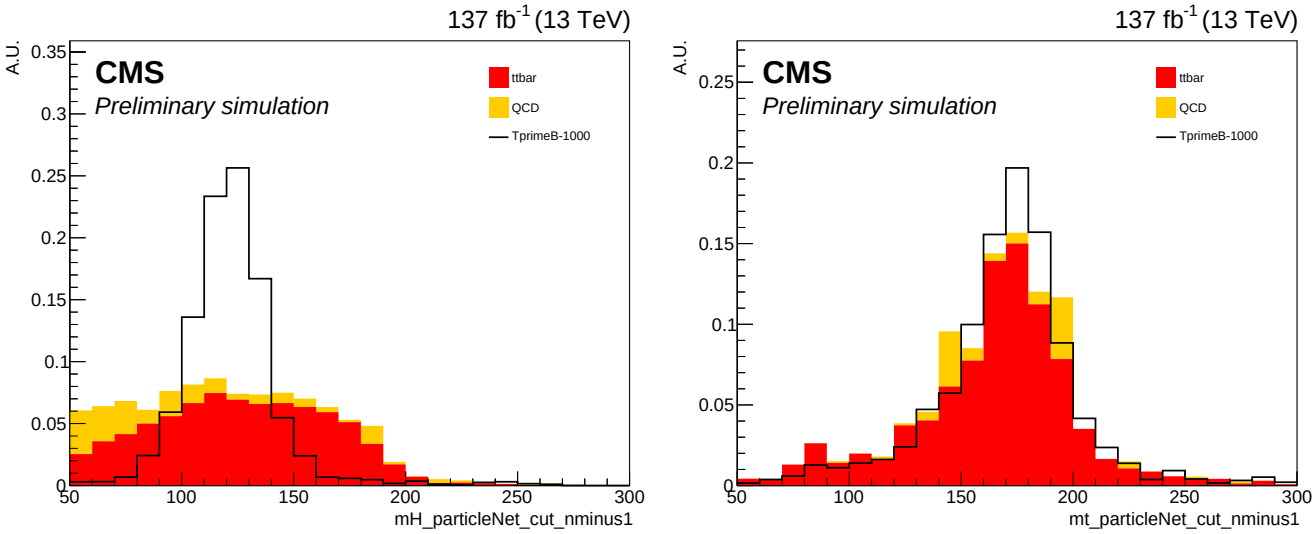

Figure 5: Shape comparison of the jet mass distributions for the Higgs (left) and top (right) jets when using the ParticleNet tagger (not mass decorrelated). The total background is represented as a stack of QCD (yellow) and ttbar (red) MC and the total is normalized to the expected number of background events. The signal (black line) is separately normalized to the expected number of signal events assuming the cross section is 1pb.

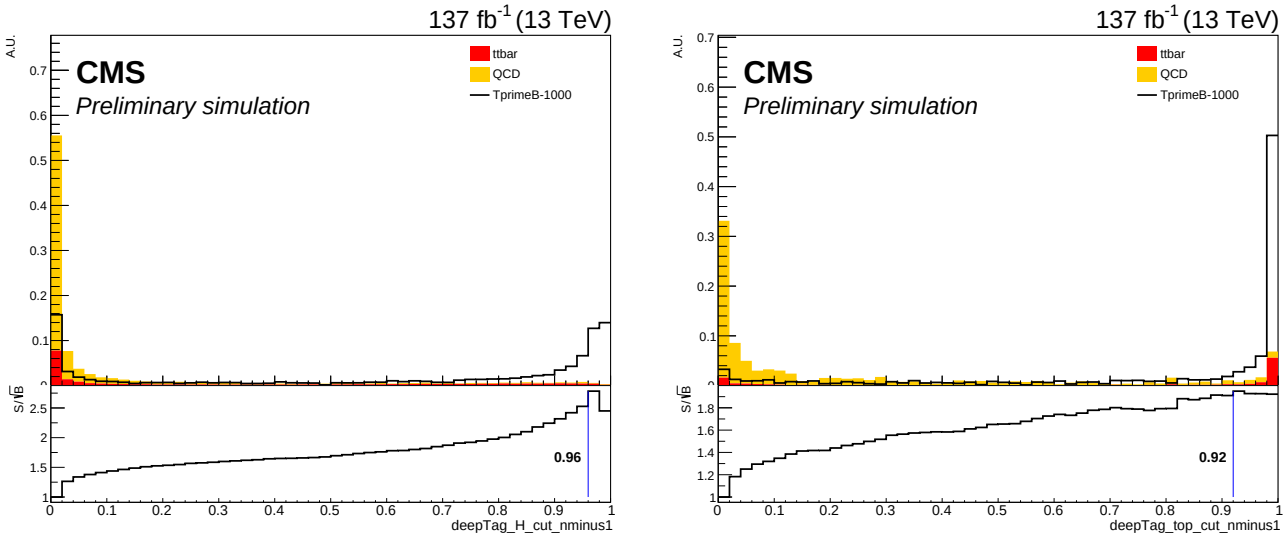

Figure 6: Shape comparison of the DeepAK8 score distributions for the Higgs (left) and top (right) jets when using the mass decorrelated DeepAK8 tagger. The total background is represented as a stack of QCD (yellow) and ttbar (red) MC and the total is normalized to the expected number of background events. The signal (black line) is separately normalized to the expected number of signal events assuming the cross section is 1pb.

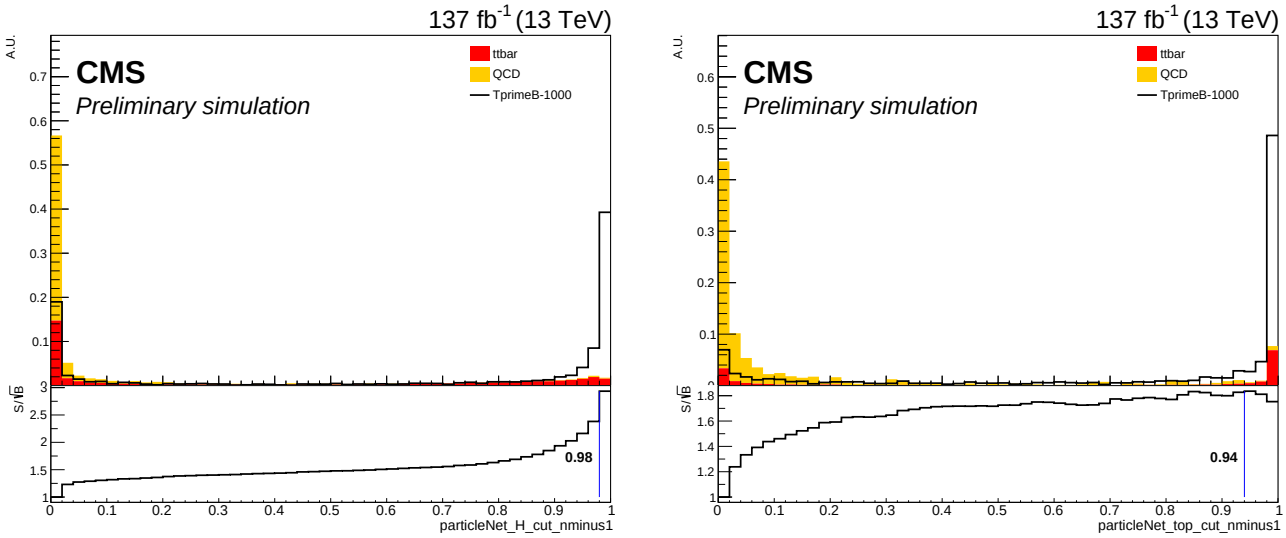

Figure 7: Shape comparison of the ParticleNet score distributions for the Higgs (left) and top (right) jets when using the mass decorrelated ParticleNet tagger. The total background is represented as a stack of QCD (yellow) and ttbar (red) MC and the total is normalized to the expected number of background events. The signal (black line) is separately normalized to the expected number of signal events assuming the cross section is 1pb.

5 Background estimation method

This analysis uses the 2D Alphabet method to build a 2D binned likelihood model that simultanously fits ttbar from MC templates while fitting QCD using a data-driven method. The data-driven method uses events in a QCD control region defined by inverting the tagging score selection on the Higgs jet. A two-dimensional polynomial called the pass-fail ratio ($R_{P/F}$) is used as the transfer function between this control region and the signal region. Additionally, there is no cut placed on the Higgs jet mass and instead, the Higgs jet mass sidebands are used to constrain the backgrounds as well as interpolate the value of the background through the Higgs mass signal region while blinded.

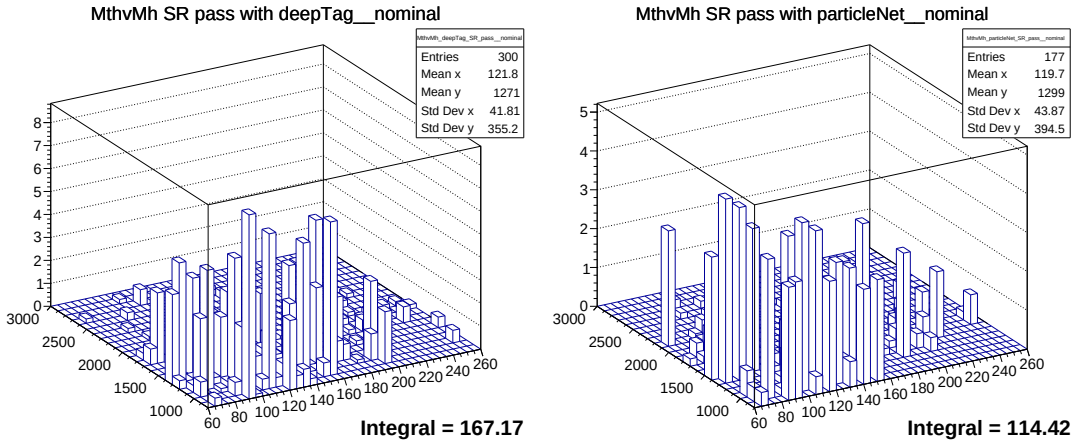

Figure 8: QCD MC simulation yields in "pass" selection for DeepAK8 (left) and ParticleNet (right). In the lower-right of each subfigured is the integrated yield (after stitching samples and normalizing to Run 2 luminosity). The legends in the upper-right show the total number of simulated events.

This method has been used successfully in B2G-19-003 and B2G-20-004. However, those two analyses used the QCD MC to assist the fit. Specifically, the $R_{P/F}^{MC}$ is calculated in simulation smoothed by a Kernel Density Estimate (KDE) and the fitted polynomial becomes the R_{ratio}. Then, $R_{P/F} = R_{P/F}^{MC} * R_{ratio}$. By doing this, the fitted function is only responsible for fitting the difference between MC and data which is often a less complex shape, reducing the number of necessary parameters and stabalizing the model.

The R_{ratio} variation of 2D Alphabet is noted because this analysis *does not* use it with the primary reason being a lack of QCD MC statistics. Figure 8 shows the QCD yield predicted by QCD simulation after the different HT-binned samples have been combined (via proper normalization to respective cross sections) and the three eras of 2016, 2017, and 2018 summed. The fluctuations from simulation statistics are large enough that even a smoothing algorithm would have a difficult time reconstructing a smooth distribution that could still lead to meaningful information for the background model.

Finally, a similar issue is faced with the $t\bar{t}$ simulation. The number of raw events in the signal region is larger than that of the QCD simulation but the distributions fluctuate enough that there were fit stability issues. This was studied with different $R_{P/F}$ parameterizations and coarser binning schemes but results were unstable. In particular, HESSE was unable to determine fit uncertainties because of "on boundary" parameters. This was true across the various $R_{P/F}$ and binning attempts.

To remedy the situation, the $t\bar{t}$ selections were reperformed with a looser selection on the Hbb tagging score (to 0.8 for DeepAK8 and ParticleNet) and the resulting distributions scaled to the integrated yield when using the optimized tagger selection. The loose working point of 0.8 was chosen based on Figs. 6 and 7 which show that the $t\bar{t}$ simulation statistics can be roughly doubled by increasing the selection window. Since the loosening of the Hbb score effectively migrates $t\bar{t}$ events from our "fail" region to the "pass" region, the possibility of biasing the shape in the "pass" to look more like the distribution in the "fail" is possible. However, the comparisons in Figs. 9 and 11 of the $t\bar{t}$ in the case of the raw selection (left) and the above "loose-and-scale" algorithm (right) show that the "fail" distributions are very similar and the "pass" distribution does not appear to be biased to look more like the "fail".

To substantiate that the resulting fit is healthier with the "loose-and-scale" method, Figs. 10 and 12 compare the nuisance parameter pulls for the DeepAK8 and ParticleNet scenarios, respectively.

Additionally, Figs. 6 and 7 show that loosening the Hbb score is more effective than loosening the top tagging score since most of the $t\bar{t}$ already lives in the signal selection of these top score distributions. Loosening the top tagging score to 0.8 was attempted and the above understanding was confirmed with little change to the final simulation statistics being observed.

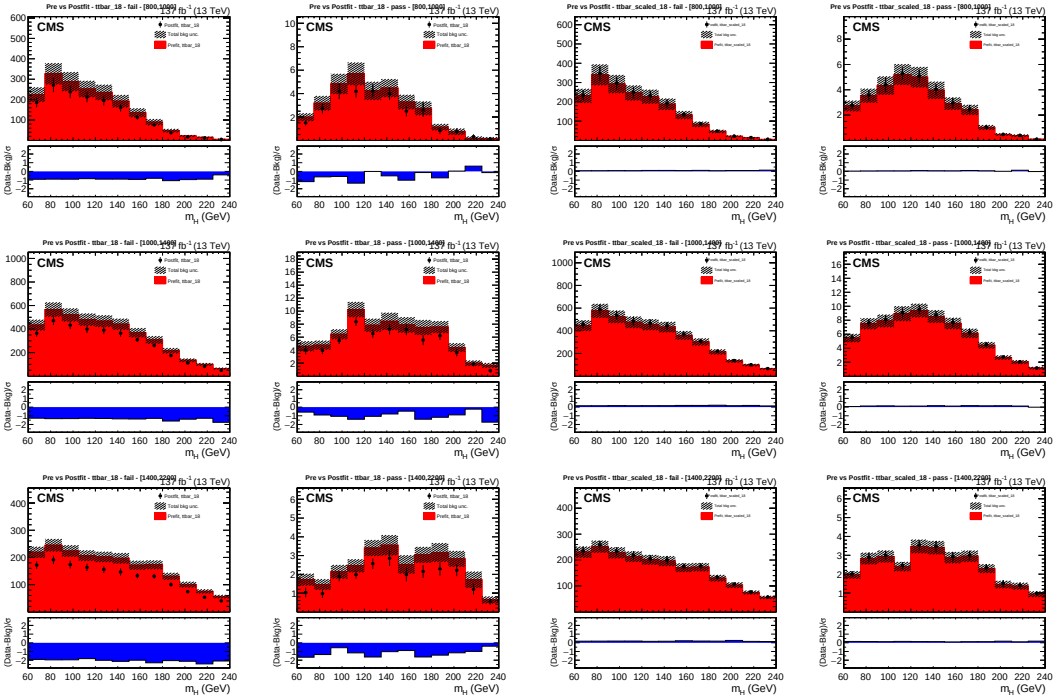

Figure 9: The m_H mass distributions of the 2018 $t\bar{t}$ simulation for the blinded background-only fit using the DeepAK8 tagger and a 0x0 $R_{P/F}$. The black points and vertical bars represent the post-fit value and uncertainty. The red histogram and shaded region represent the pre-fit value and uncertainty.

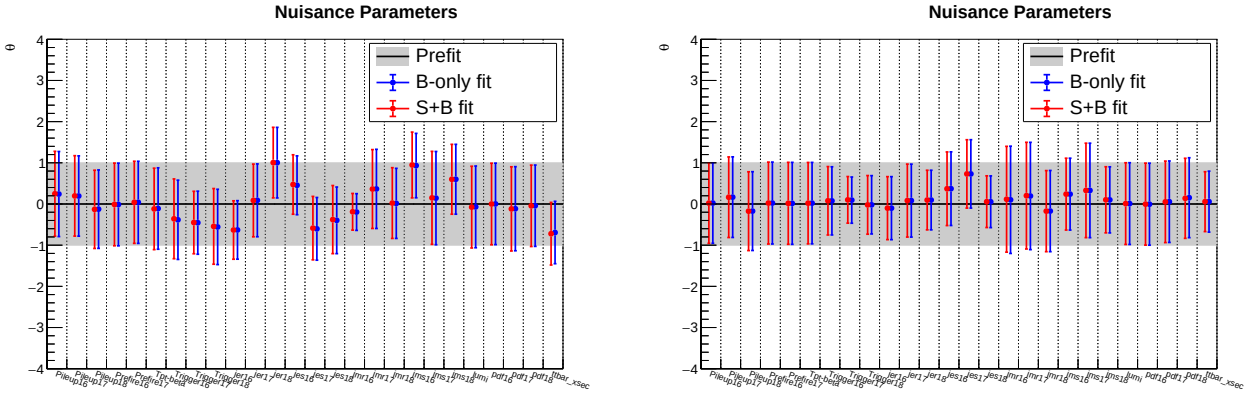

Figure 10: The nuisance parameter pulls for the blinded fits of the DeepAK8 based selection using a 0x0 $R_{P/F}$ for the raw $t\bar{t}$ MC (left) and $t\bar{t}$ MC with a looser selection and scaled down (right).

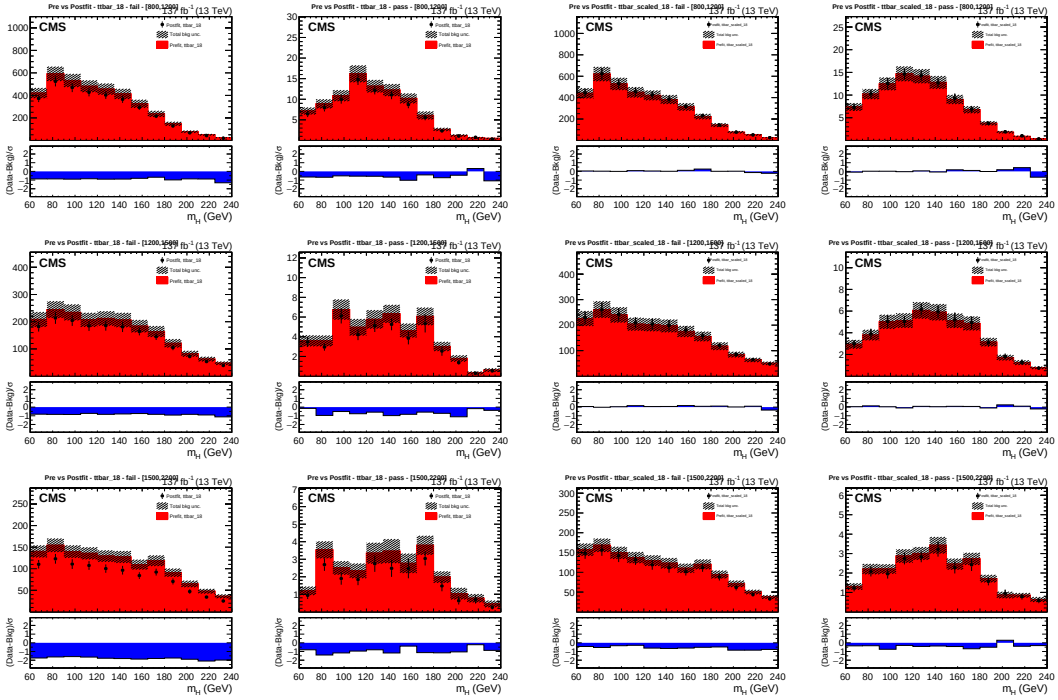

Figure 11: The m_H mass distributions of the 2018 $t\bar{t}$ simulation for the blinded background-only fit using the ParticleNet tagger and a 0x0 $R_{P/F}$. The black points and vertical bars represent the post-fit value and uncertainty. The red histogram and shaded region represent the pre-fit value and uncertainty.

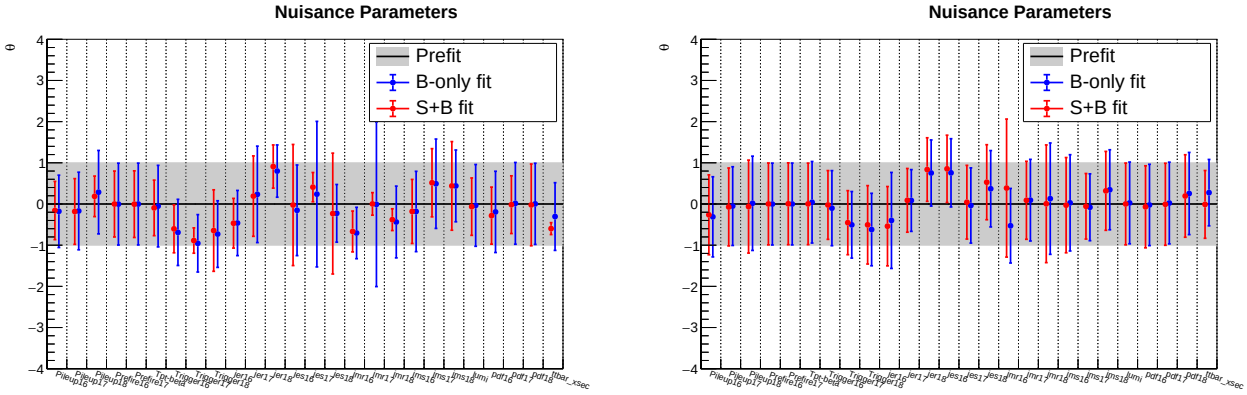

Figure 12: The nuisance parameter pulls for the blinded fits of the DeepAK8 based selection using a 0x0 $R_{P/F}$ for the raw $t\bar{t}$ MC (left) and $t\bar{t}$ MC with a looser selection and scaled down (right).

6 Blinded fits to data

6.1 DeepAK8 selections

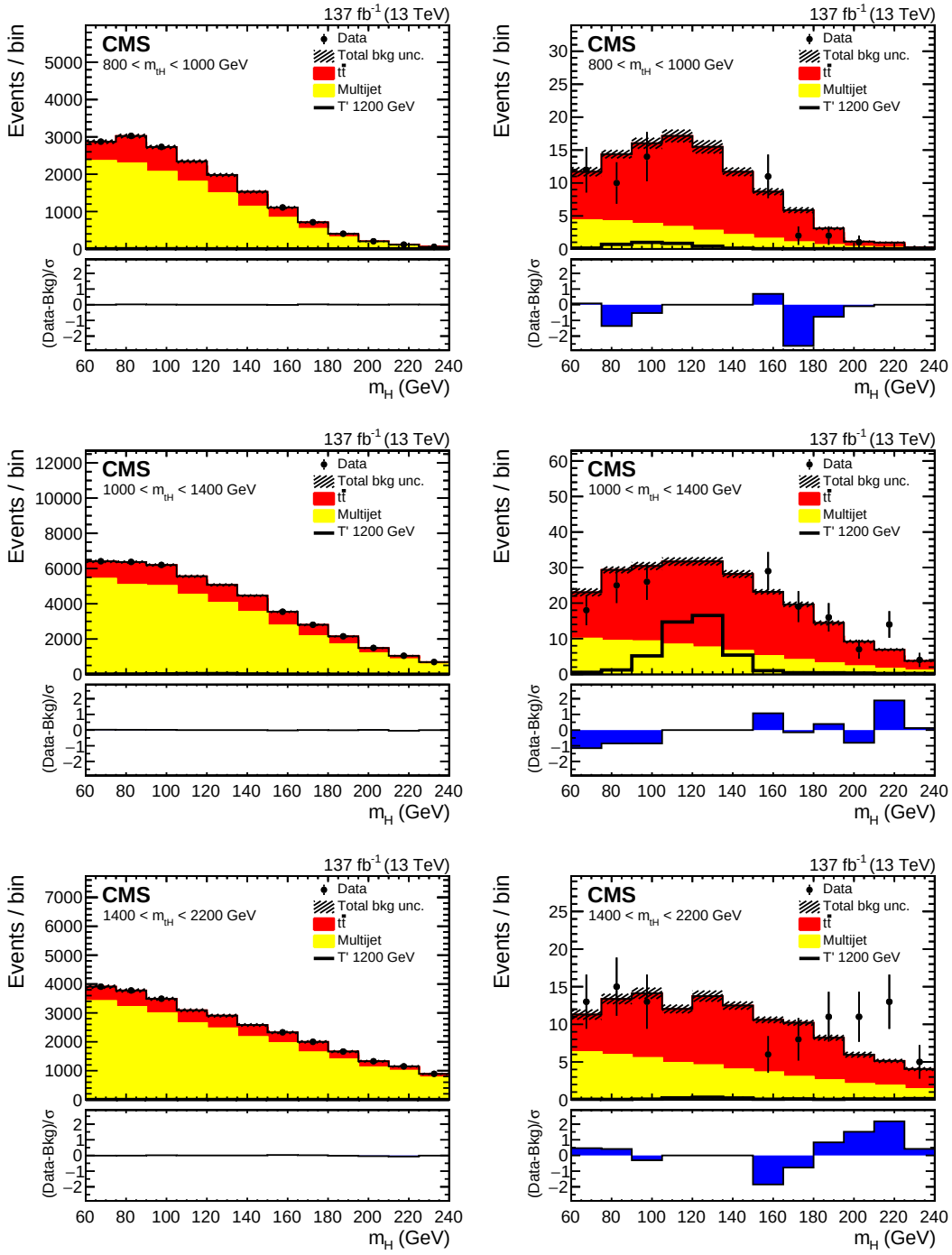

Figure 13: The m_H mass distributions for the blinded background-only fit using the DeepAK8 tagger and a 0x0 $R_{P/F}$. A 1200 GeV T' signal is normalized to 0.1 pb and plotted with the backgrounds to show relative shapes and yields.

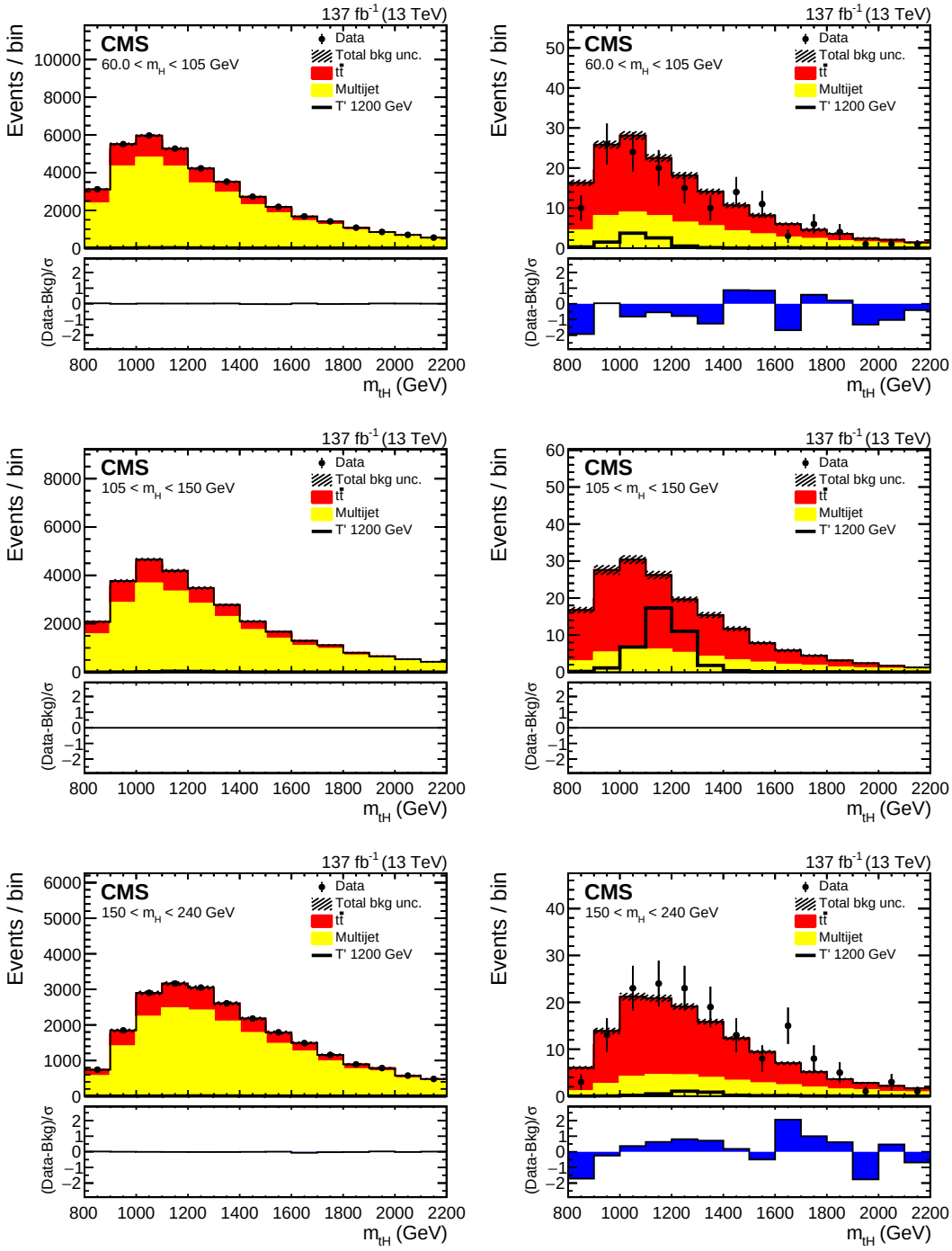

Figure 14: The m_{tH} mass distributions for the blinded background-only fit using the DeepAK8 tagger and a 0x0 $R_{P/F}$. A 1200 GeV T' signal is normalized to 0.1 pb and plotted with the backgrounds to show relative shapes and yields.

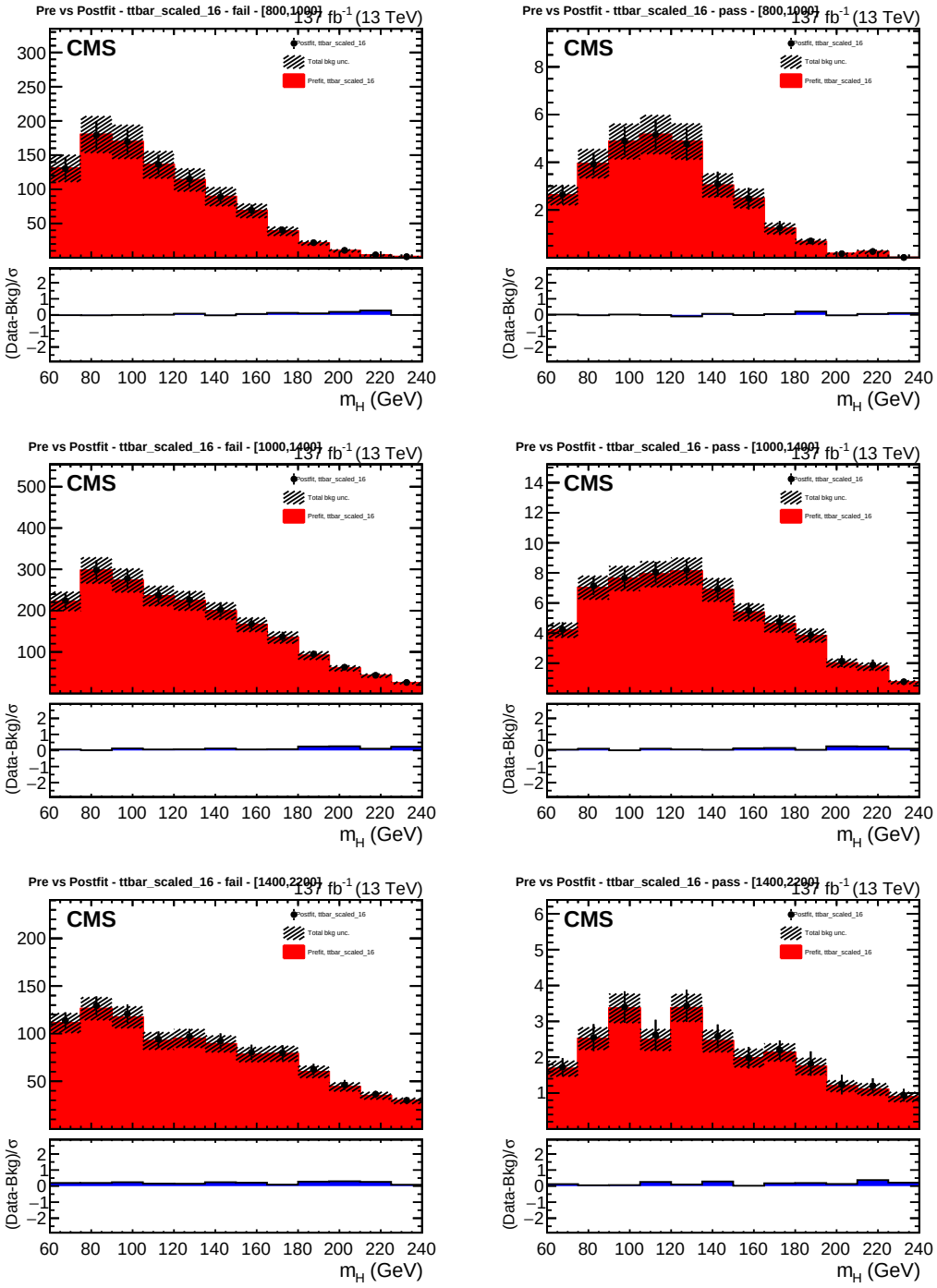

Figure 15: The m_H mass distributions of just the 2016 $t\bar{t}$ component of the blinded background-only fit using the DeepAK8 tagger and a 0x0 $R_{P/F}$. The red histogram with shaded area represent the pre-fit distribution and uncertainty while the black points represent the equivalent post-fit distribution and uncertainty.

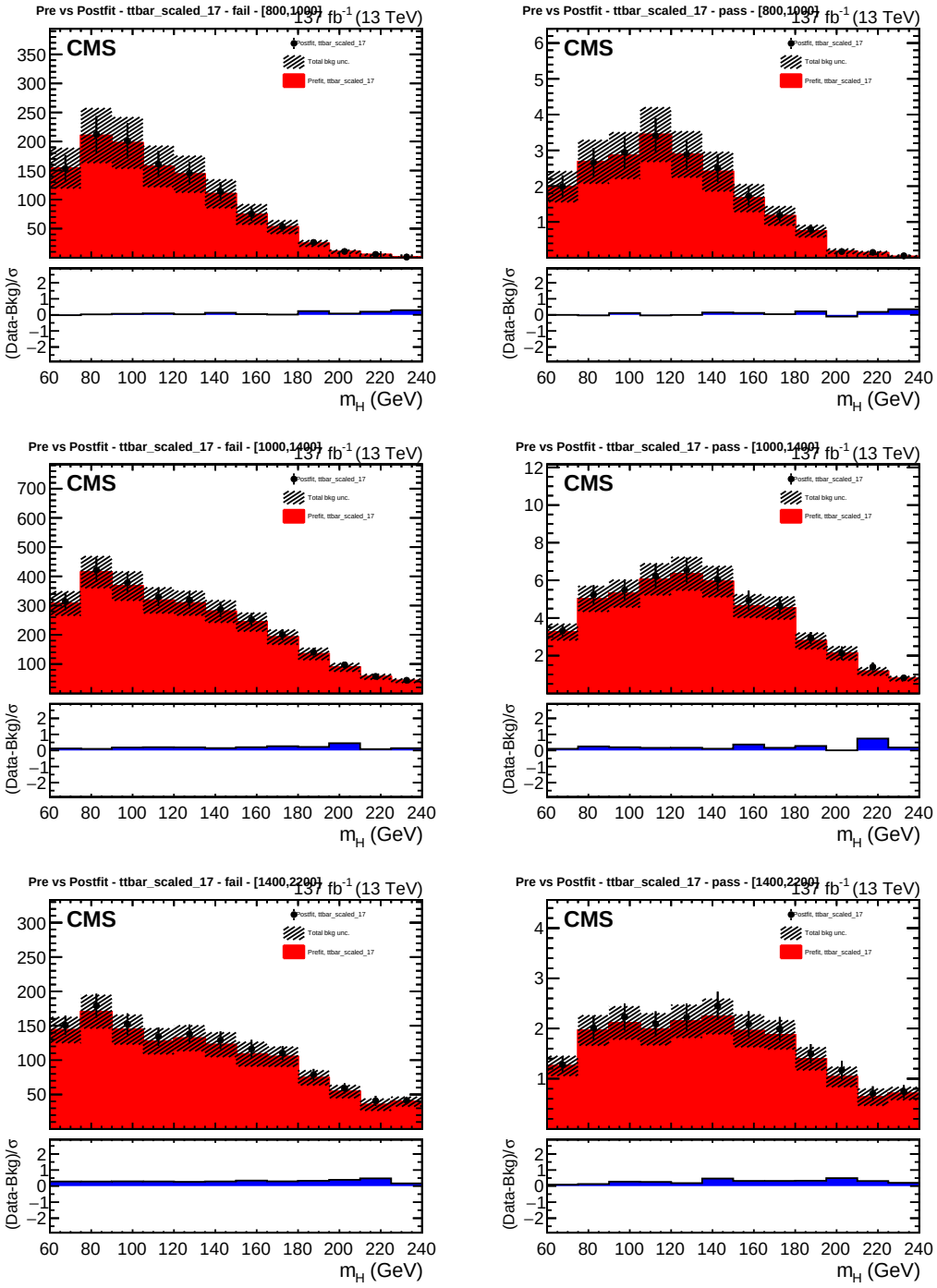

Figure 16: The m_H mass distributions of just the 2017 $t\bar{t}$ component of the blinded background-only fit using the DeepAK8 tagger and a 0x0 $R_{P/F}$. The red histogram with shaded area represent the pre-fit distribution and uncertainty while the black points represent the equivalent post-fit distribution and uncertainty.

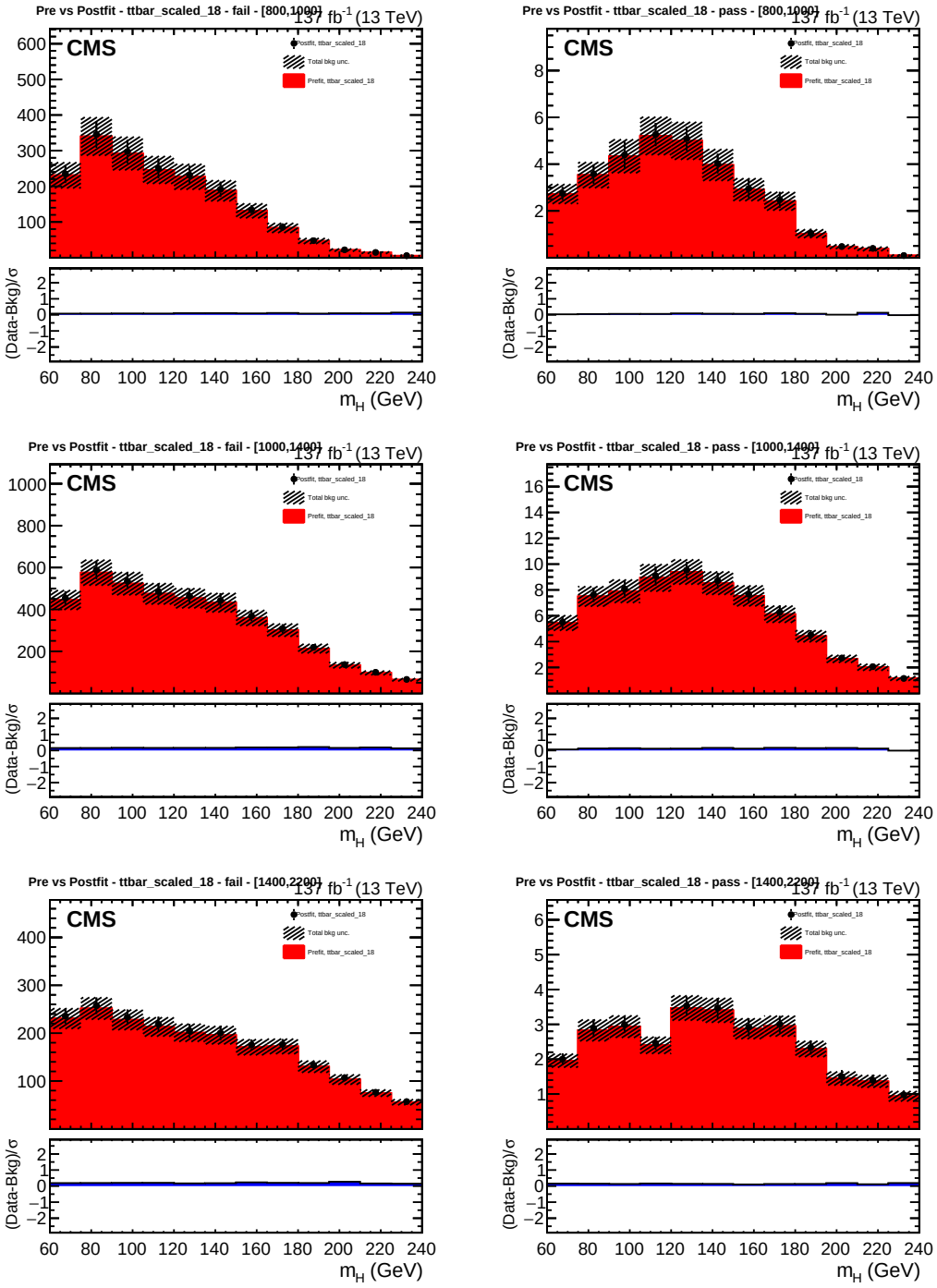

Figure 17: The m_H mass distributions of just the 2018 $t\bar{t}$ component of the blinded background-only fit using the DeepAK8 tagger and a 0x0 $R_{P/F}$. The red histogram with shaded area represent the pre-fit distribution and uncertainty while the black points represent the equivalent post-fit distribution and uncertainty.

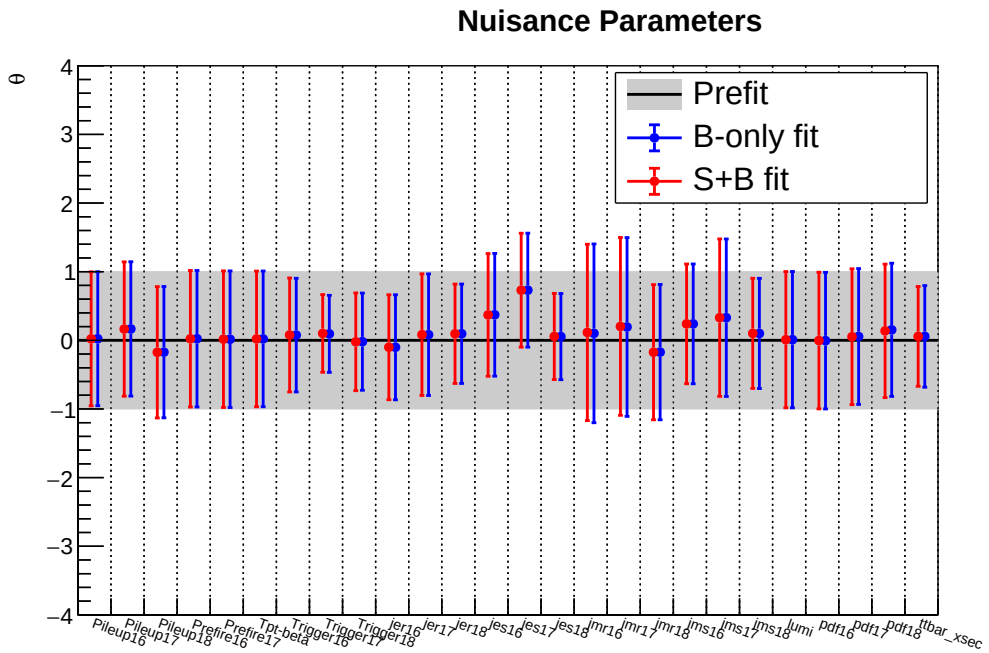

Figure 18: The nuisance parameter pulls for the blinded fits of the DeepAK8 based selection using a 0x0 $R_{P/F}$.

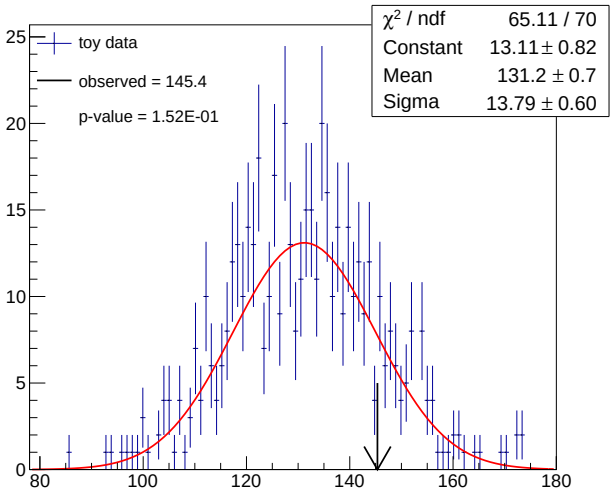

Figure 19: The Goodness of Fit for the blinded background-only fit of the DeepAK8 based selection using a 0x0 $R_{P/F}$.

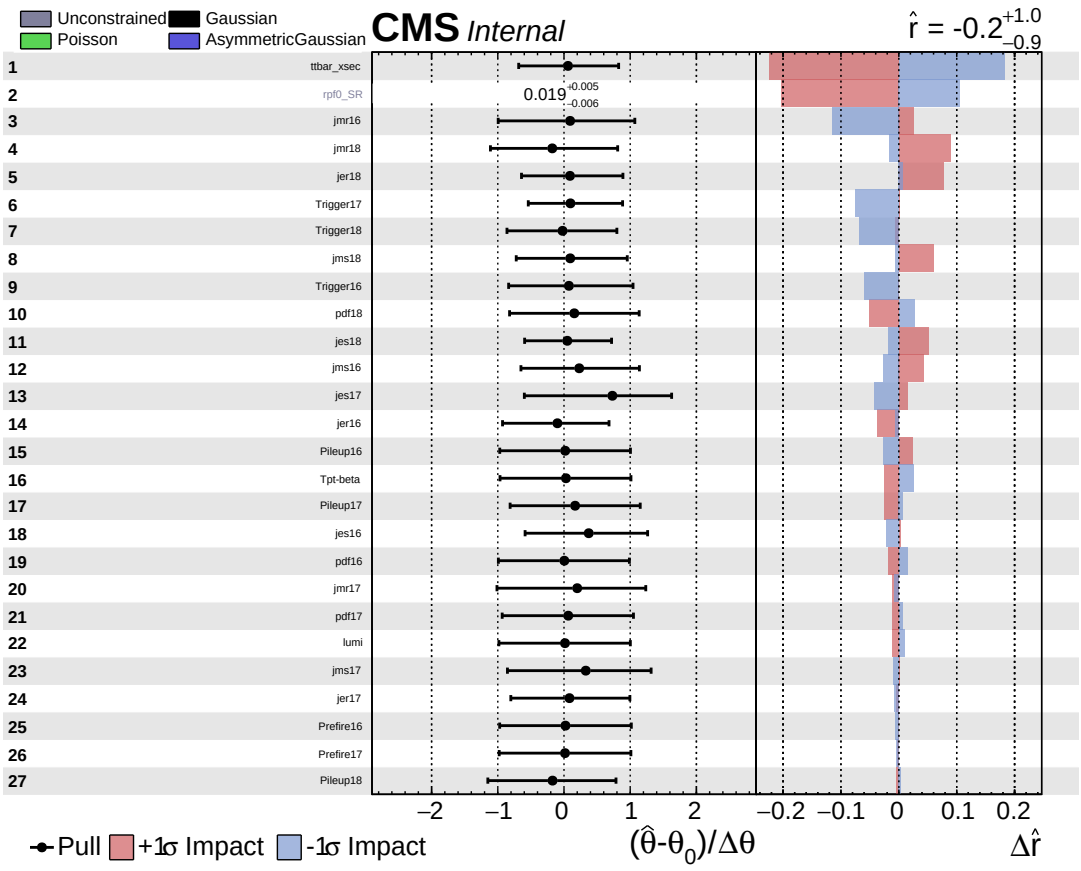

Figure 20: The nuisance parameter impacts on the final measured value of the signal strength, r, for the blinded background-only fit of the DeepAK8 based selection using a 0x0 $R_{P/F}$.

6.2 ParticleNet selections

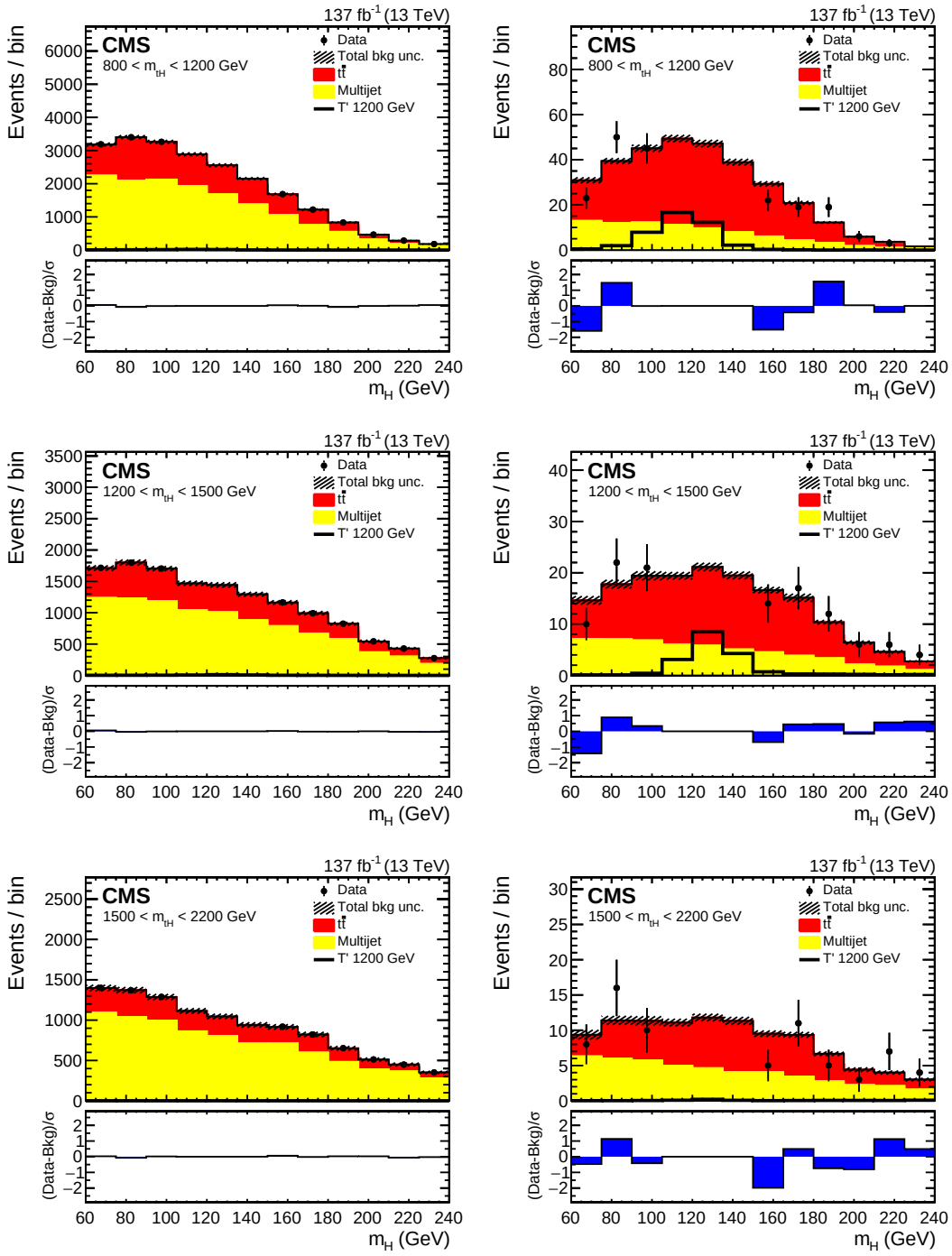

Figure 21: The m_H mass distributions for the blinded background-only fit using the ParticleNet tagger and a 0x0 $R_{P/F}$. A 1200 GeV T' signal is normalized to 0.1 pb and plotted with the backgrounds to show relative shapes and yields.

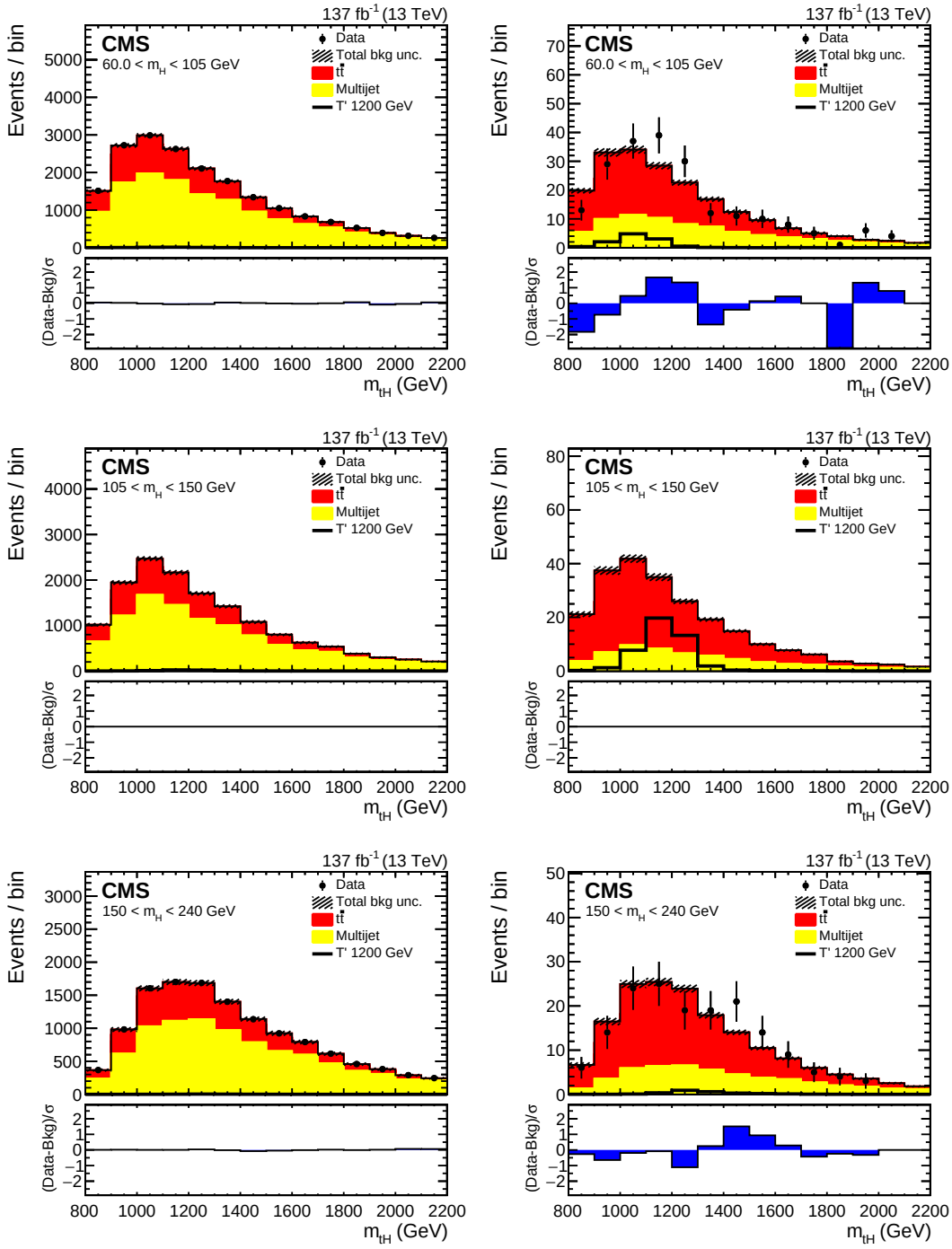

Figure 22: The m_H mass distributions for the blinded background-only fit using the ParticleNet tagger and a 0x0 $R_{P/F}$. A 1200 GeV T' signal is normalized to 0.1 pb and plotted with the backgrounds to show relative shapes and yields.

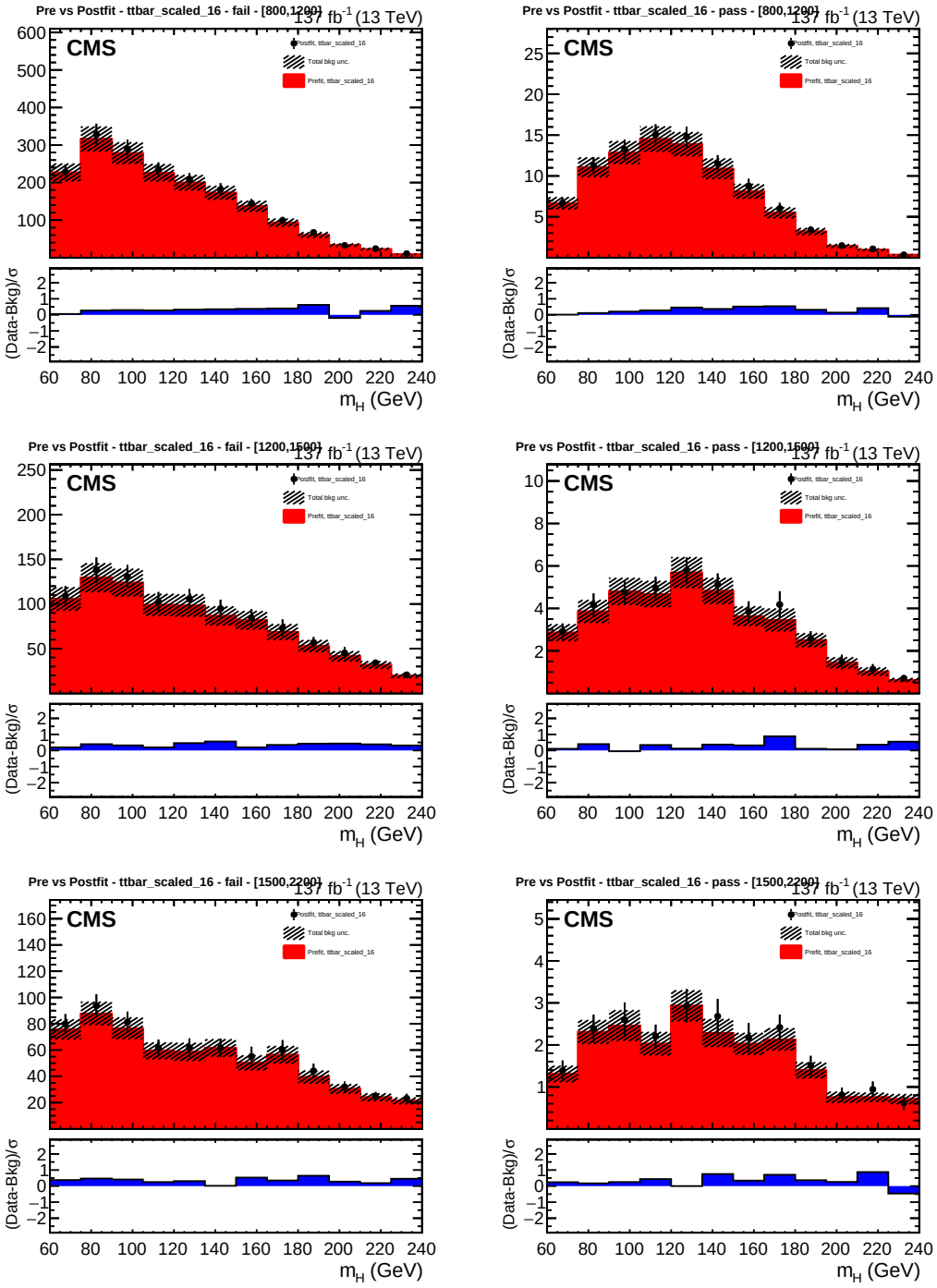

Figure 23: The m_H mass distributions of just the 2016 $t\bar{t}$ component of the blinded background-only fit using the ParticleNet tagger and a 0x0 $R_{P/F}$. The red histogram with shaded area represent the pre-fit distribution and uncertainty while the black points represent the equivalent post-fit distribution and uncertainty.

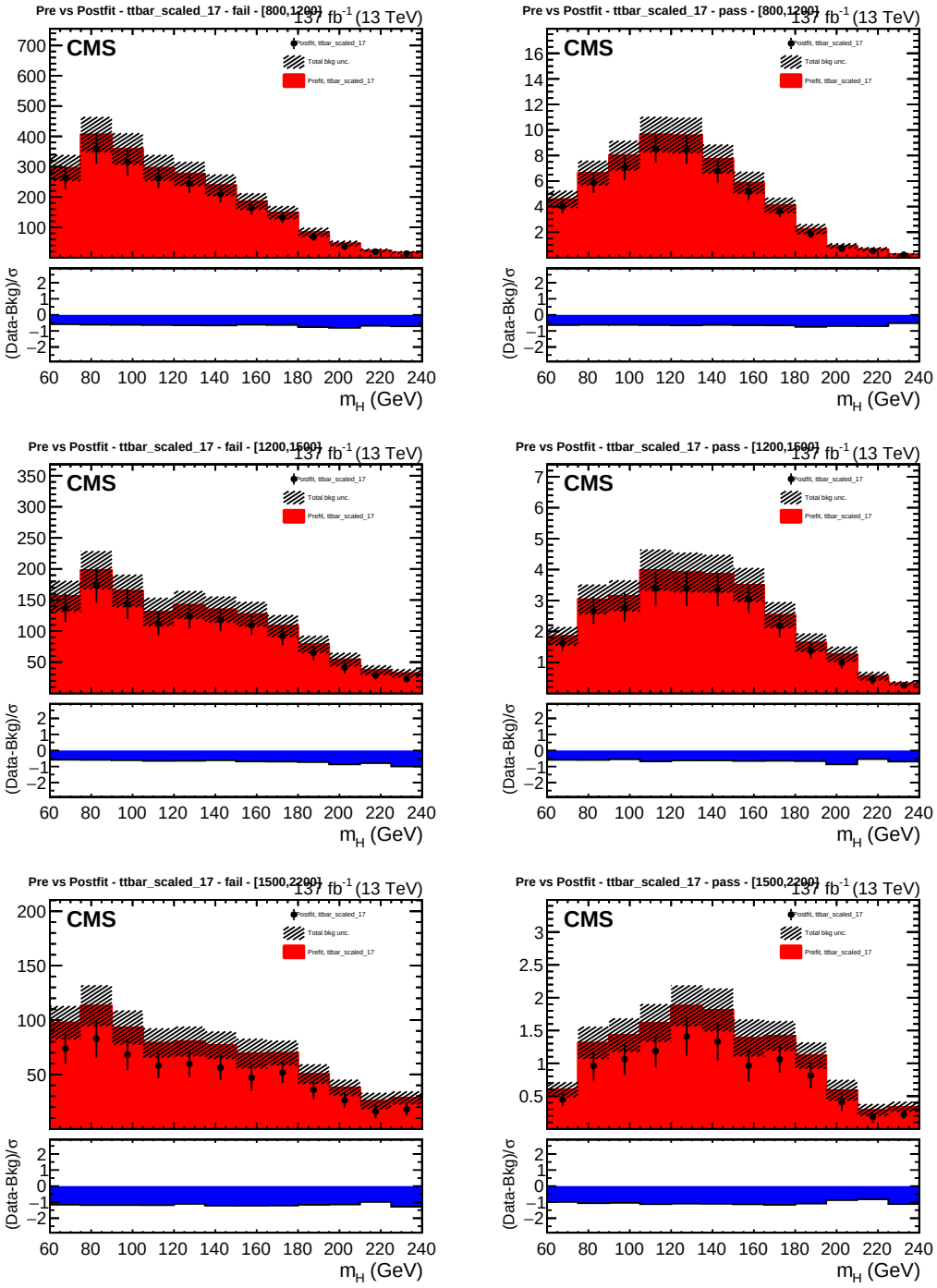

Figure 24: The m_H mass distributions of just the 2017 $t\bar{t}$ component of the blinded background-only fit using the ParticleNet tagger and a 0x0 $R_{P/F}$. The red histogram with shaded area represent the pre-fit distribution and uncertainty while the black points represent the equivalent post-fit distribution and uncertainty.

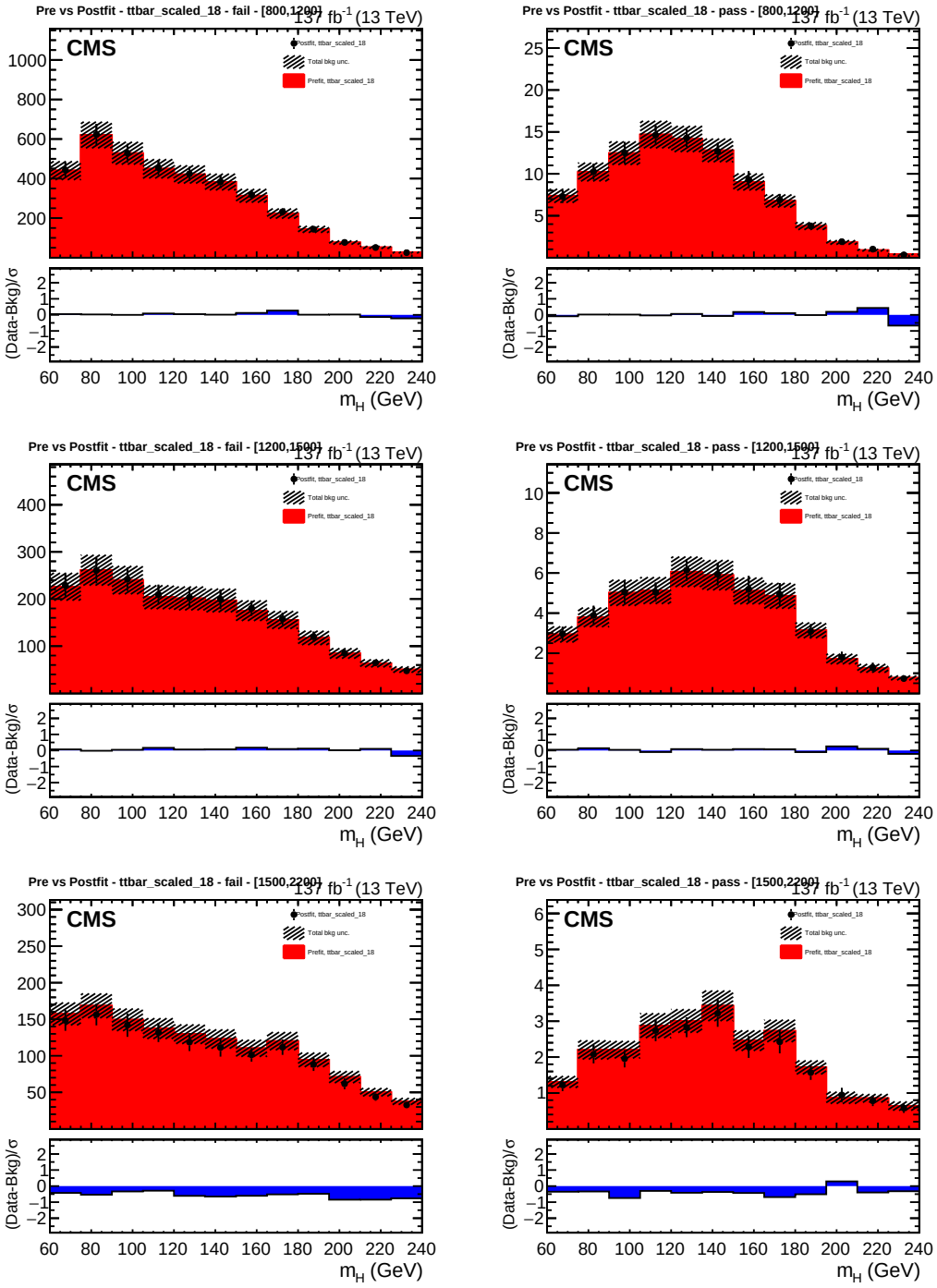

Figure 25: The m_H mass distributions of just the 2018 $t\bar{t}$ component of the blinded background-only fit using the ParticleNet tagger and a 0x0 $R_{P/F}$. The red histogram with shaded area represent the pre-fit distribution and uncertainty while the black points represent the equivalent post-fit distribution and uncertainty.

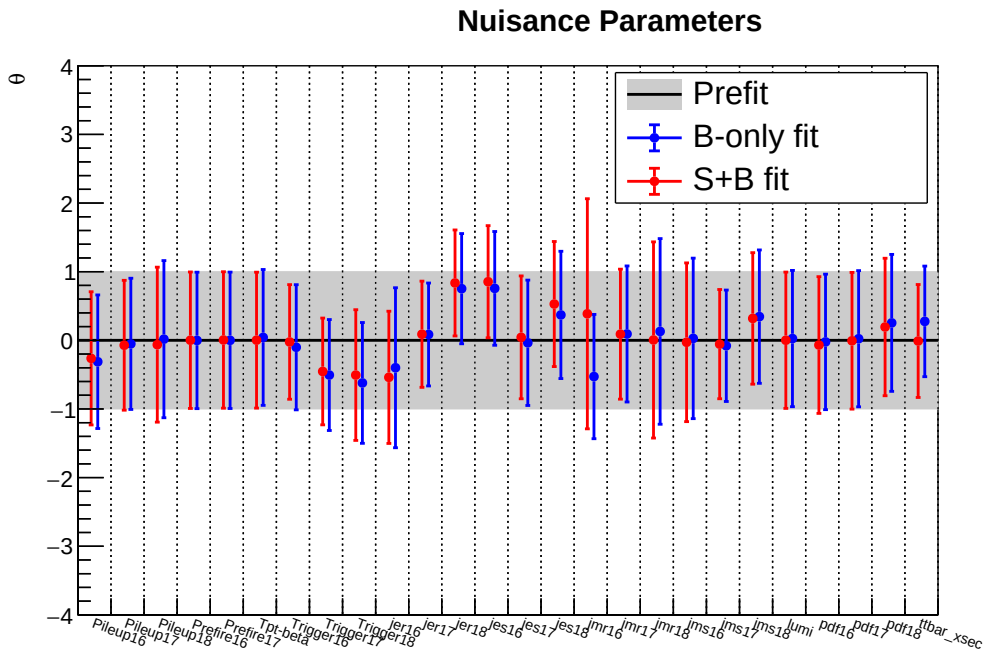

Figure 26: The nuisance parameter pulls for the blinded fits of the ParticleNet based selection using a 0x0 $R_{P/F}$.

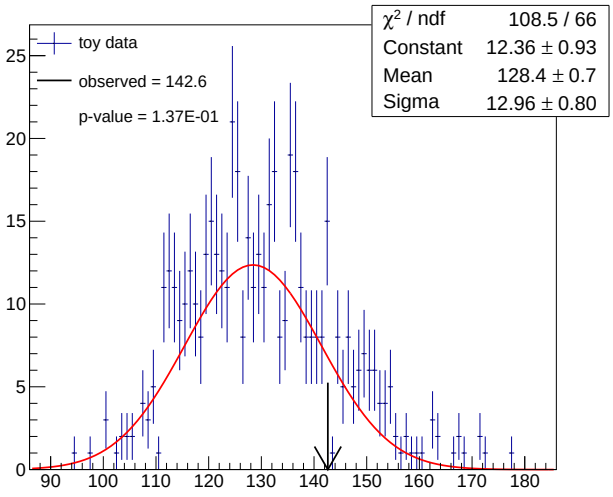

Figure 27: The Goodness of Fit for the blinded background-only fit of the ParticleNet based selection using a 0x0 $R_{P/F}$.

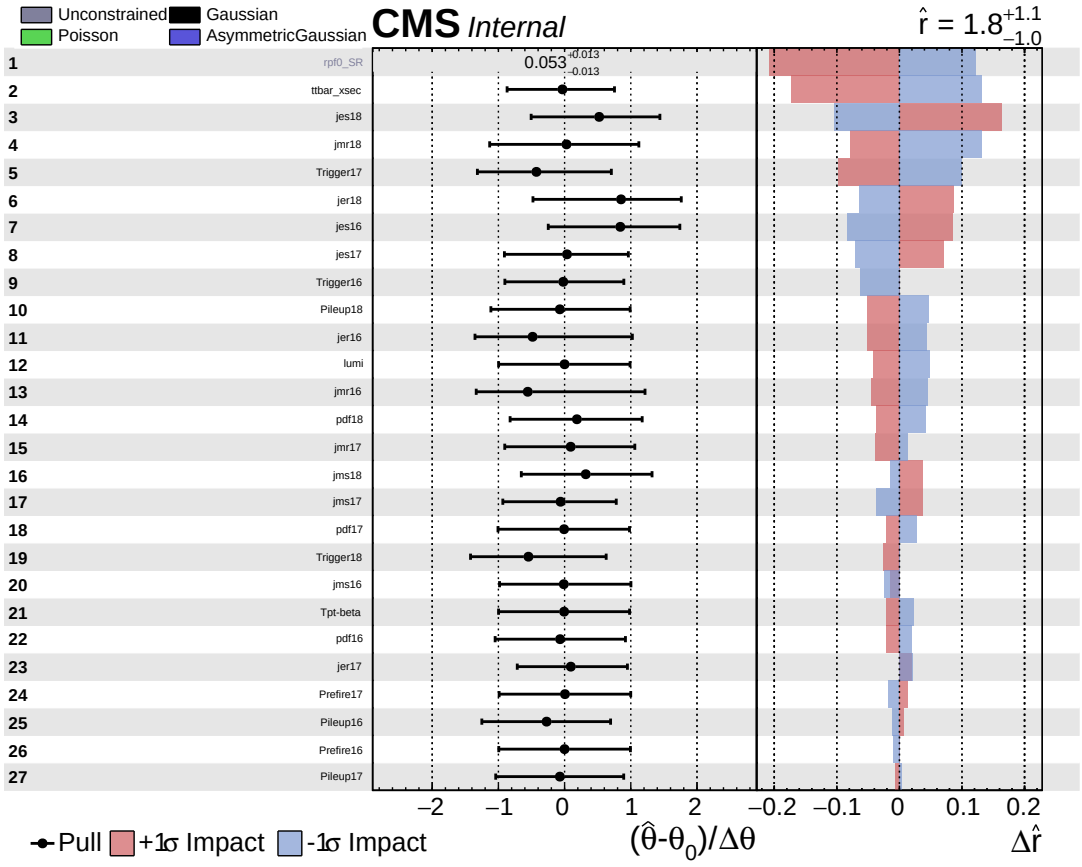

Figure 28: The nuisance parameter impacts on the final measured value of the signal strength, r, for the blinded background-only fit of the ParticleNet based selection using a 0x0 $R_{P/F}$.

7 Blinded signal injection tests

Signal injection tests are performed where the pseudo-data is generated from the post-fit background-only model with r signal added. The following tests are for a 1200 GeV $T' \to tH$ siganl.

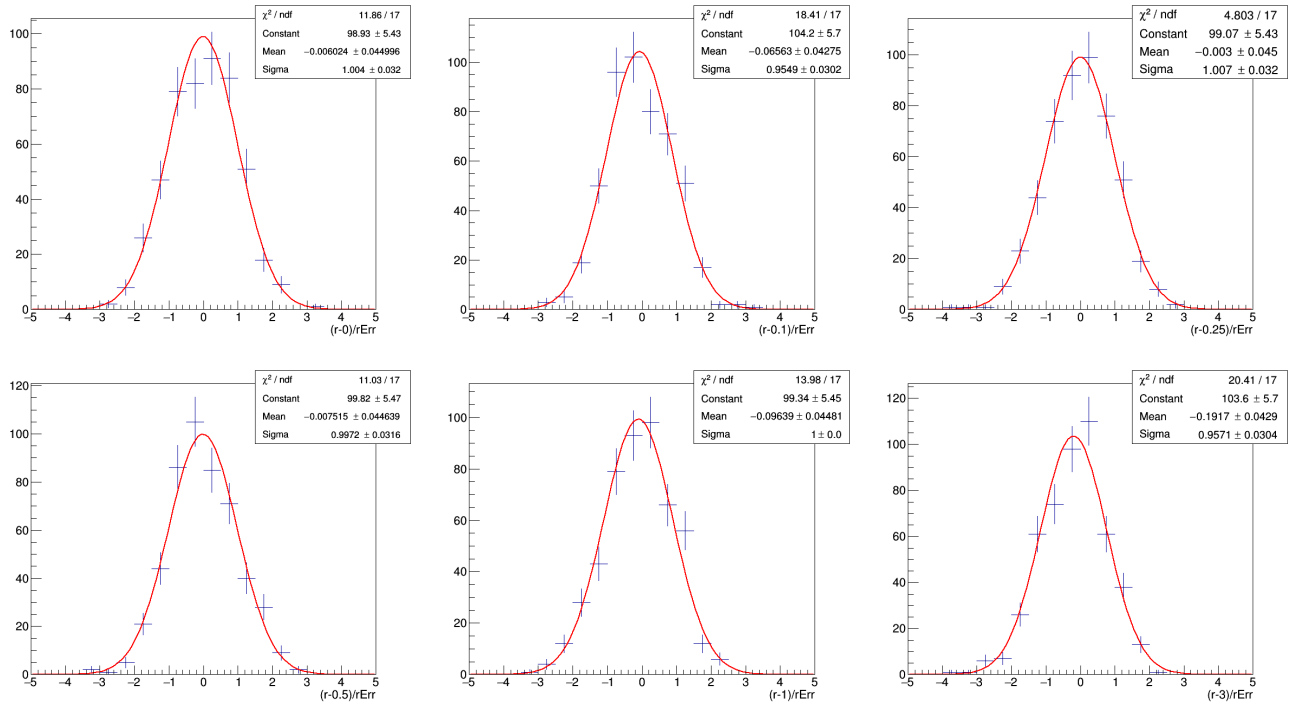

Figure 29: DeepAK8 signal injection tests. The pull on r is plotted in order from left to right, top to bottom: $r = 0$, $r = 0.1$, $r = 0.25$, $r = 0.5$, $r = 1$, $r = 3$

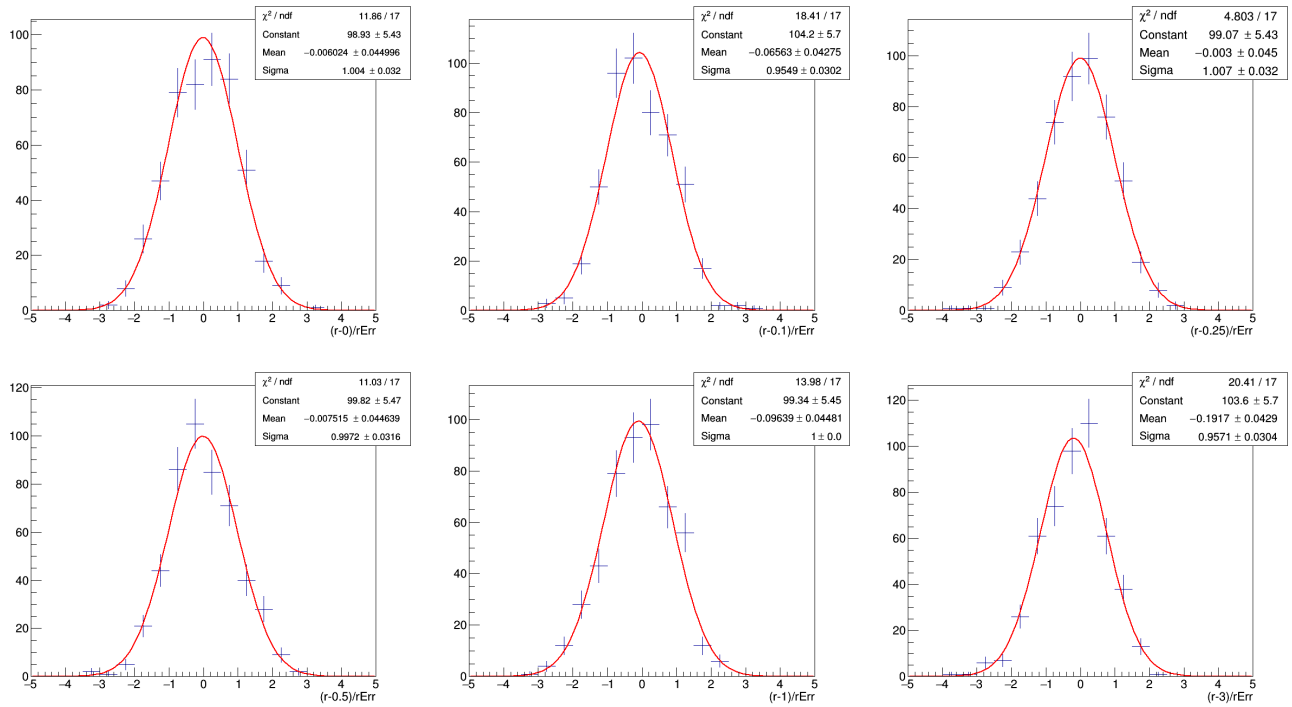

Figure 30: ParticleNet signal injection tests. The pull on r is plotted in order from left to right, top to bottom: $r = 0$, $r = 0.1$, $r = 0.25$, $r = 0.5$, $r = 1$, $r = 3$

8 Blinded expected limits

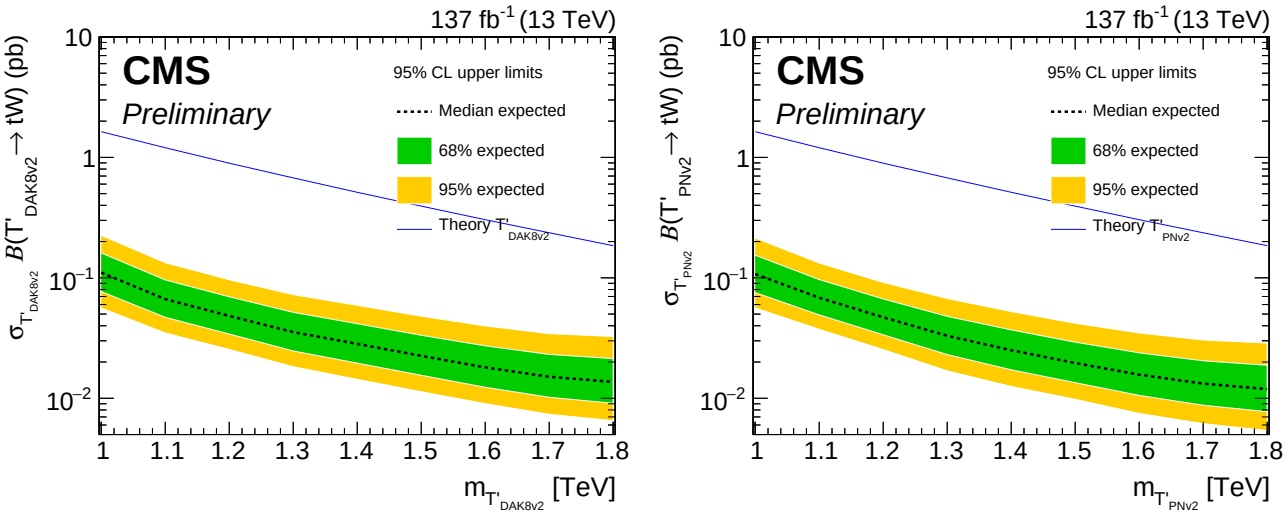

Figure 31: Blinded expected limits for $T' \to tH$ when using the DeepAK8 (left) and ParticleNet (right) taggers.

9 Data and simulation samples

2016

Setname	DAS location
TprimeB 800 GeV	/TprimeBToTH_M-800_LH_TuneCP5_PSweights_13TeV-madgraph_pythia8/ RunIISummer19UL16NanoAODv2-106X_mcRun2_asymptotic_v15-v1/NANOAODSIM
TprimeB 900 GeV	/TprimeBToTH_M-900_LH_TuneCP5_PSweights_13TeV-madgraph_pythia8/ RunIISummer19UL16NanoAODv2-106X_mcRun2_asymptotic_v15-v1/NANOAODSIM
TprimeB 1000 GeV	/TprimeBToTH_M-1000_LH_TuneCP5_PSweights_13TeV-madgraph_pythia8/ RunIISummer19UL16NanoAODv2-106X_mcRun2_asymptotic_v15-v1/NANOAODSIM
TprimeB 1100 GeV	/TprimeBToTH_M-1100_LH_TuneCP5_PSweights_13TeV-madgraph_pythia8/ RunIISummer19UL16NanoAODv2-106X_mcRun2_asymptotic_v15-v1/NANOAODSIM
TprimeB 1200 GeV	/TprimeBToTH_M-1200_LH_TuneCP5_PSweights_13TeV-madgraph_pythia8/ RunIISummer19UL16NanoAODv2-106X_mcRun2_asymptotic_v15-v1/NANOAODSIM
TprimeB 1300 GeV	/TprimeBToTH_M-1300_LH_TuneCP5_PSweights_13TeV-madgraph_pythia8/ RunIISummer19UL16NanoAODv2-106X_mcRun2_asymptotic_v15-v1/NANOAODSIM
TprimeB 1400 GeV	/TprimeBToTH_M-1400_LH_TuneCP5_PSweights_13TeV-madgraph_pythia8/ RunIISummer19UL16NanoAODv2-106X_mcRun2_asymptotic_v15-v1/NANOAODSIM
TprimeB 1500 GeV	/TprimeBToTH_M-1500_LH_TuneCP5_PSweights_13TeV-madgraph_pythia8/ RunIISummer19UL16NanoAODv2-106X_mcRun2_asymptotic_v15-v1/NANOAODSIM
TprimeB 1600 GeV	/TprimeBToTH_M-1600_LH_TuneCP5_PSweights_13TeV-madgraph_pythia8/ RunIISummer19UL16NanoAODv2-106X_mcRun2_asymptotic_v15-v1/NANOAODSIM
TprimeB 1700 GeV	/TprimeBToTH_M-1700_LH_TuneCP5_PSweights_13TeV-madgraph_pythia8/ RunIISummer19UL16NanoAODv2-106X_mcRun2_asymptotic_v15-v1/NANOAODSIM
TprimeB 1800 GeV	/TprimeBToTH_M-1800_LH_TuneCP5_PSweights_13TeV-madgraph_pythia8/ RunIISummer19UL16NanoAODv2-106X_mcRun2_asymptotic_v15-v1/NANOAODSIM
ttbar-allhad	/TTToHadronic_TuneCP5_13TeV-powheg-pythia8/RunIISummer19UL16NanoAODv2-106X_ mcRun2_asymptotic_v15-v1/NANOAODSIM
ttbar-semilep	/TTToSemiLeptonic_TuneCP5_13TeV-powheg-pythia8/RunIISummer19UL16NanoAODv2-106X_ mcRun2_asymptotic_v15-v1/NANOAODSIM
QCDHT700	/QCD_HT700to1000_TuneCP5_PSWeights_13TeV-madgraphMLM-pythia8/ RunIISummer19UL16NanoAODv2-106X_mcRun2_asymptotic_v15-v1/NANOAODSIM
QCDHT1000	/QCD_HT1000to1500_TuneCP5_PSWeights_13TeV-madgraphMLM-pythia8/ RunIISummer19UL16NanoAODv2-106X_mcRun2_asymptotic_v15-v1/NANOAODSIM
QCDHT1500	/QCD_HT1500to2000_TuneCP5_PSWeights_13TeV-madgraphMLM-pythia8/ RunIISummer19UL16NanoAODv2-106X_mcRun2_asymptotic_v15-v1/NANOAODSIM
QCDHT2000	/QCD_HT2000toInf_TuneCP5_PSWeights_13TeV-madgraphMLM-pythia8/ RunIISummer19UL16NanoAODv2-106X_mcRun2_asymptotic_v15-v1/NANOAODSIM
DataB1	/JetHT/Run2016B-ver1_HIPM_UL2016_MiniAODv1_NanoAODv2-v1/NANOAOD
DataB2	/JetHT/Run2016B-ver2_HIPM_UL2016_MiniAODv1_NanoAODv2-v1/NANOAOD
DataC	/JetHT/Run2016C-UL2016_MiniAODv1_NanoAODv2-v1/NANOAOD
DataD	/JetHT/Run2016D-UL2016_MiniAODv1_NanoAODv2-v1/NANOAOD
DataE	/JetHT/Run2016E-UL2016_MiniAODv1_NanoAODv2-v1/NANOAOD
DataF	/JetHT/Run2016F-UL2016_MiniAODv1_NanoAODv2-v2/NANOAOD
DataG	/JetHT/Run2016G-UL2016_MiniAODv1_NanoAODv2-v1/NANOAOD
DataH	/JetHT/Run2016H-UL2016_MiniAODv1_NanoAODv2-v1/NANOAOD

2017

Setname	DAS location
TprimeB 800 GeV	/TprimeBToTH_M-800_LH_TuneCP5_PSweights_13TeV-madgraph_pythia8/ RunIISummer19UL17NanoAODv2-106X_mc2017_realistic_v8-v1/NANOAODSIM
TprimeB 900 GeV	/TprimeBToTH_M-900_LH_TuneCP5_PSweights_13TeV-madgraph_pythia8/ RunIISummer19UL17NanoAODv2-106X_mc2017_realistic_v8-v1/NANOAODSIM
TprimeB 1000 GeV	/TprimeBToTH_M-1000_LH_TuneCP5_PSweights_13TeV-madgraph_pythia8/ RunIISummer19UL17NanoAODv2-106X_mc2017_realistic_v8-v1/NANOAODSIM
TprimeB 1100 GeV	/TprimeBToTH_M-1100_LH_TuneCP5_PSweights_13TeV-madgraph_pythia8/ RunIISummer19UL17NanoAODv2-106X_mc2017_realistic_v8-v1/NANOAODSIM
TprimeB 1200 GeV	/TprimeBToTH_M-1200_LH_TuneCP5_PSweights_13TeV-madgraph_pythia8/ RunIISummer19UL17NanoAODv2-106X_mc2017_realistic_v8-v1/NANOAODSIM
TprimeB 1300 GeV	/TprimeBToTH_M-1300_LH_TuneCP5_PSweights_13TeV-madgraph_pythia8/ RunIISummer19UL17NanoAODv2-106X_mc2017_realistic_v8-v1/NANOAODSIM
TprimeB 1400 GeV	/TprimeBToTH_M-1400_LH_TuneCP5_PSweights_13TeV-madgraph_pythia8/ RunIISummer19UL17NanoAODv2-106X_mc2017_realistic_v8-v1/NANOAODSIM
TprimeB 1500 GeV	/TprimeBToTH_M-1500_LH_TuneCP5_PSweights_13TeV-madgraph_pythia8/ RunIISummer19UL17NanoAODv2-106X_mc2017_realistic_v8-v1/NANOAODSIM
TprimeB 1600 GeV	/TprimeBToTH_M-1600_LH_TuneCP5_PSweights_13TeV-madgraph_pythia8/ RunIISummer19UL17NanoAODv2-106X_mc2017_realistic_v8-v1/NANOAODSIM
TprimeB 1700 GeV	/TprimeBToTH_M-1700_LH_TuneCP5_PSweights_13TeV-madgraph_pythia8/ RunIISummer19UL17NanoAODv2-106X_mc2017_realistic_v8-v1/NANOAODSIM
TprimeB 1800 GeV	/TprimeBToTH_M-1800_LH_TuneCP5_PSweights_13TeV-madgraph_pythia8/ RunIISummer19UL17NanoAODv2-106X_mc2017_realistic_v8-v1/NANOAODSIM
ttbar-allhad	/TTToHadronic_TuneCP5_13TeV-powheg-pythia8/RunIISummer19UL17NanoAODv2-106X_ mc2017_realistic_v8-v1/NANOAODSIM
ttbar-semilep	/TTToSemiLeptonic_TuneCP5_13TeV-powheg-pythia8/RunIISummer19UL17NanoAODv2-106X_ mc2017_realistic_v8-v1/NANOAODSIM
QCDHT700	/QCD_HT700to1000_TuneCP5_PSWeights_13TeV-madgraphMLM-pythia8/ RunIISummer19UL17NanoAODv2-106X_mc2017_realistic_v8-v1/NANOAODSIM
QCDHT1000	/QCD_HT1000to1500_TuneCP5_PSWeights_13TeV-madgraphMLM-pythia8/ RunIISummer19UL17NanoAODv2-106X_mc2017_realistic_v8-v1/NANOAODSIM
QCDHT1500	/QCD_HT1500to2000_TuneCP5_PSWeights_13TeV-madgraphMLM-pythia8/ RunIISummer19UL17NanoAODv2-106X_mc2017_realistic_v8-v1/NANOAODSIM
QCDHT2000	/QCD_HT2000toInf_TuneCP5_PSWeights_13TeV-madgraphMLM-pythia8/ RunIISummer19UL17NanoAODv2-106X_mc2017_realistic_v8-v1/NANOAODSIM
DataB	/JetHT/Run2017B-UL2017_MiniAODv1_NanoAODv2-v1/NANOAOD
DataC	/JetHT/Run2017C-UL2017_MiniAODv1_NanoAODv2-v1/NANOAOD
DataD	/JetHT/Run2017D-UL2017_MiniAODv1_NanoAODv2-v1/NANOAOD
DataE	/JetHT/Run2017E-UL2017_MiniAODv1_NanoAODv2-v1/NANOAOD
DataF	/JetHT/Run2017F-UL2017_MiniAODv1_NanoAODv2-v2/NANOAOD

2018

Setname	DAS location
TprimeB 800 GeV	/TprimeBToTH_M-800_LH_TuneCP5_PSweights_13TeV-madgraph_pythia8/ RunIISummer19UL18NanoAODv2-106X_upgrade2018_realistic_v15_L1v1-v1/NANOAODSIM
TprimeB 900 GeV	/TprimeBToTH_M-900_LH_TuneCP5_PSweights_13TeV-madgraph_pythia8/ RunIISummer19UL18NanoAODv2-106X_upgrade2018_realistic_v15_L1v1-v1/NANOAODSIM
TprimeB 1000 GeV	/TprimeBToTH_M-1000_LH_TuneCP5_PSweights_13TeV-madgraph_pythia8/ RunIISummer19UL18NanoAODv2-106X_upgrade2018_realistic_v15_L1v1-v1/NANOAODSIM
TprimeB 1100 GeV	/TprimeBToTH_M-1100_LH_TuneCP5_PSweights_13TeV-madgraph_pythia8/ RunIISummer19UL18NanoAODv2-106X_upgrade2018_realistic_v15_L1v1-v1/NANOAODSIM
TprimeB 1200 GeV	/TprimeBToTH_M-1200_LH_TuneCP5_PSweights_13TeV-madgraph_pythia8/ RunIISummer19UL18NanoAODv2-106X_upgrade2018_realistic_v15_L1v1-v1/NANOAODSIM
TprimeB 1300 GeV	/TprimeBToTH_M-1300_LH_TuneCP5_PSweights_13TeV-madgraph_pythia8/ RunIISummer19UL18NanoAODv2-106X_upgrade2018_realistic_v15_L1v1-v1/NANOAODSIM
TprimeB 1400 GeV	/TprimeBToTH_M-1400_LH_TuneCP5_PSweights_13TeV-madgraph_pythia8/ RunIISummer19UL18NanoAODv2-106X_upgrade2018_realistic_v15_L1v1-v1/NANOAODSIM
TprimeB 1500 GeV	/TprimeBToTH_M-1500_LH_TuneCP5_PSweights_13TeV-madgraph_pythia8/ RunIISummer19UL18NanoAODv2-106X_upgrade2018_realistic_v15_L1v1-v1/NANOAODSIM
TprimeB 1600 GeV	/TprimeBToTH_M-1600_LH_TuneCP5_PSweights_13TeV-madgraph_pythia8/ RunIISummer19UL18NanoAODv2-106X_upgrade2018_realistic_v15_L1v1-v1/NANOAODSIM
TprimeB 1700 GeV	/TprimeBToTH_M-1700_LH_TuneCP5_PSweights_13TeV-madgraph_pythia8/ RunIISummer19UL18NanoAODv2-106X_upgrade2018_realistic_v15_L1v1-v1/NANOAODSIM
TprimeB 1800 GeV	/TprimeBToTH_M-1800_LH_TuneCP5_PSweights_13TeV-madgraph_pythia8/ RunIISummer19UL18NanoAODv2-106X_upgrade2018_realistic_v15_L1v1-v1/NANOAODSIM
ttbar-allhad	/TTToHadronic_TuneCP5_13TeV-powheg-pythia8/RunIISummer19UL18NanoAODv2-106X_ upgrade2018_realistic_v15_L1v1-v1/NANOAODSIM
ttbar-semilep	/TTToSemiLeptonic_TuneCP5_13TeV-powheg-pythia8/RunIISummer19UL18NanoAODv2-106X_ upgrade2018_realistic_v15_L1v1-v1/NANOAODSIM
QCDHT700	/QCD_HT700to1000_TuneCP5_PSWeights_13TeV-madgraphMLM-pythia8/ RunIISummer19UL18NanoAODv2-106X_upgrade2018_realistic_v15_L1v1-v1/NANOAODSIM
QCDHT1000	/QCD_HT1000to1500_TuneCP5_PSWeights_13TeV-madgraphMLM-pythia8/ RunIISummer19UL18NanoAODv2-106X_upgrade2018_realistic_v15_L1v1-v1/NANOAODSIM
QCDHT1500	/QCD_HT1500to2000_TuneCP5_PSWeights_13TeV-madgraphMLM-pythia8/ RunIISummer19UL18NanoAODv2-106X_upgrade2018_realistic_v15_L1v1-v1/NANOAODSIM
QCDHT2000	/QCD_HT2000toInf_TuneCP5_PSWeights_13TeV-madgraphMLM-pythia8/ RunIISummer19UL18NanoAODv2-106X_upgrade2018_realistic_v15_L1v1-v1/NANOAODSIM
DataA	/JetHT/Run2018A-UL2018_MiniAODv1_NanoAODv2-v1/NANOAOD
DataB	/JetHT/Run2018B-UL2018_MiniAODv1_NanoAODv2-v1/NANOAOD
DataC	/JetHT/Run2018C-UL2018_MiniAODv1_NanoAODv2-v1/NANOAOD
DataD	/JetHT/Run2018D-UL2018_MiniAODv1_NanoAODv2-v1/NANOAOD

10 Fit results with variations of the $R_{P/F}$

10.1 $R_{P/F}$ pol0 by pol1

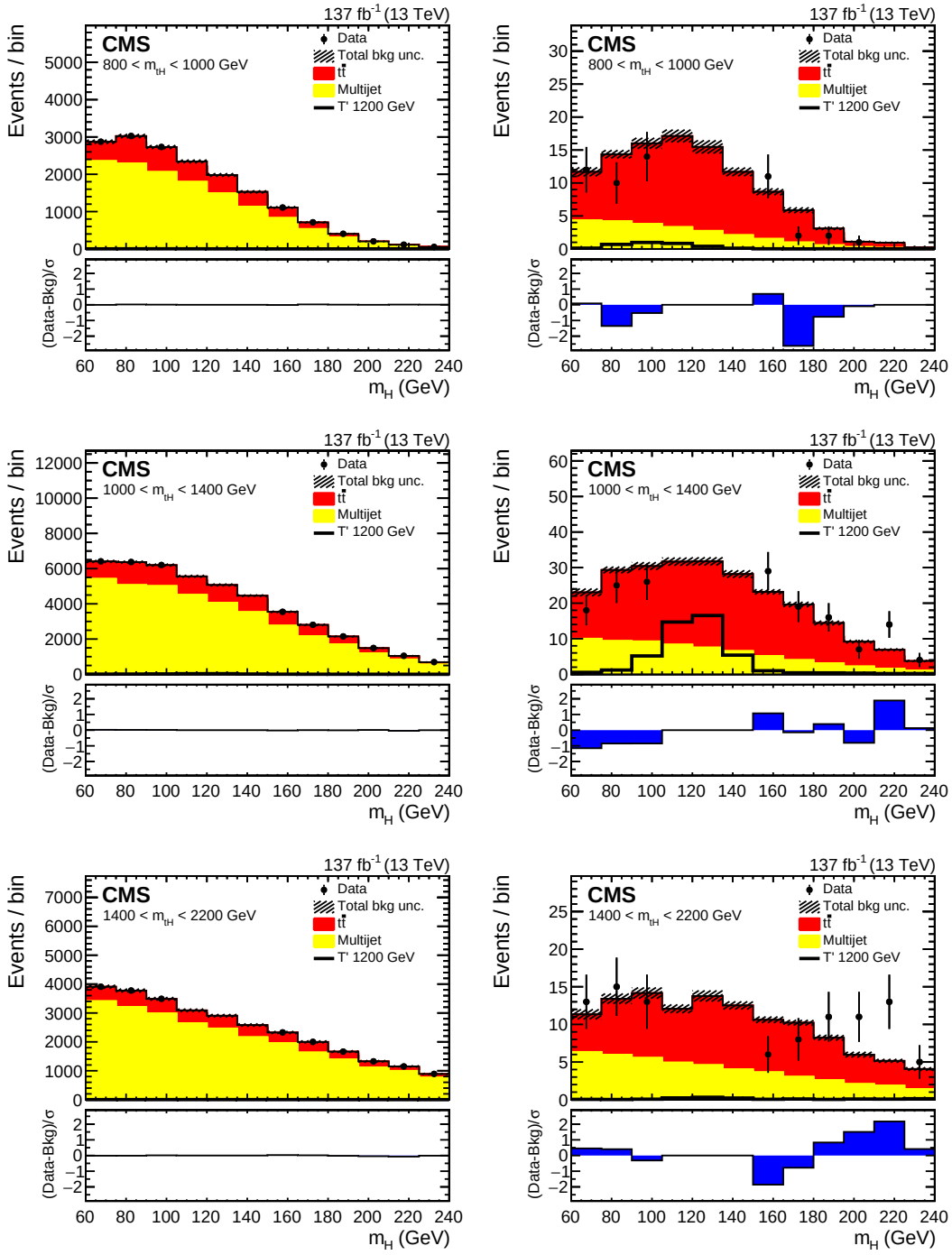

Figure 32: The m_H mass distributions for the blinded background-only fit using the DeepAK8 tagger and a 0x1 $R_{P/F}$. A 1200 GeV T' signal is normalized to 0.1 pb and plotted with the backgrounds to show relative shapes and yields.

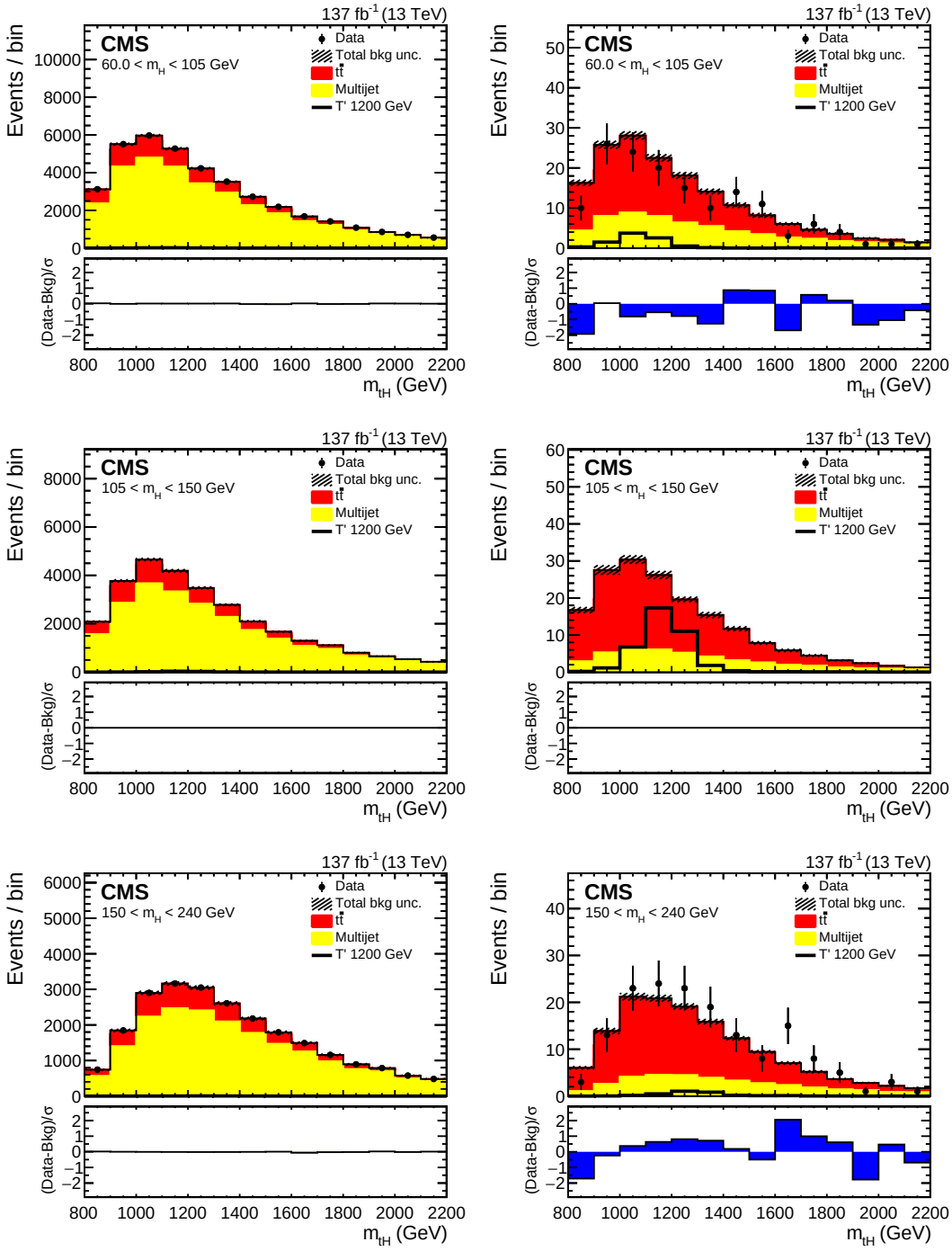

Figure 33: The m_{tH} mass distributions for the blinded background-only fit using the DeepAK8 tagger and a 0x1 $R_{P/F}$. A 1200 GeV T' signal is normalized to 0.1 pb and plotted with the backgrounds to show relative shapes and yields.

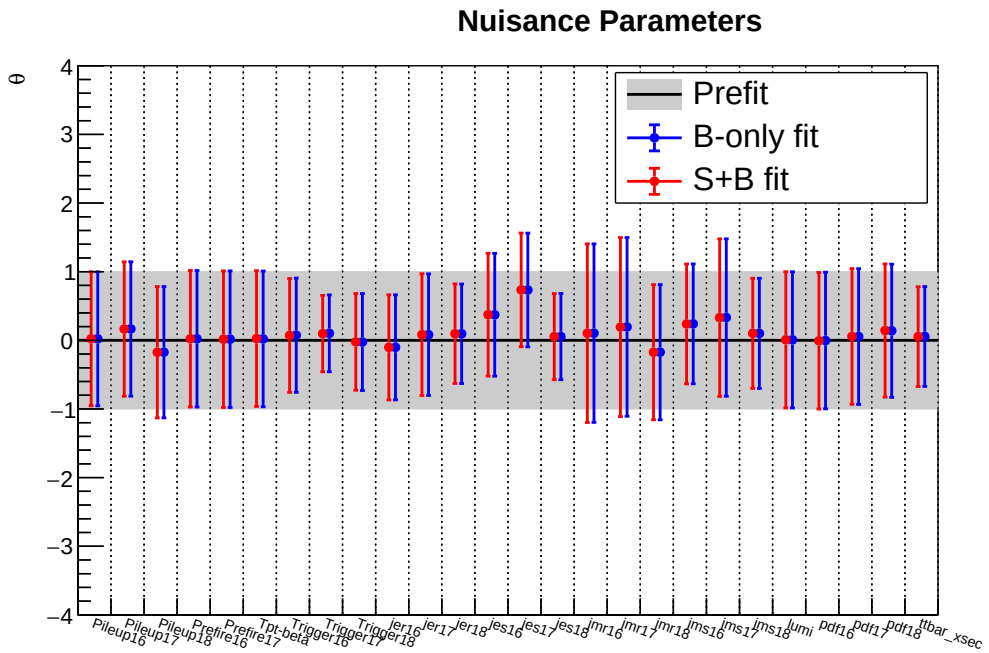

Figure 34: The nuisance parameter pulls for the blinded fits of the DeepAK8 based selection using a 0x1 $R_{P/F}$.

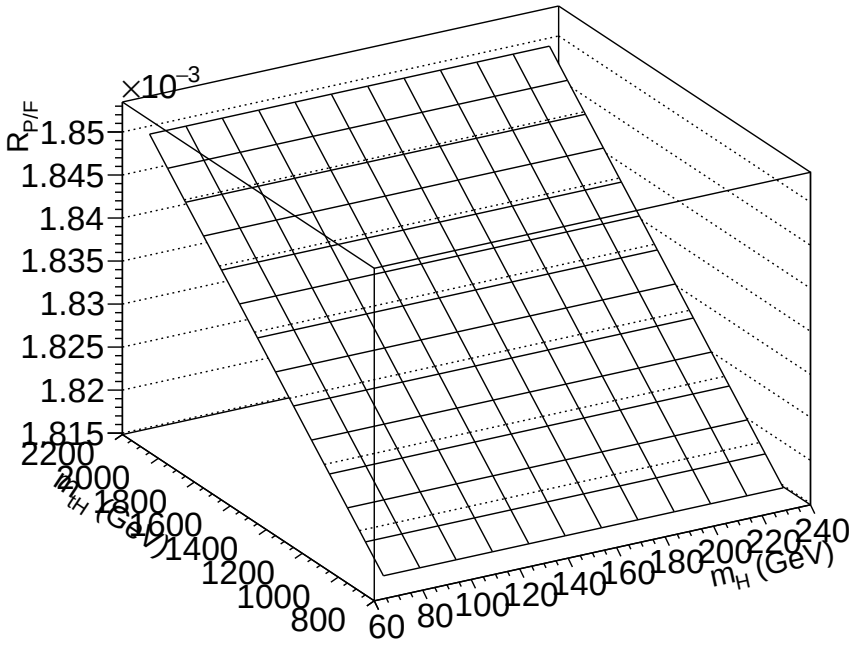

Figure 35: The post-fit $R_{P/F}$ for the blinded fits of the DeepAK8 based selection using a 0x1 $R_{P/F}$.

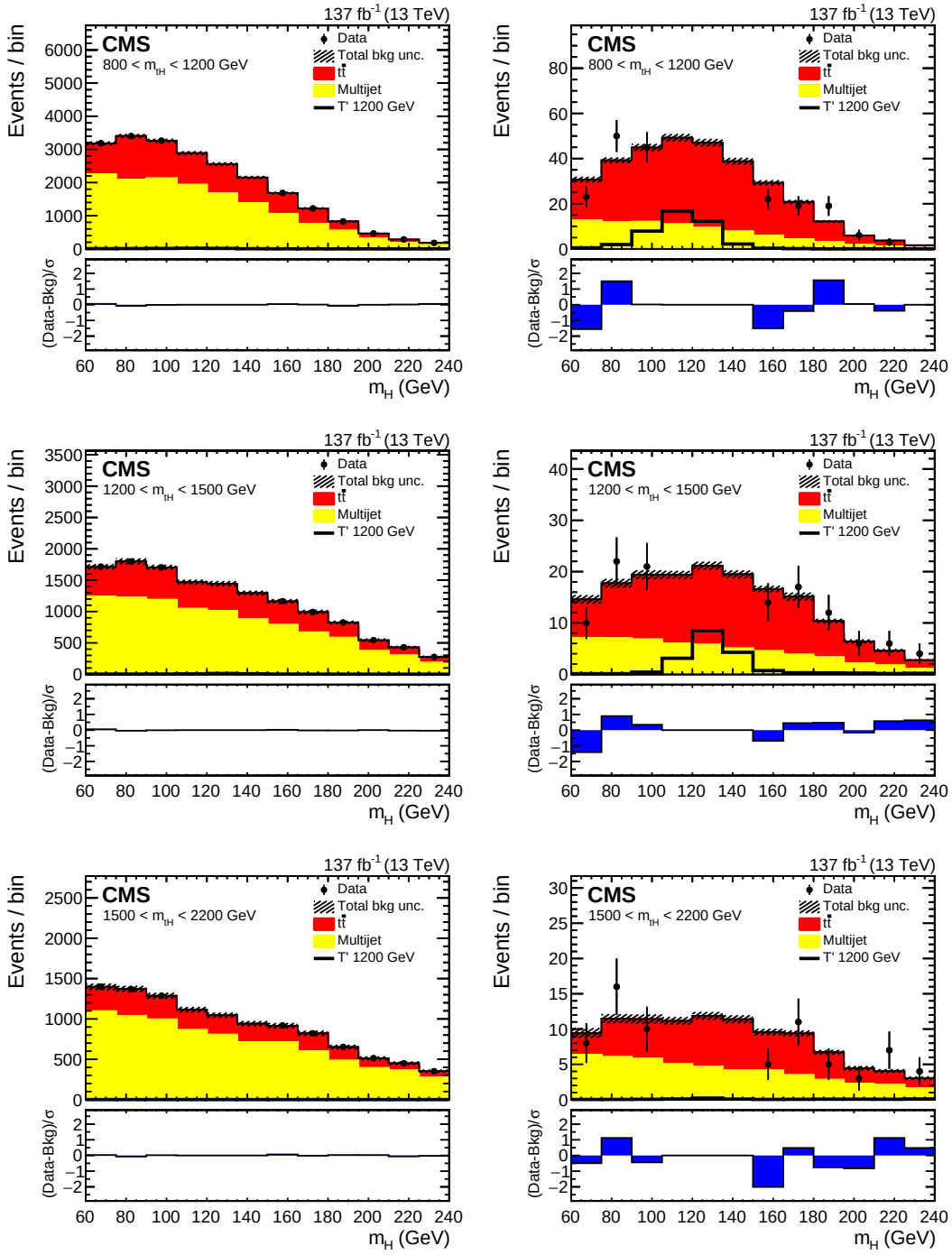

Figure 36: The m_H mass distributions for the blinded background-only fit using the ParticleNet tagger and a 0x1 $R_{P/F}$. A 1200 GeV T' signal is normalized to 0.1 pb and plotted with the backgrounds to show relative shapes and yields.

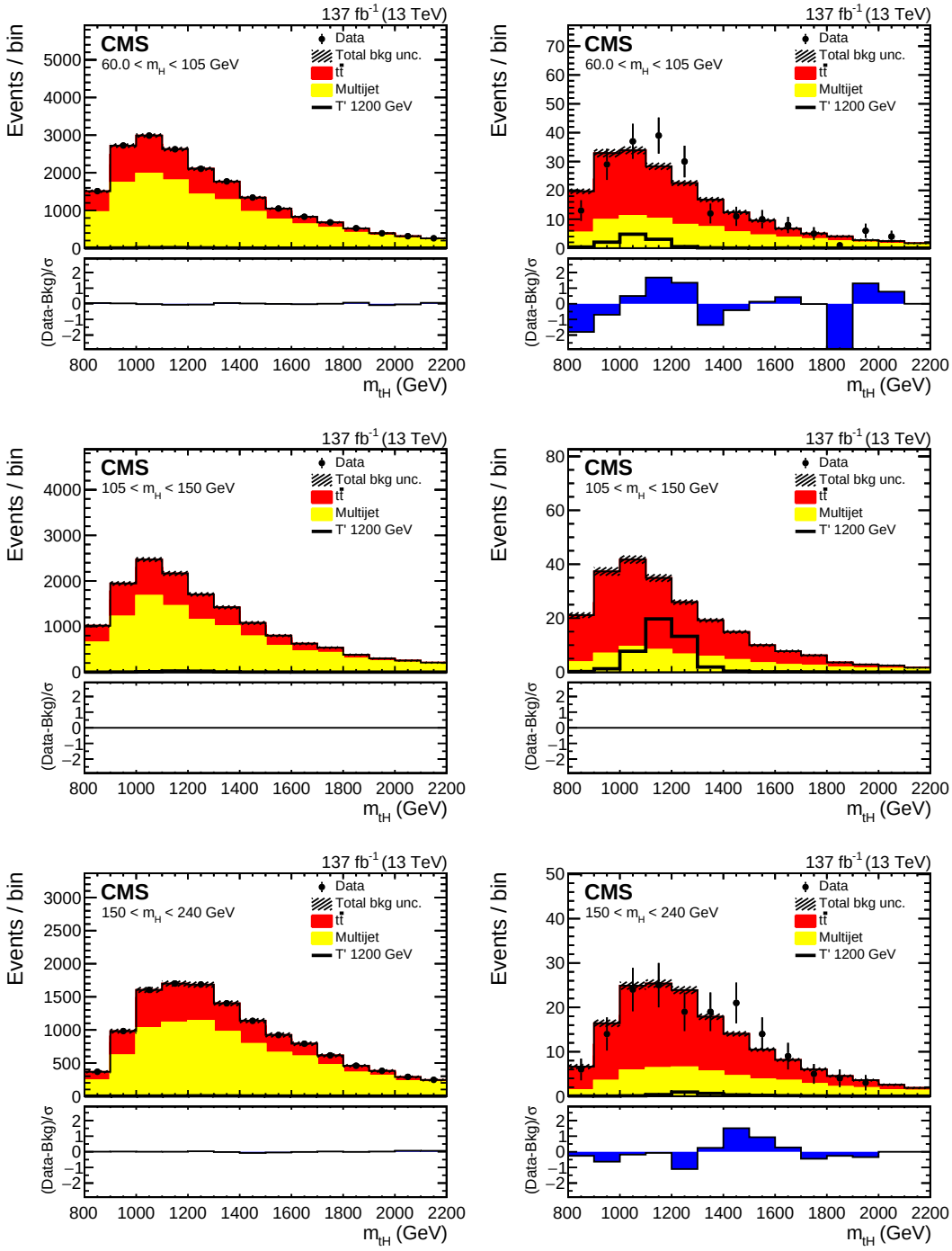

Figure 37: The m_{tH} mass distributions for the blinded background-only fit using the ParticleNet tagger and a 0x1 $R_{P/F}$. A 1200 GeV T' signal is normalized to 0.1 pb and plotted with the backgrounds to show relative shapes and yields.

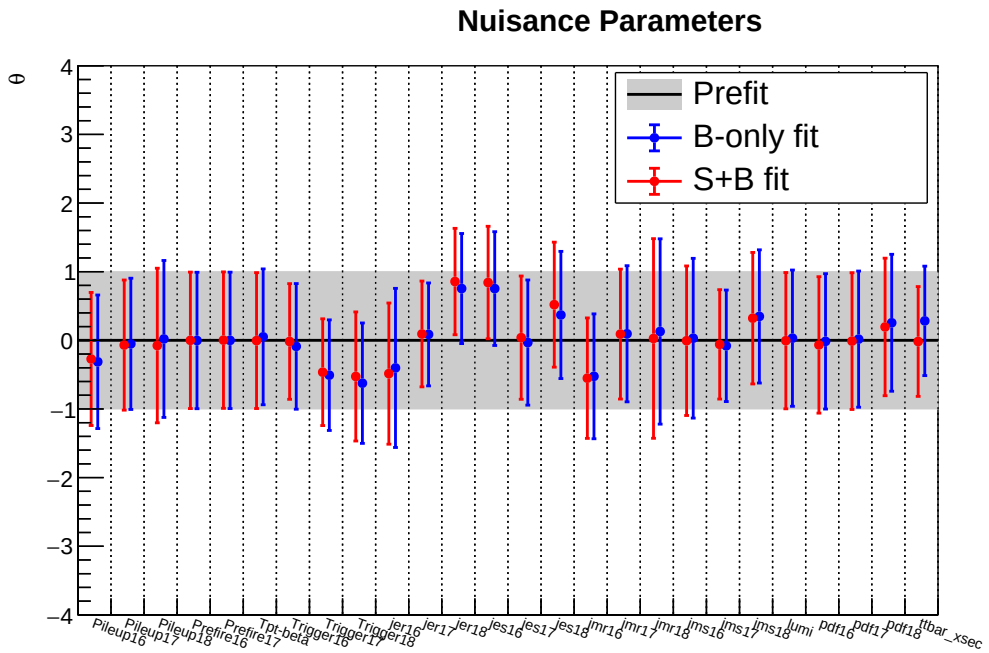

Figure 38: The nuisance parameter pulls for the blinded fits of the ParticleNet based selection using a 0x1 $R_{P/F}$.

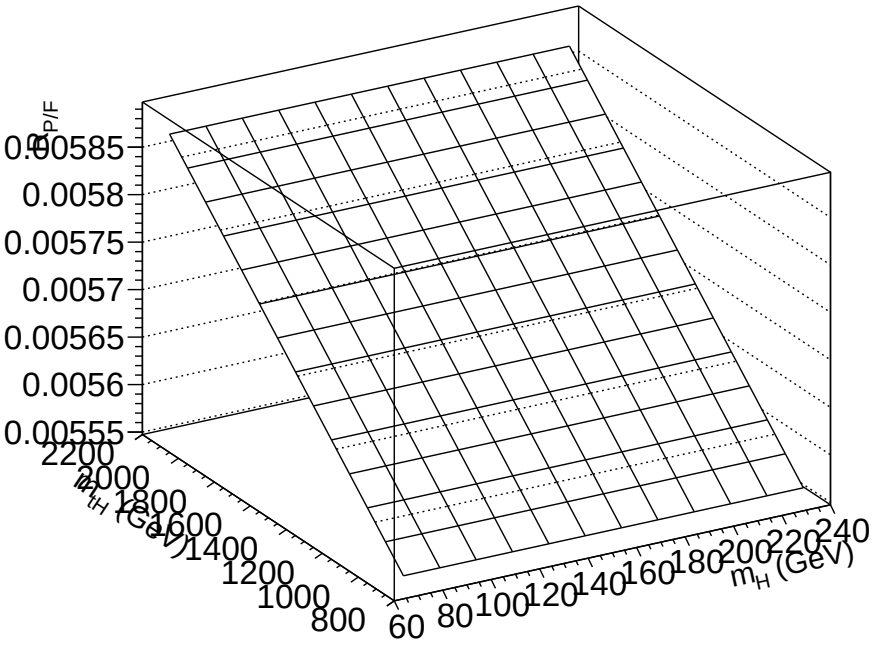

Figure 39: The post-fit $R_{P/F}$ for the blinded fits of the ParticleNet based selection using a 0x1 $R_{P/F}$.

10.2 $R_{P/F}$ pol1 by pol0

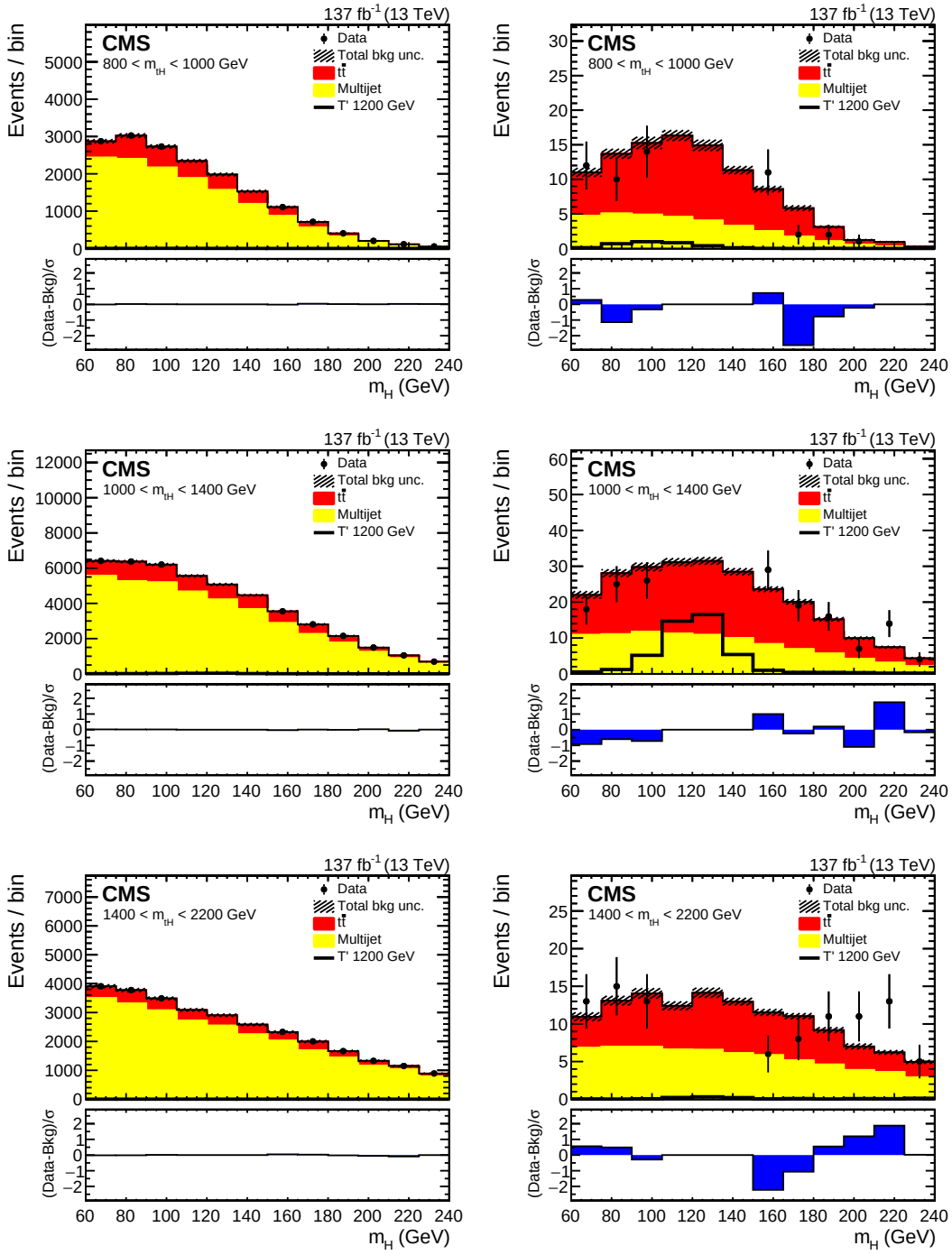

Figure 40: The m_H mass distributions for the blinded background-only fit using the DeepAK8 tagger and a 1x0 $R_{P/F}$. A 1200 GeV T' signal is normalized to 0.1 pb and plotted with the backgrounds to show relative shapes and yields.

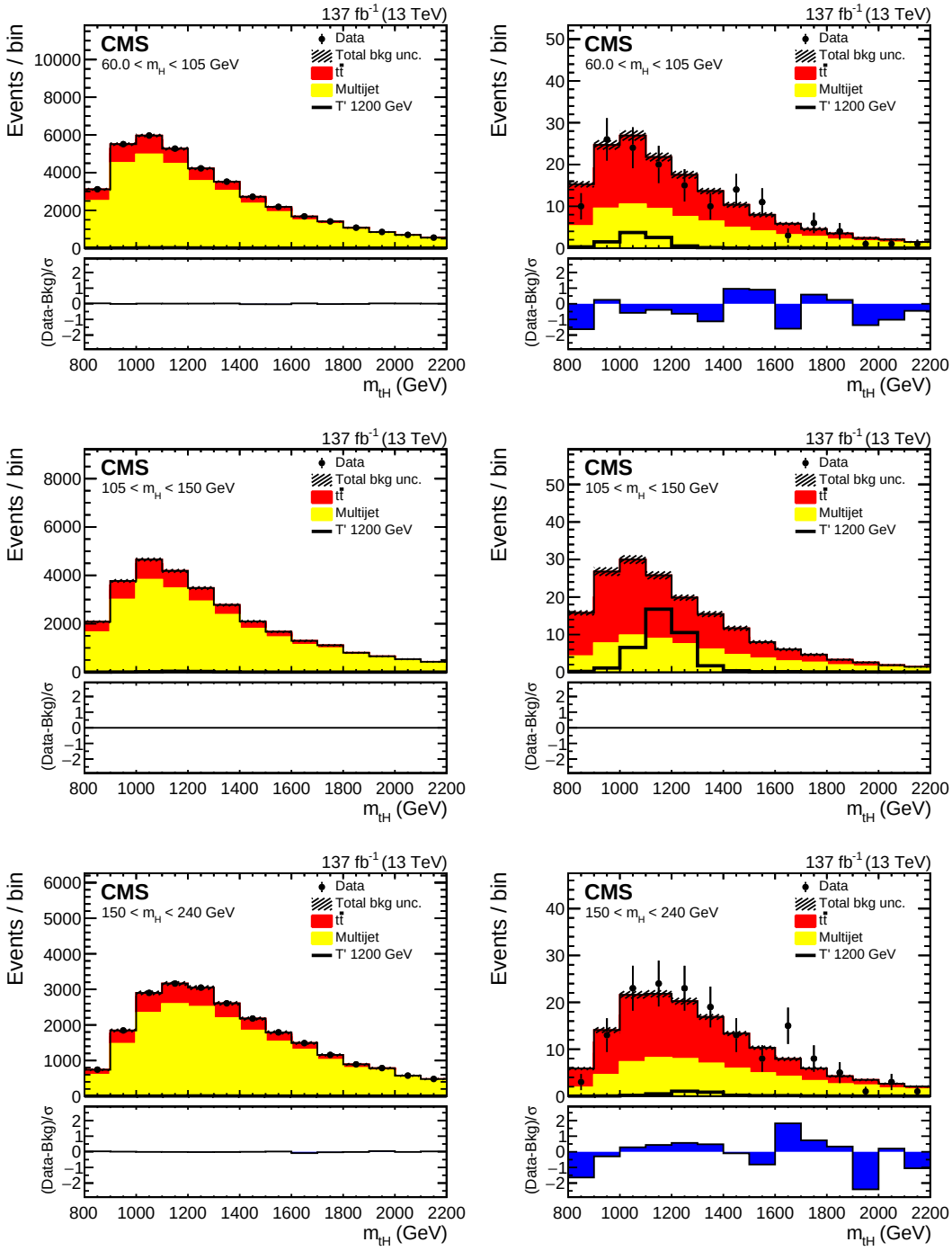

Figure 41: The m_{tH} mass distributions for the blinded background-only fit using the DeepAK8 tagger and a 1x0 $R_{P/F}$. A 1200 GeV T' signal is normalized to 0.1 pb and plotted with the backgrounds to show relative shapes and yields.

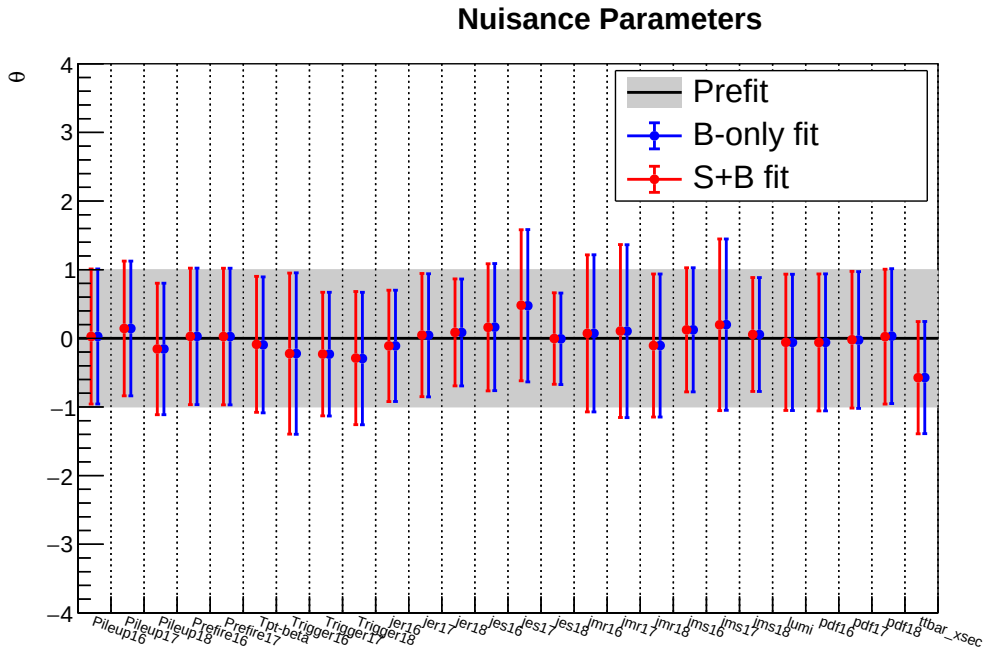

Figure 42: The nuisance parameter pulls for the blinded fits of the DeepAK8 based selection using a 1x0 $R_{P/F}$.

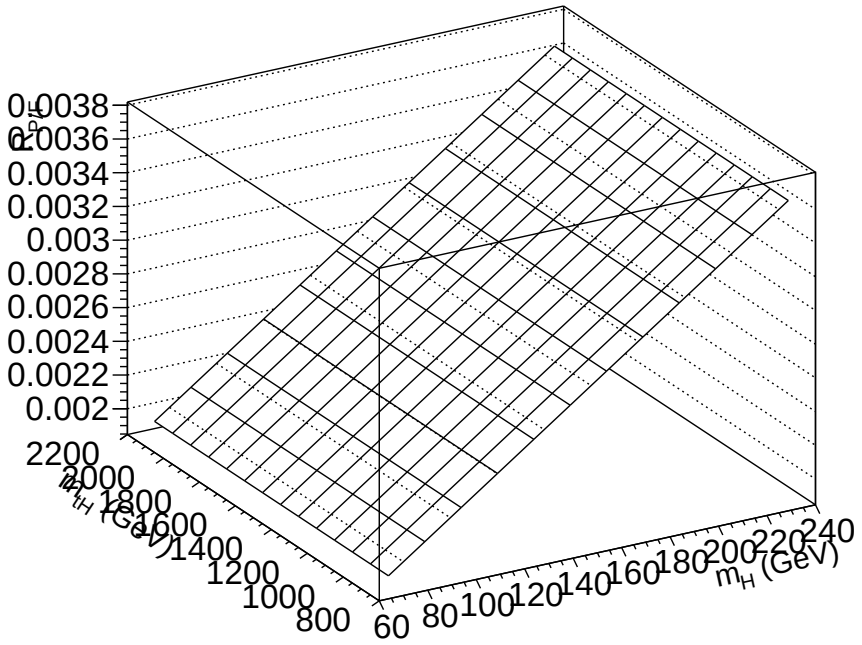

Figure 43: The post-fit $R_{P/F}$ for the blinded fits of the DeepAK8 based selection using a 1x0 $R_{P/F}$.

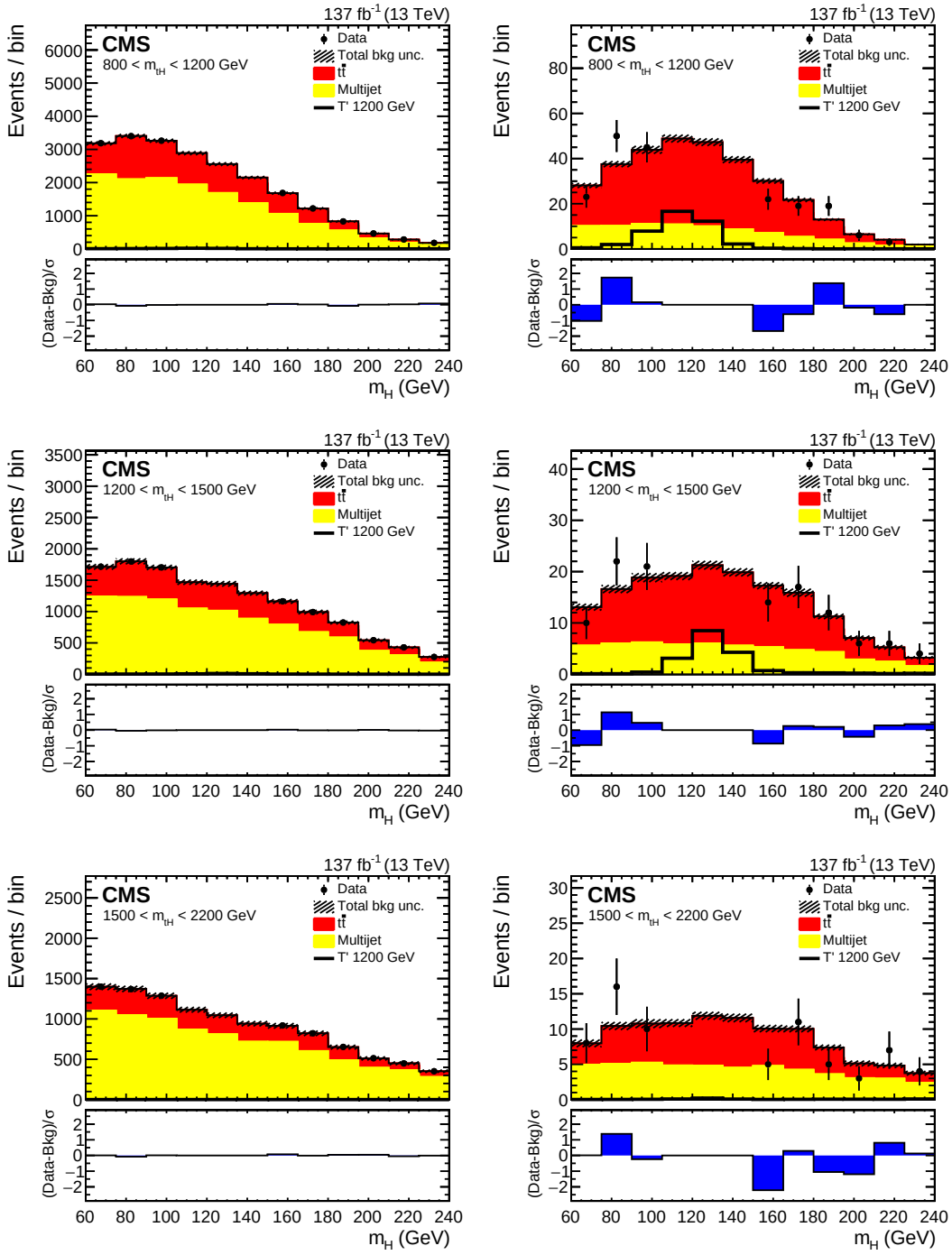

Figure 44: The m_H mass distributions for the blinded background-only fit using the ParticleNet tagger and a 1x0 $R_{P/F}$. A 1200 GeV T' signal is normalized to 0.1 pb and plotted with the backgrounds to show relative shapes and yields.

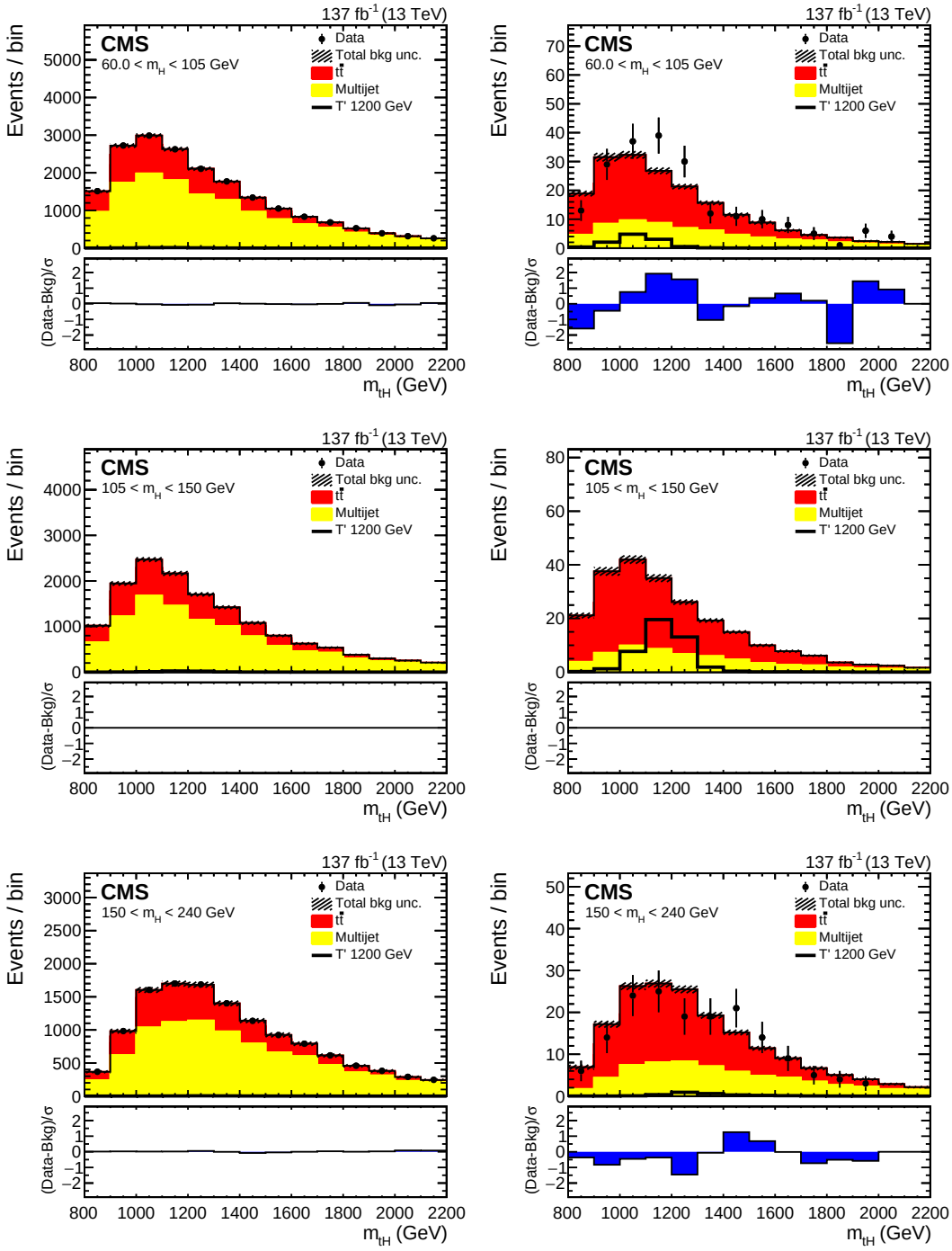

Figure 45: The m_{tH} mass distributions for the blinded background-only fit using the ParticleNet tagger and a 1x0 $R_{P/F}$. A 1200 GeV T' signal is normalized to 0.1 pb and plotted with the backgrounds to show relative shapes and yields.

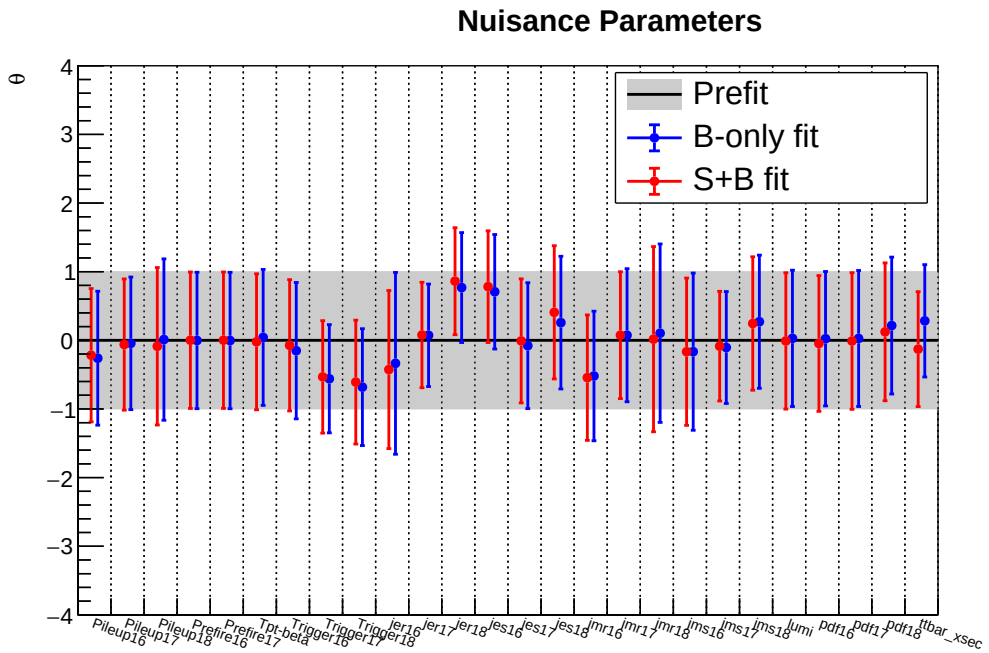

Figure 46: The nuisance parameter pulls for the blinded fits of the ParticleNet based selection using a 1x0 $R_{P/F}$.

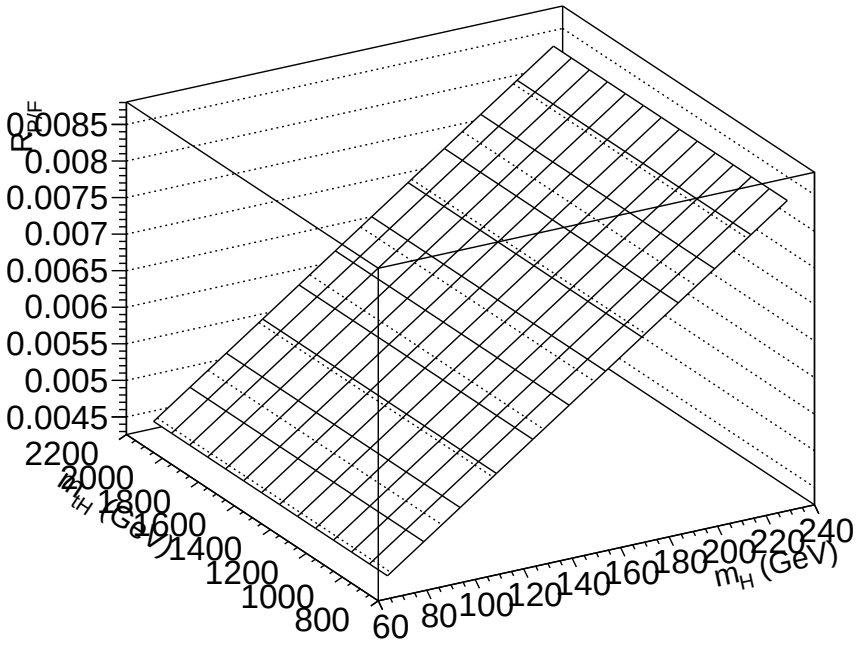

Figure 47: The post-fit $R_{P/F}$ for the blinded fits of the ParticleNet based selection using a 1x0 $R_{P/F}$.

10.3 $R_{P/F}$ pol1 by pol1

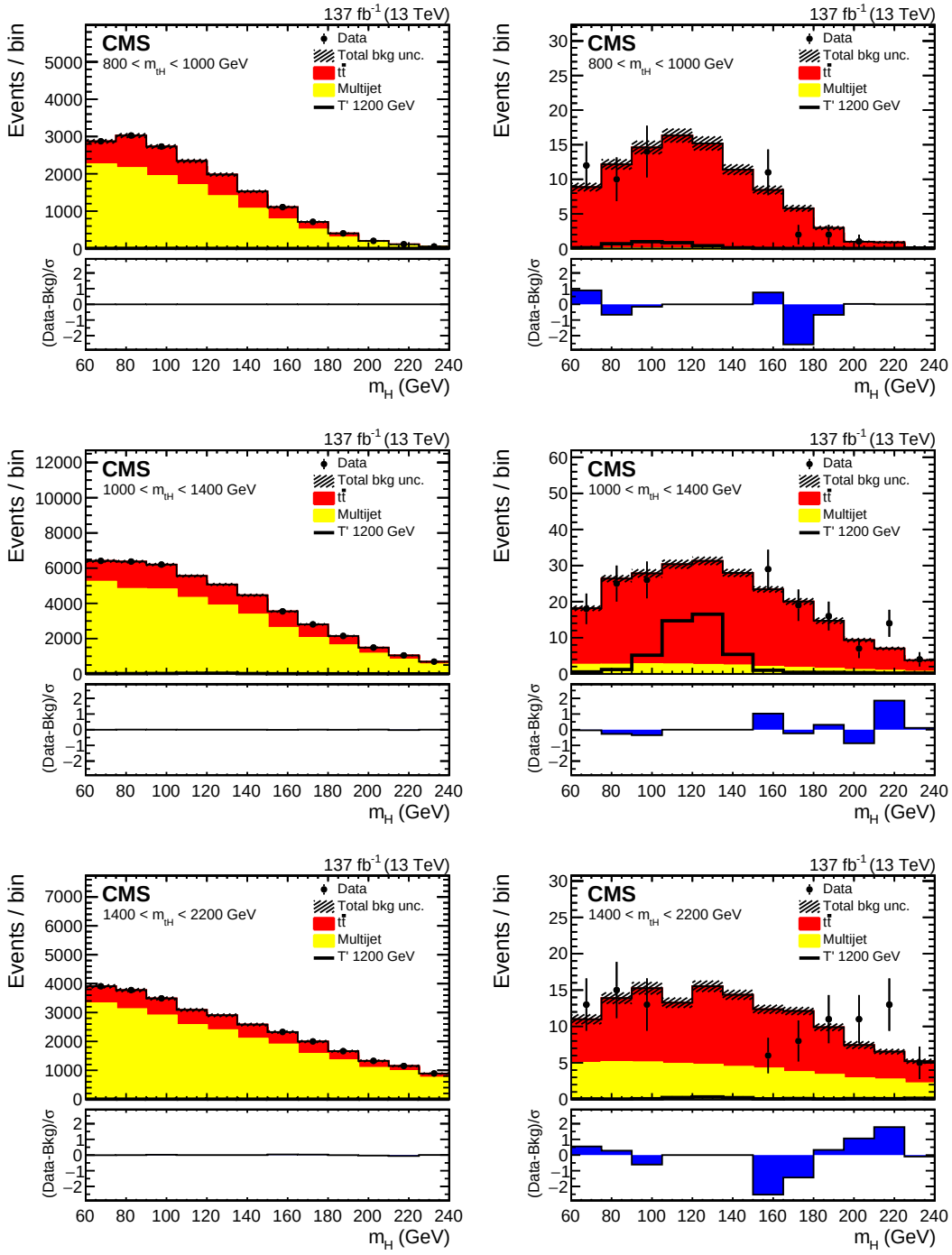

Figure 48: The m_H mass distributions for the blinded background-only fit using the DeepAK8 tagger and a 1x1 $R_{P/F}$. A 1200 GeV T' signal is normalized to 0.1 pb and plotted with the backgrounds to show relative shapes and yields.

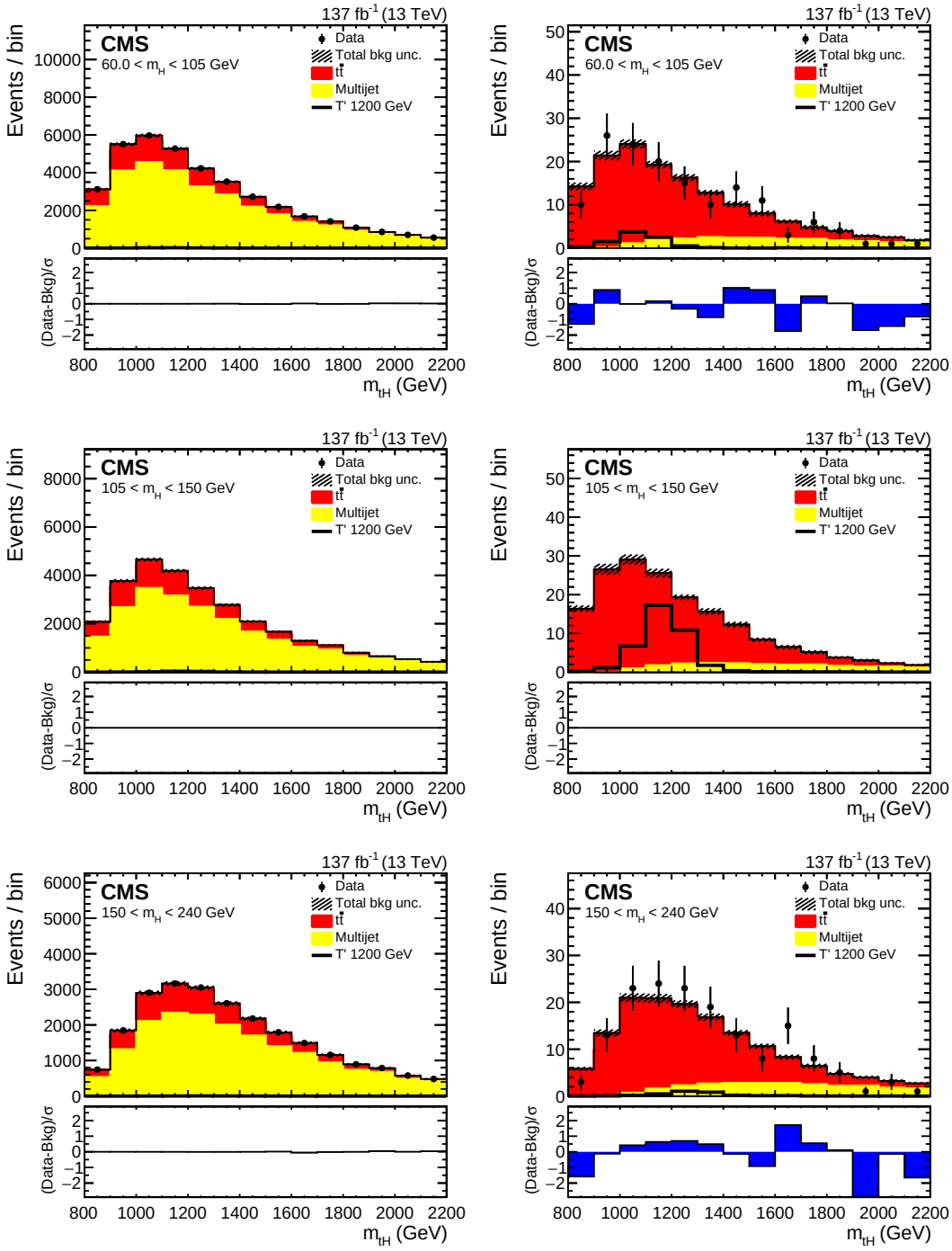

Figure 49: The m_{tH} mass distributions for the blinded background-only fit using the DeepAK8 tagger and a 1x1 $R_{P/F}$. A 1200 GeV T' signal is normalized to 0.1 pb and plotted with the backgrounds to show relative shapes and yields.

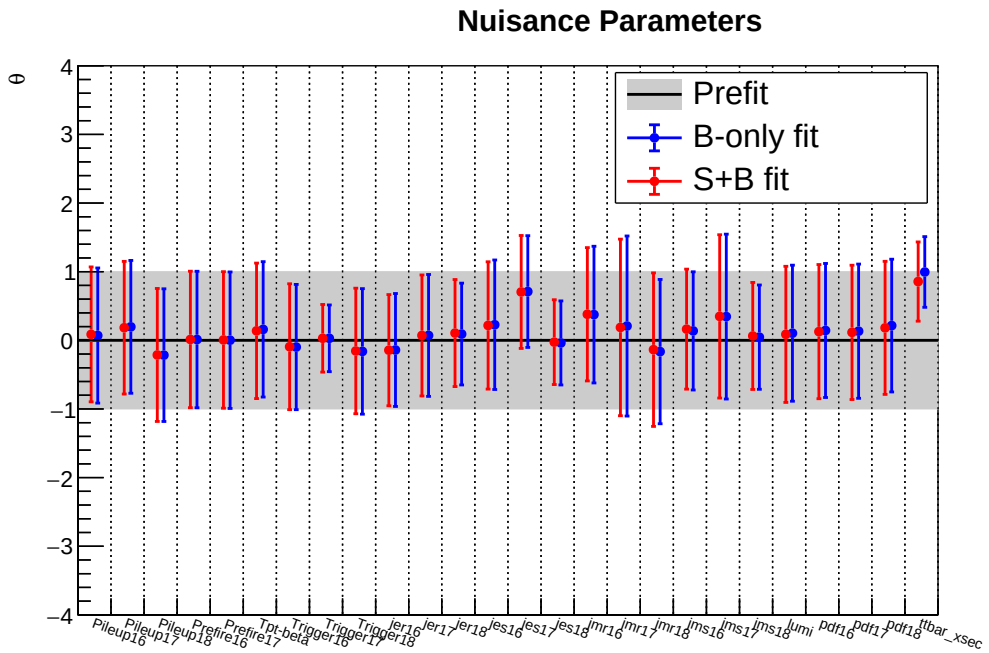

Figure 50: The nuisance parameter pulls for the blinded fits of the DeepAK8 based selection using a 1x1 $R_{P/F}$.

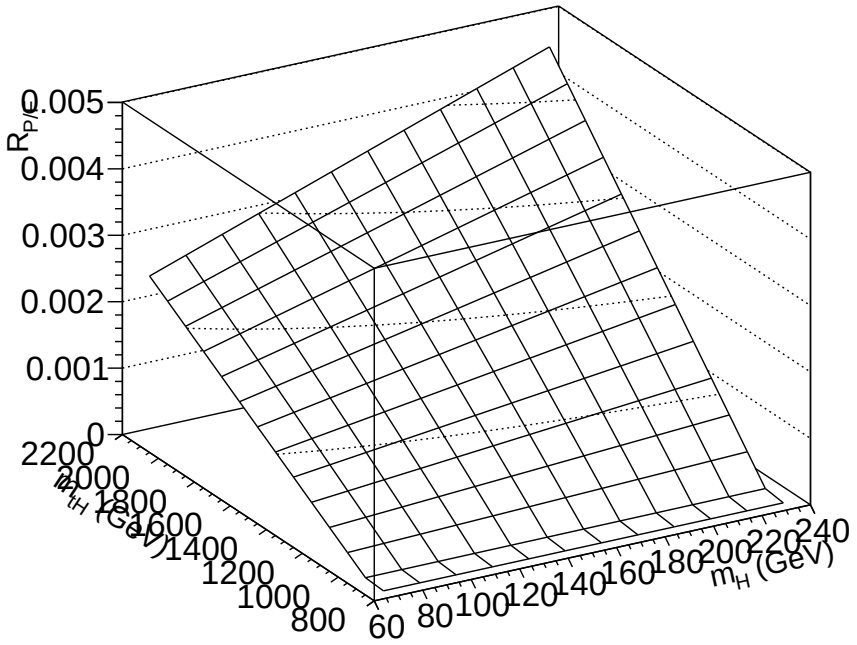

Figure 51: The post-fit $R_{P/F}$ for the blinded fits of the DeepAK8 based selection using a 1x1 $R_{P/F}$.

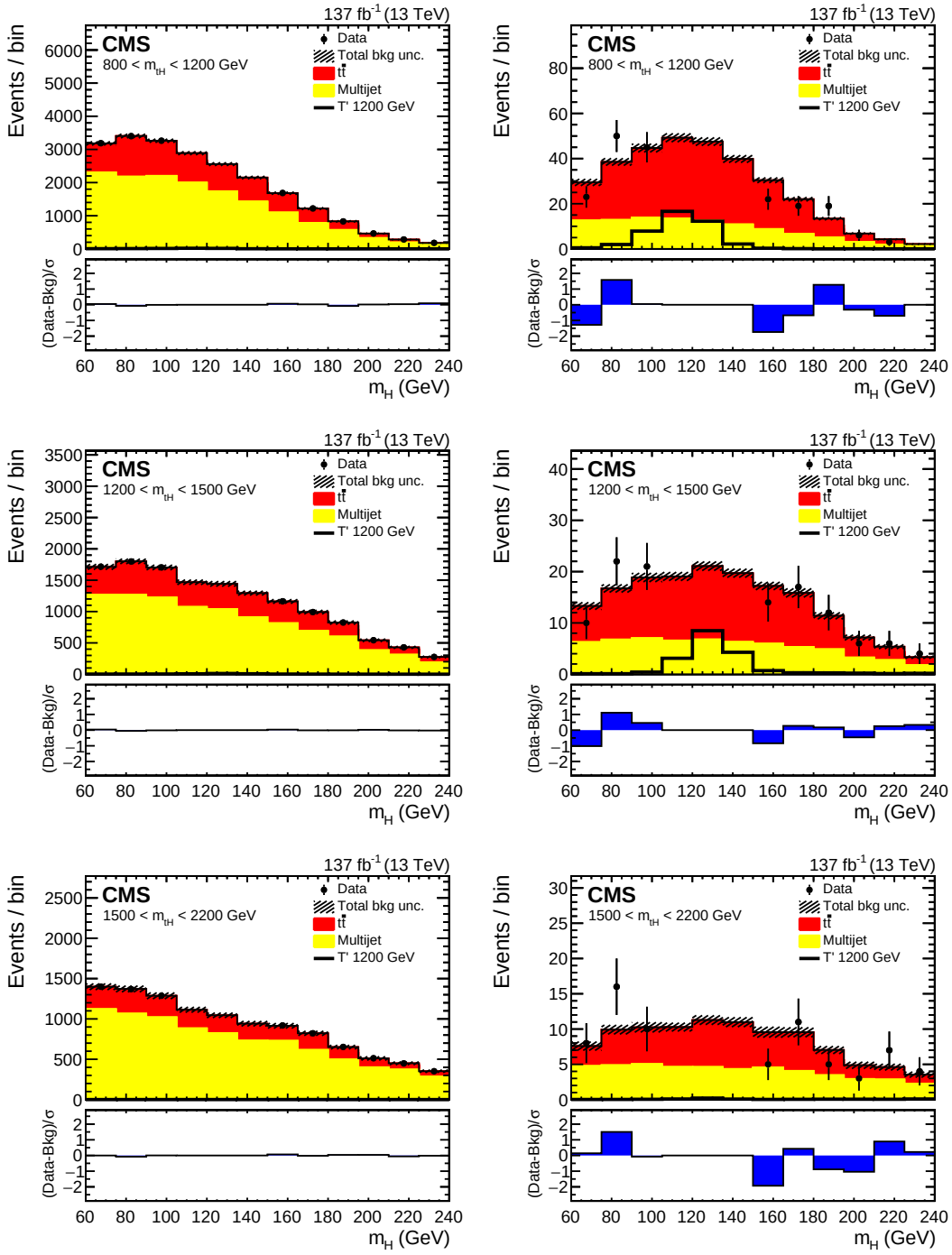

Figure 52: The m_H mass distributions for the blinded background-only fit using the ParticleNet tagger and a 1x1 $R_{P/F}$. A 1200 GeV T' signal is normalized to 0.1 pb and plotted with the backgrounds to show relative shapes and yields.

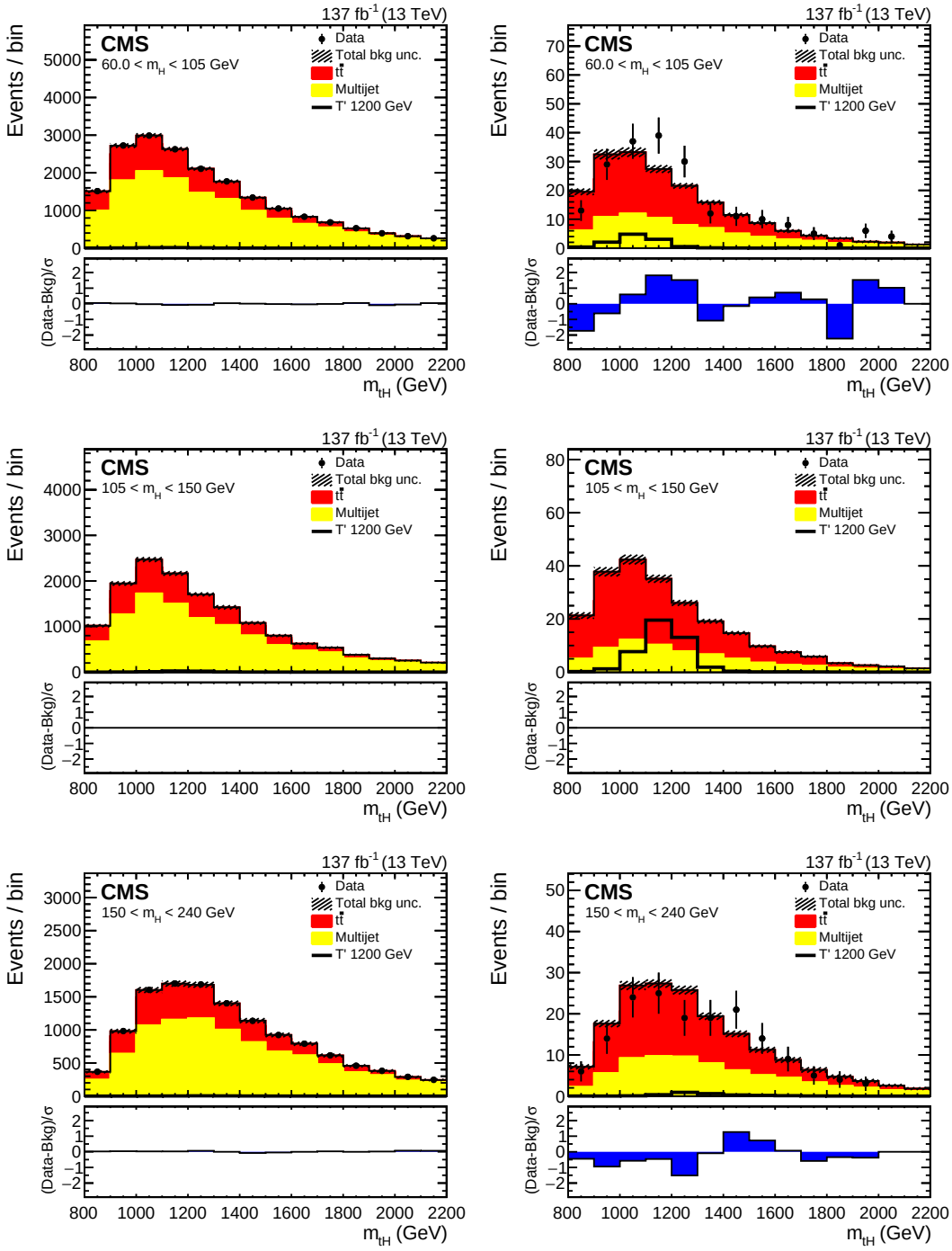

Figure 53: The m_{tH} mass distributions for the blinded background-only fit using the ParticleNet tagger and a 1x1 $R_{P/F}$. A 1200 GeV T' signal is normalized to 0.1 pb and plotted with the backgrounds to show relative shapes and yields.

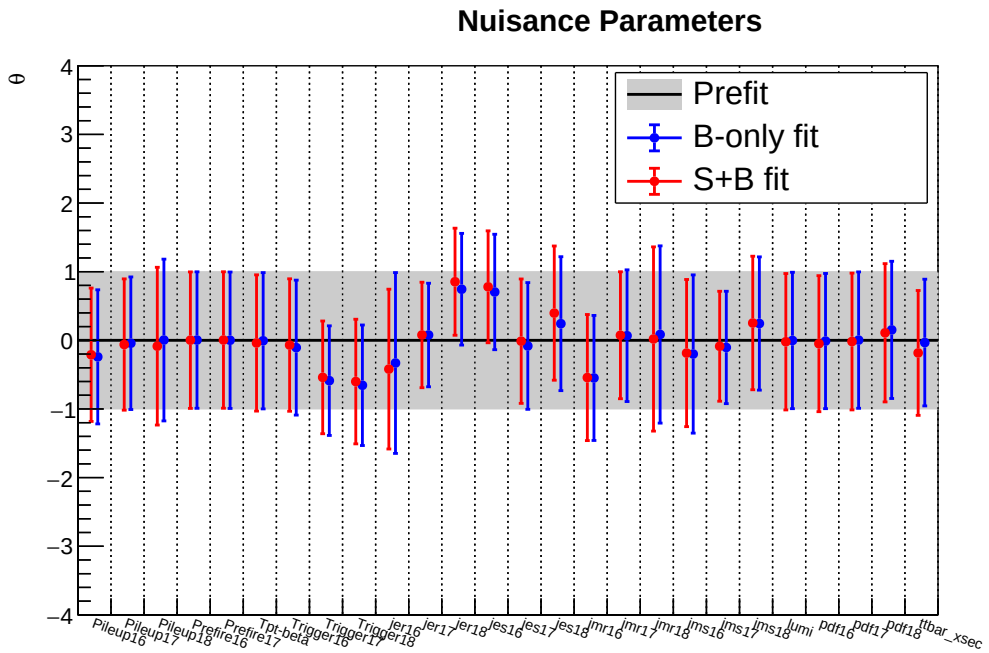

Figure 54: The nuisance parameter pulls for the blinded fits of the ParticleNet based selection using a 1x1 $R_{P/F}$.

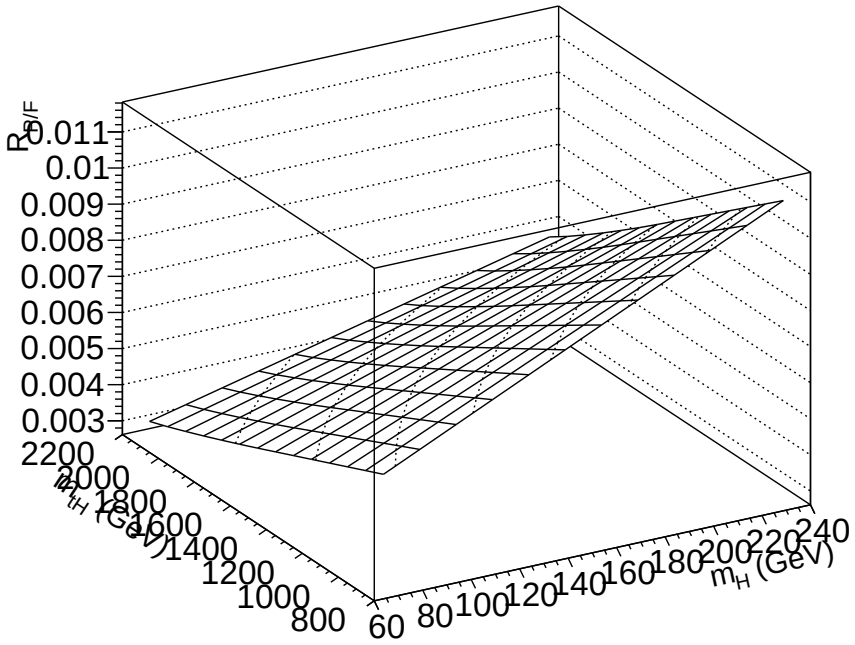

Figure 55: The post-fit $R_{P/F}$ for the blinded fits of the ParticleNet based selection using a 1x1 $R_{P/F}$.

10.4 $R_{P/F}$ pol2 by pol1

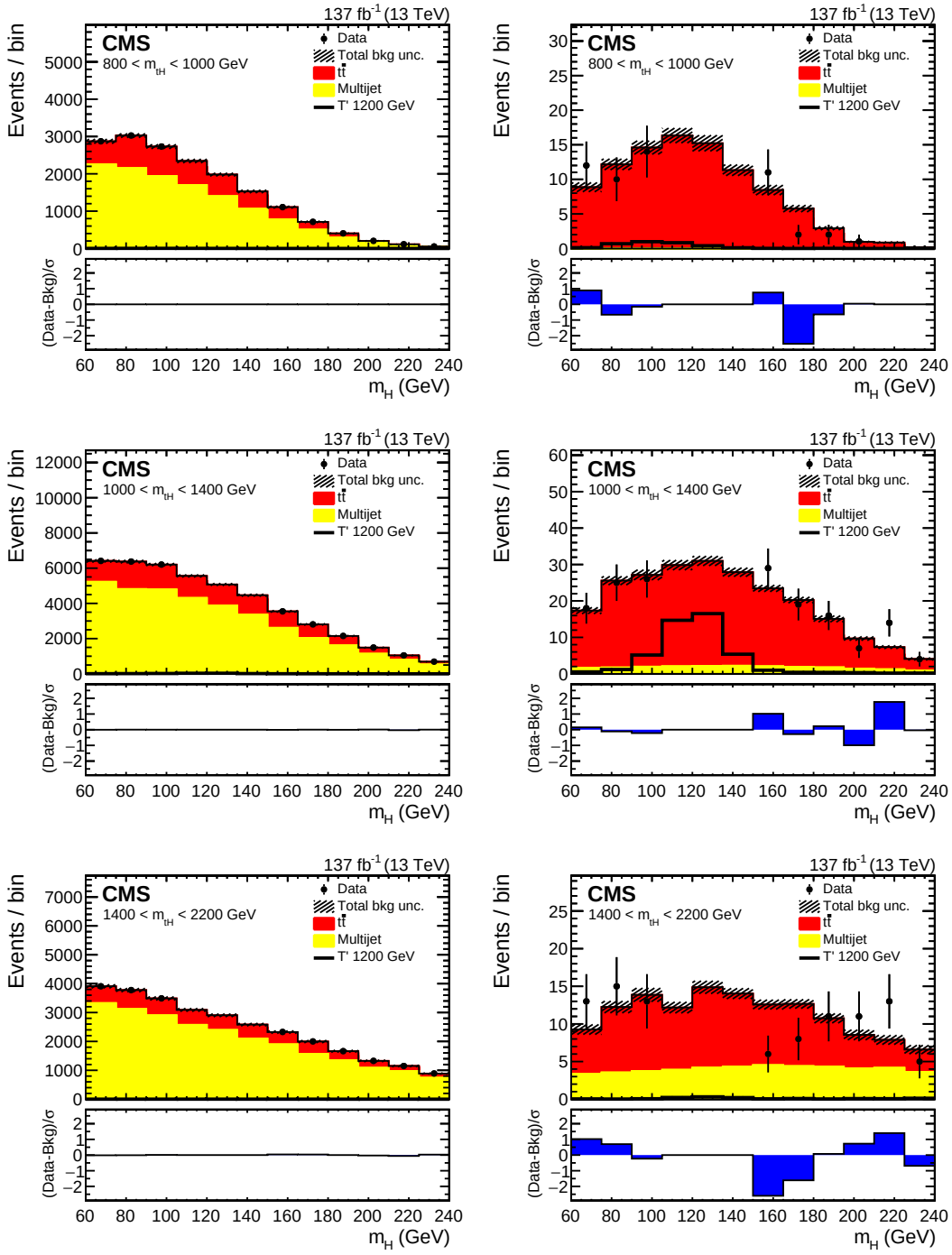

Figure 56: The m_H mass distributions for the blinded background-only fit using the DeepAK8 tagger and a 2x1 $R_{P/F}$. A 1200 GeV T' signal is normalized to 0.1 pb and plotted with the backgrounds to show relative shapes and yields.

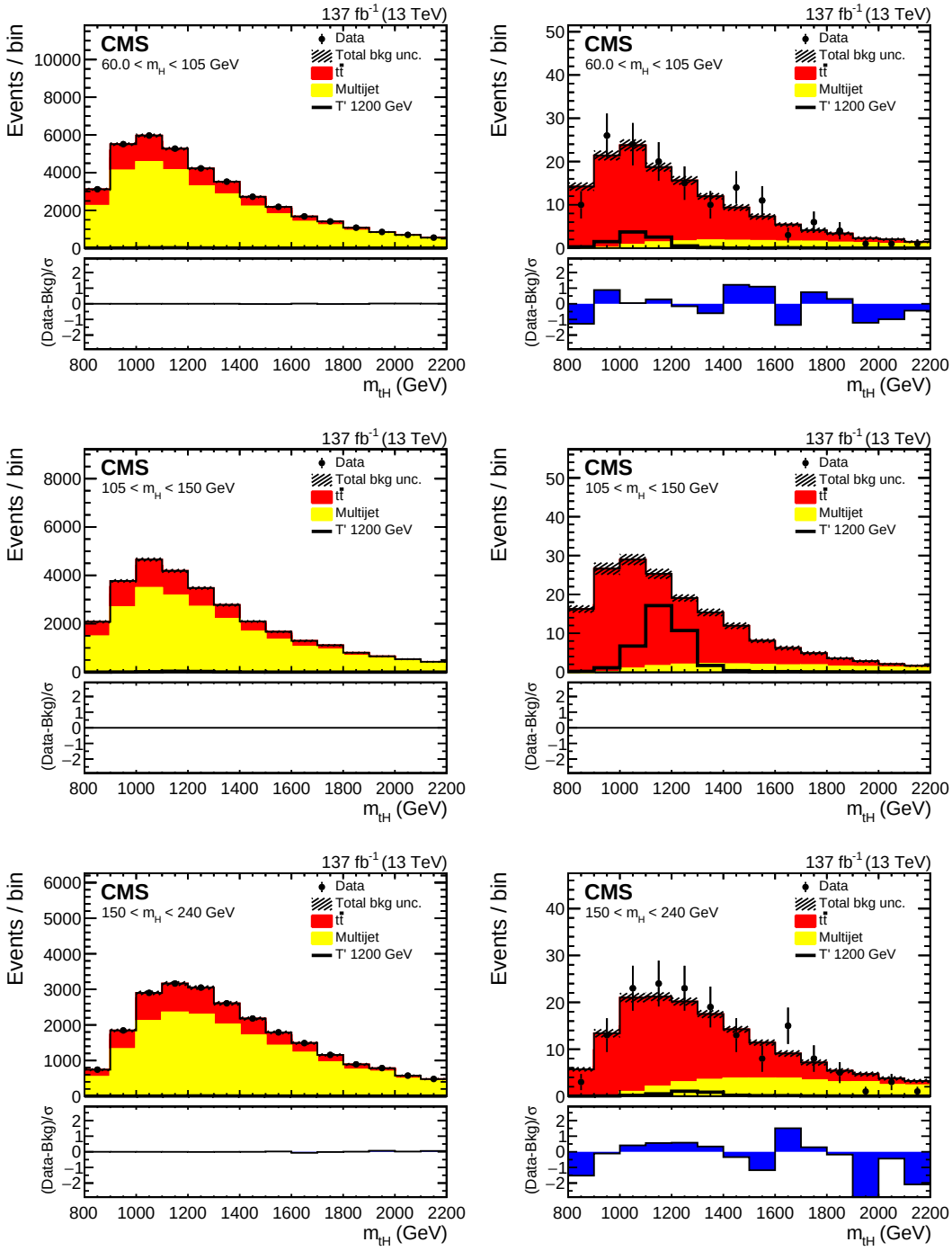

Figure 57: The m_{tH} mass distributions for the blinded background-only fit using the DeepAK8 tagger and a 2x1 $R_{P/F}$. A 1200 GeV T' signal is normalized to 0.1 pb and plotted with the backgrounds to show relative shapes and yields.

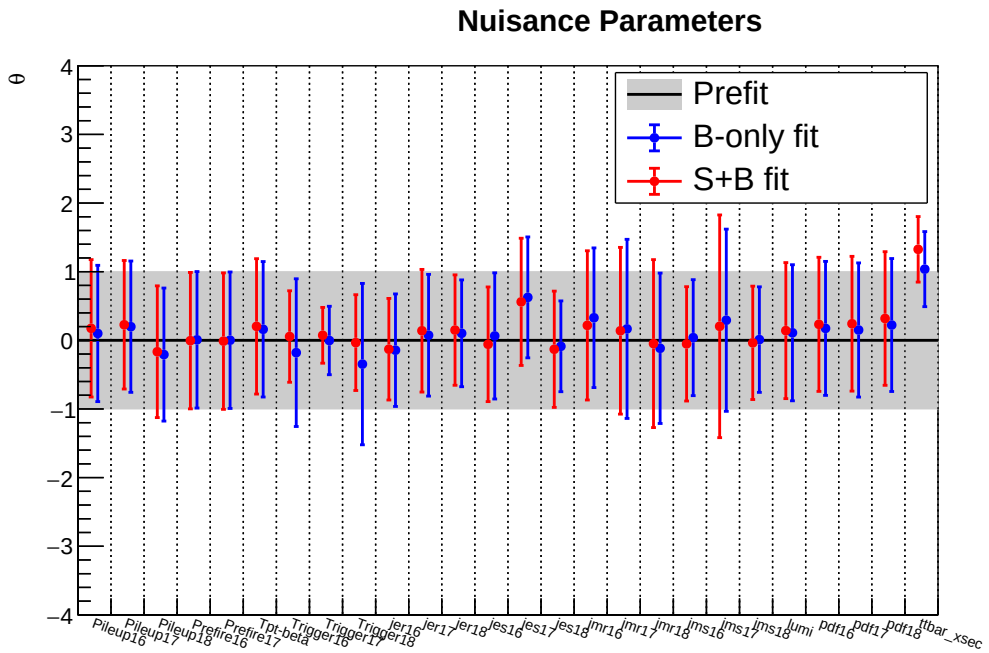

Figure 58: The nuisance parameter pulls for the blinded fits of the DeepAK8 based selection using a 2x1 $R_{P/F}$.

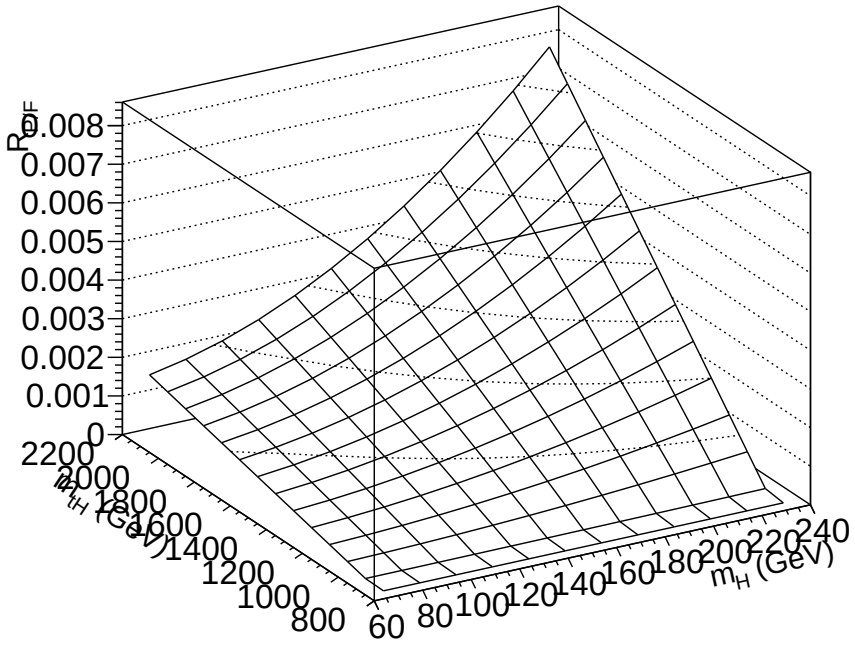

Figure 59: The post-fit $R_{P/F}$ for the blinded fits of the DeepAK8 based selection using a 2x1 $R_{P/F}$.

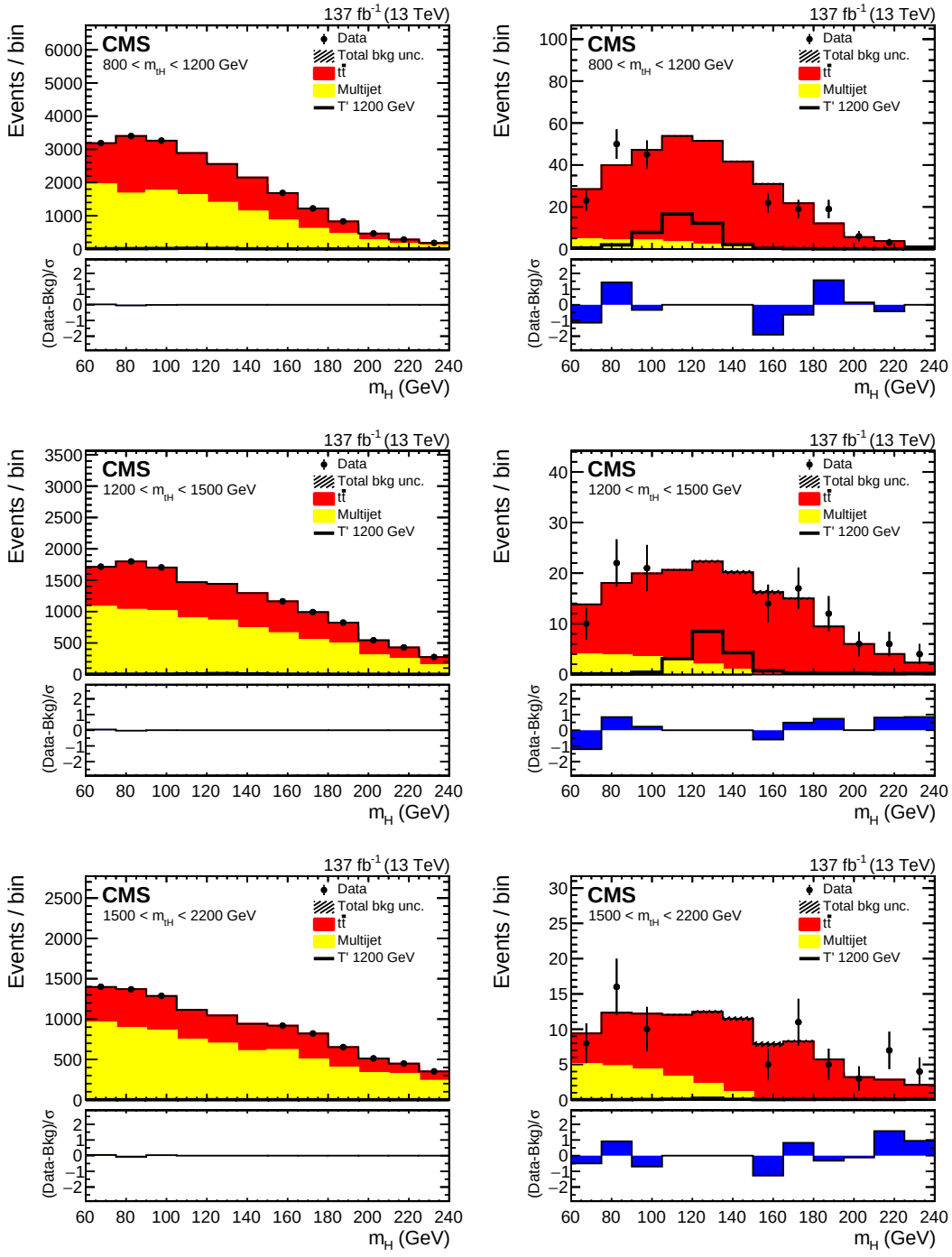

Figure 60: The m_H mass distributions for the blinded background-only fit using the ParticleNet tagger and a 2x1 $R_{P/F}$. A 1200 GeV T' signal is normalized to 0.1 pb and plotted with the backgrounds to show relative shapes and yields.

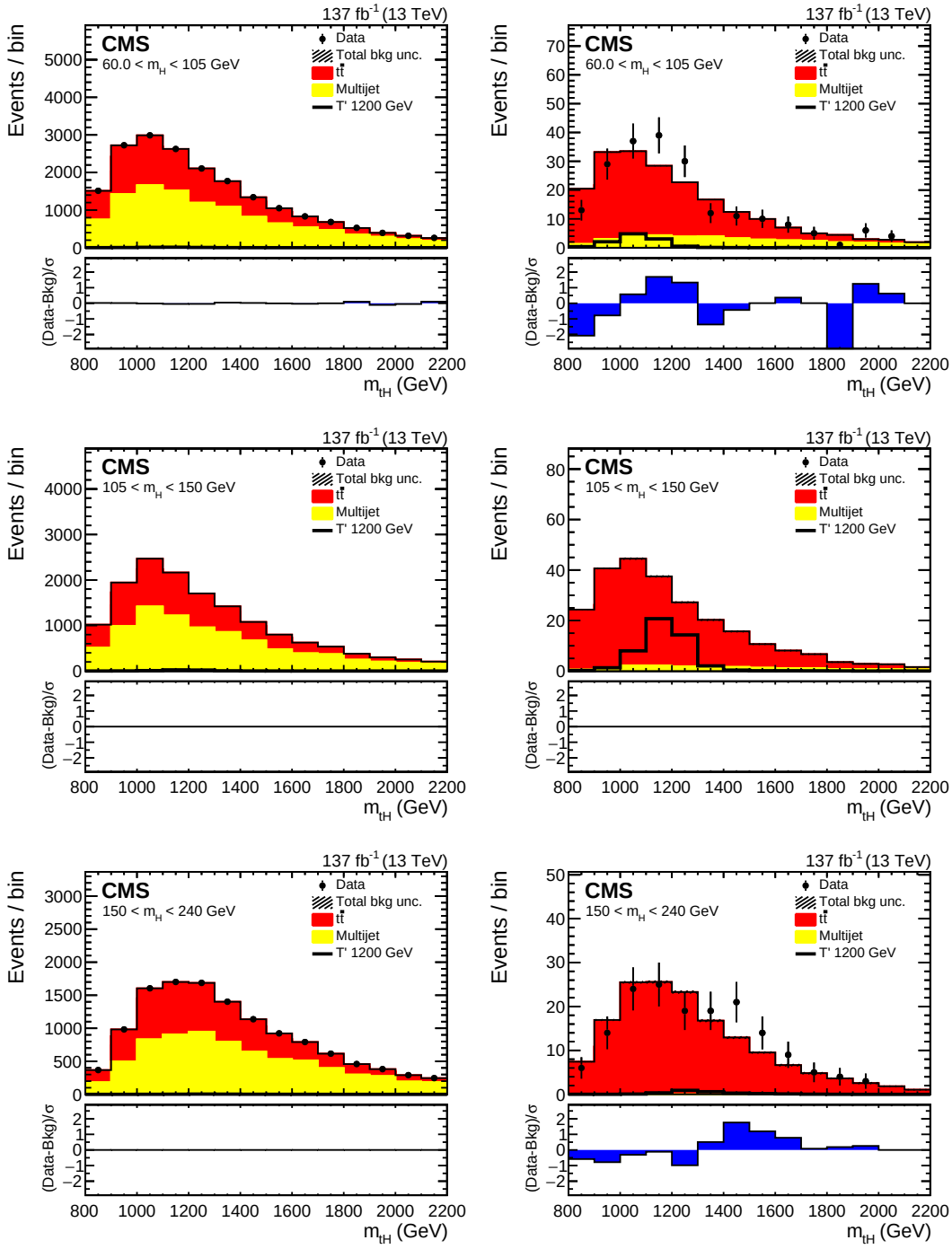

Figure 61: The m_{tH} mass distributions for the blinded background-only fit using the ParticleNet tagger and a 2x1 $R_{P/F}$. A 1200 GeV T' signal is normalized to 0.1 pb and plotted with the backgrounds to show relative shapes and yields.

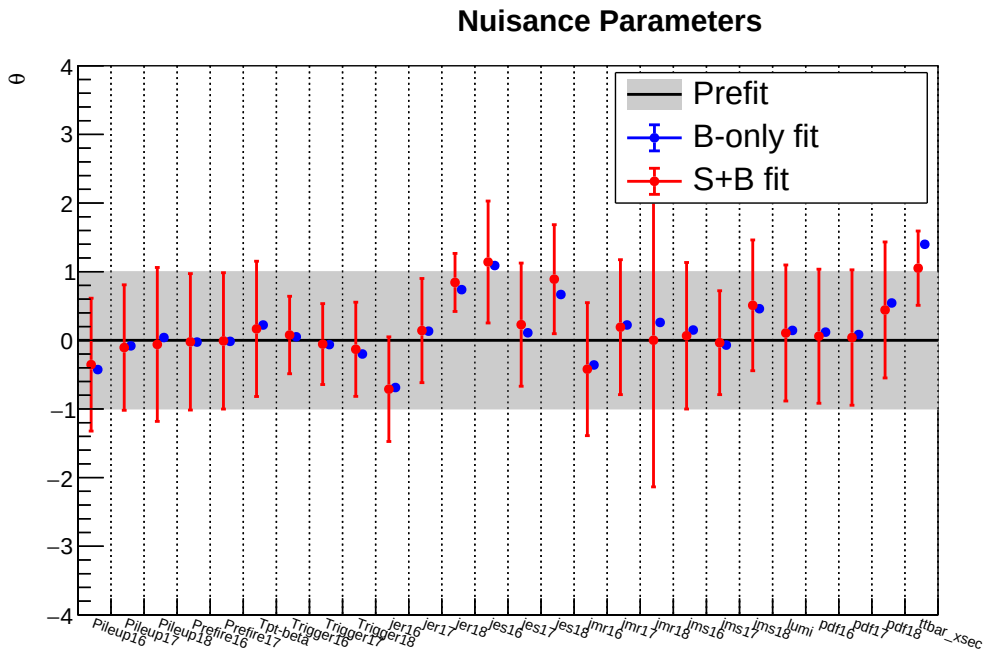

Figure 62: The nuisance parameter pulls for the blinded fits of the ParticleNet based selection using a 2x1 $R_{P/F}$.

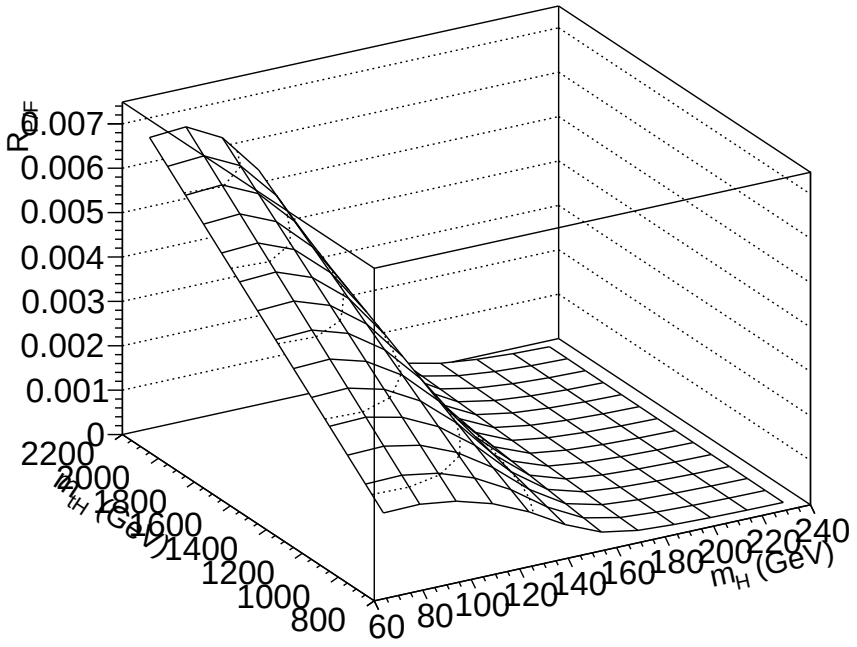

Figure 63: The post-fit $R_{P/F}$ for the blinded fits of the ParticleNet based selection using a 2x1 $R_{P/F}$.

10.5 $R_{P/F}$ pol1 by pol2

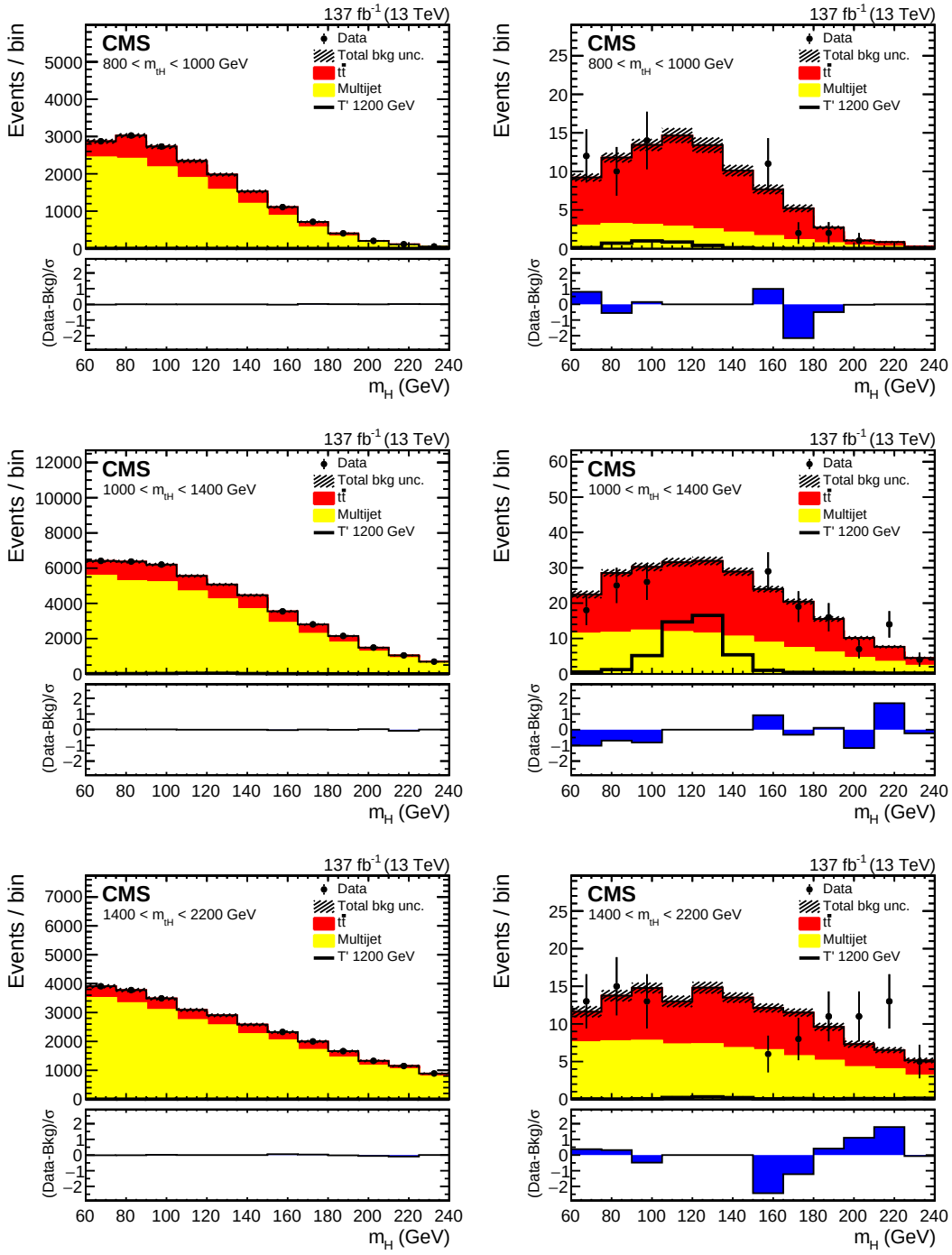

Figure 64: The m_H mass distributions for the blinded background-only fit using the DeepAK8 tagger and a 1x2 $R_{P/F}$. A 1200 GeV T' signal is normalized to 0.1 pb and plotted with the backgrounds to show relative shapes and yields.

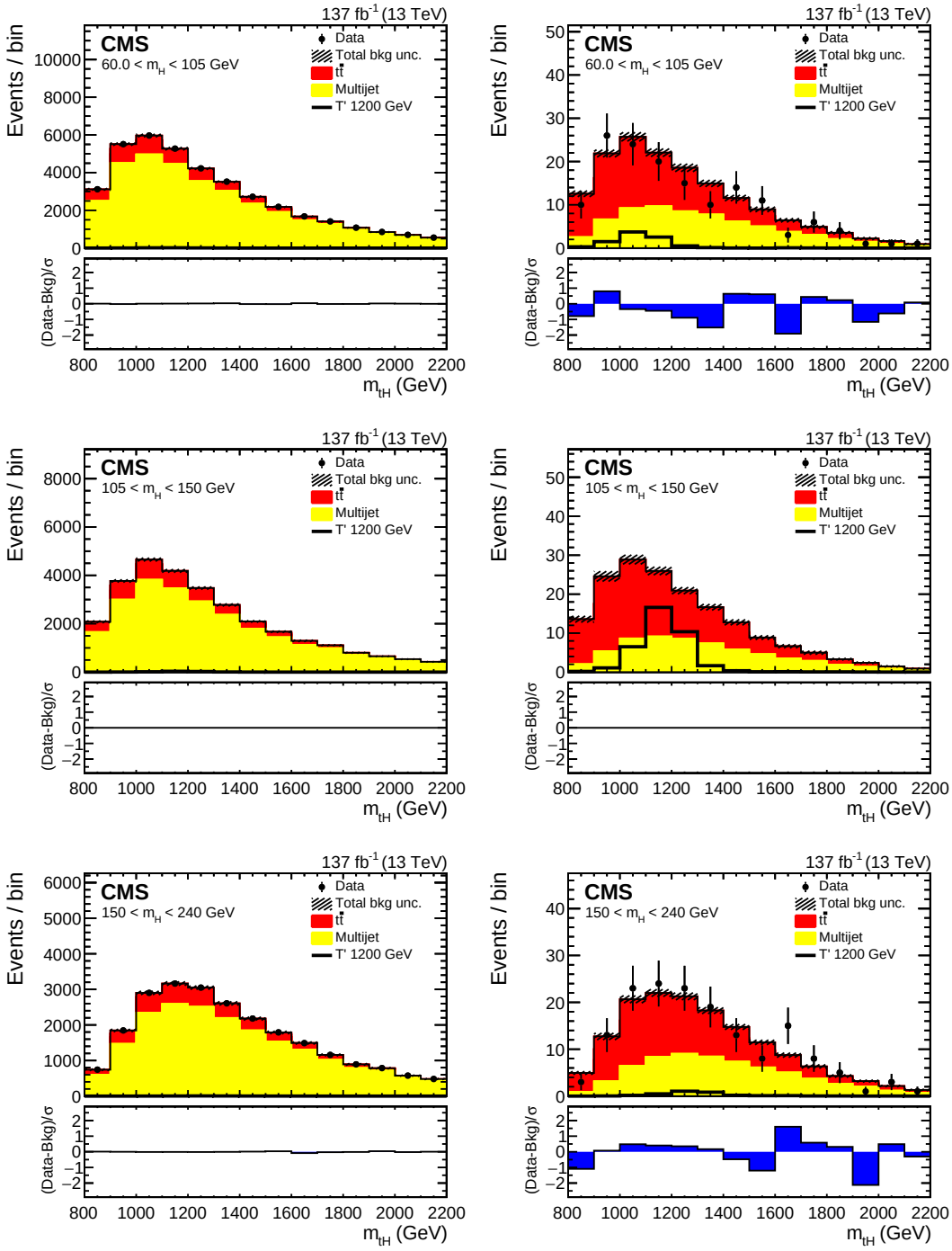

Figure 65: The m_{tH} mass distributions for the blinded background-only fit using the DeepAK8 tagger and a 1x2 $R_{P/F}$. A 1200 GeV T' signal is normalized to 0.1 pb and plotted with the backgrounds to show relative shapes and yields.

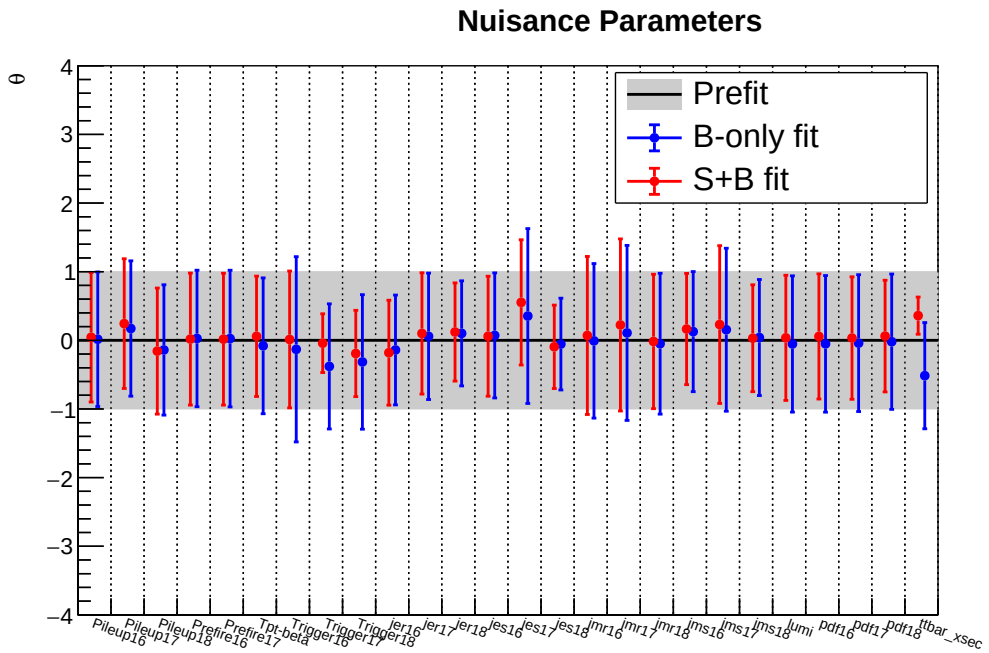

Figure 66: The nuisance parameter pulls for the blinded fits of the DeepAK8 based selection using a 1x2 $R_{P/F}$.

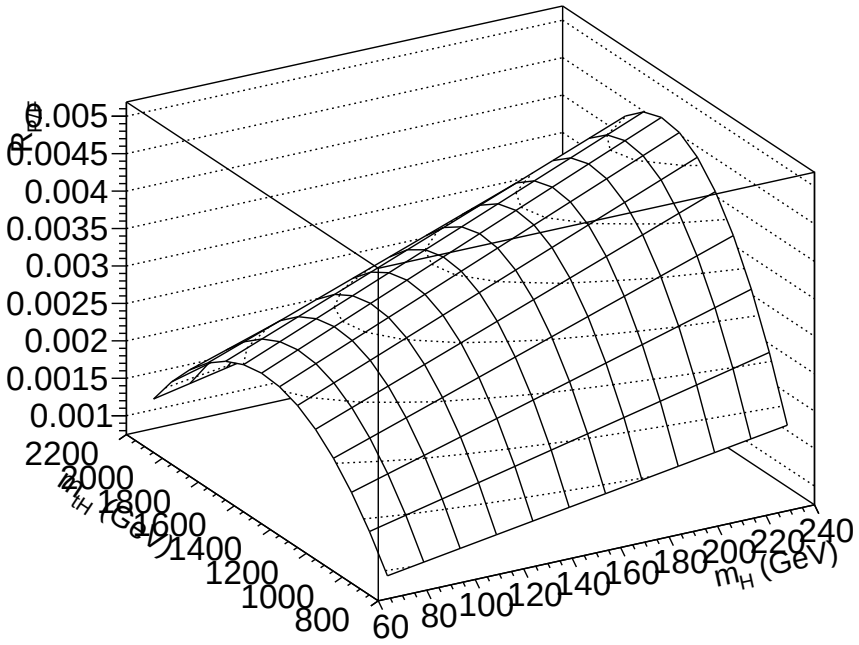

Figure 67: The post-fit $R_{P/F}$ for the blinded fits of the DeepAK8 based selection using a 1x2 $R_{P/F}$.

PARTICLENET FIT DID NOT CONVERGE

10.6 $R_{P/F}$ pol2 by pol2

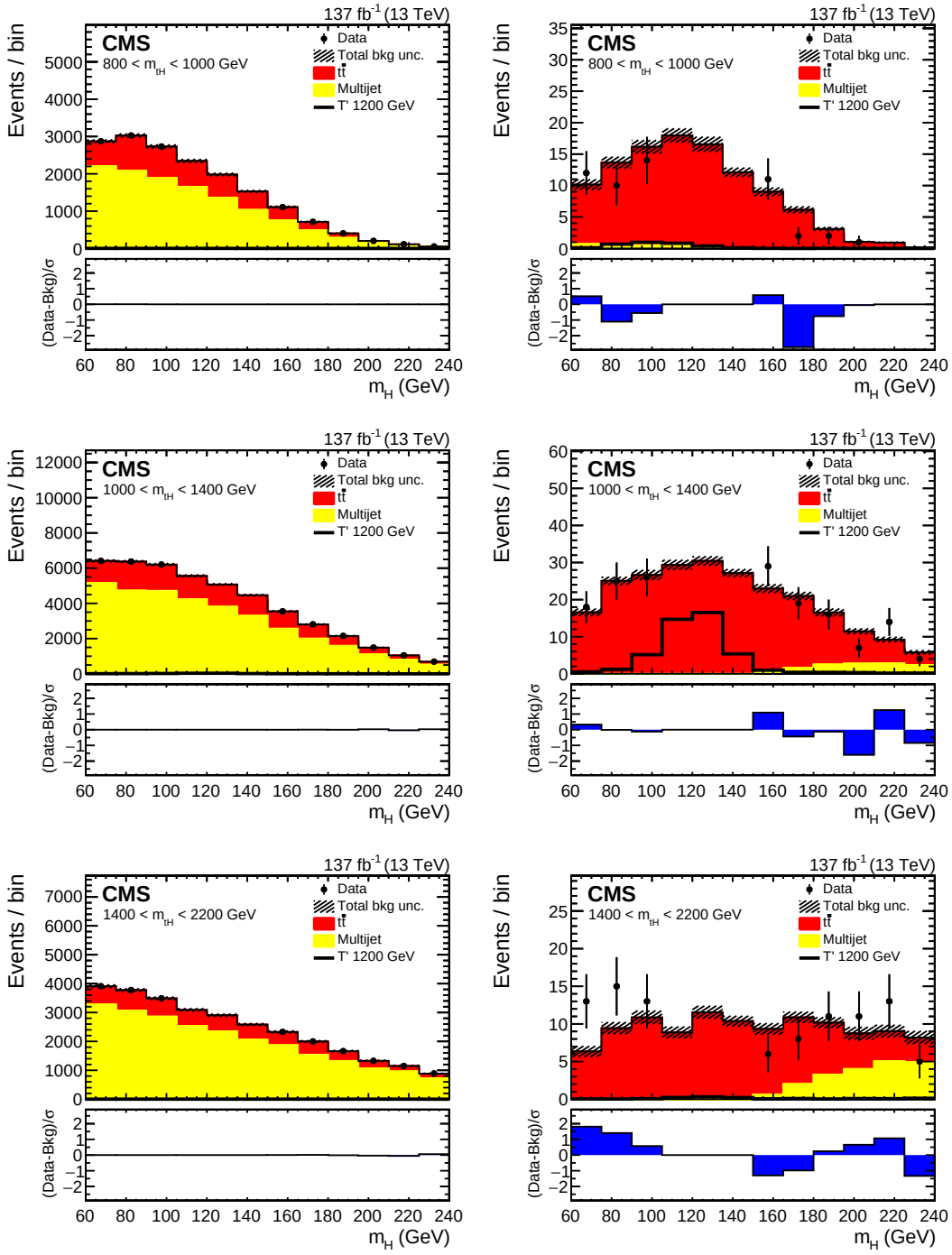

Figure 68: The m_H mass distributions for the blinded background-only fit using the DeepAK8 tagger and a 2x2 $R_{P/F}$. A 1200 GeV T' signal is normalized to 0.1 pb and plotted with the backgrounds to show relative shapes and yields.

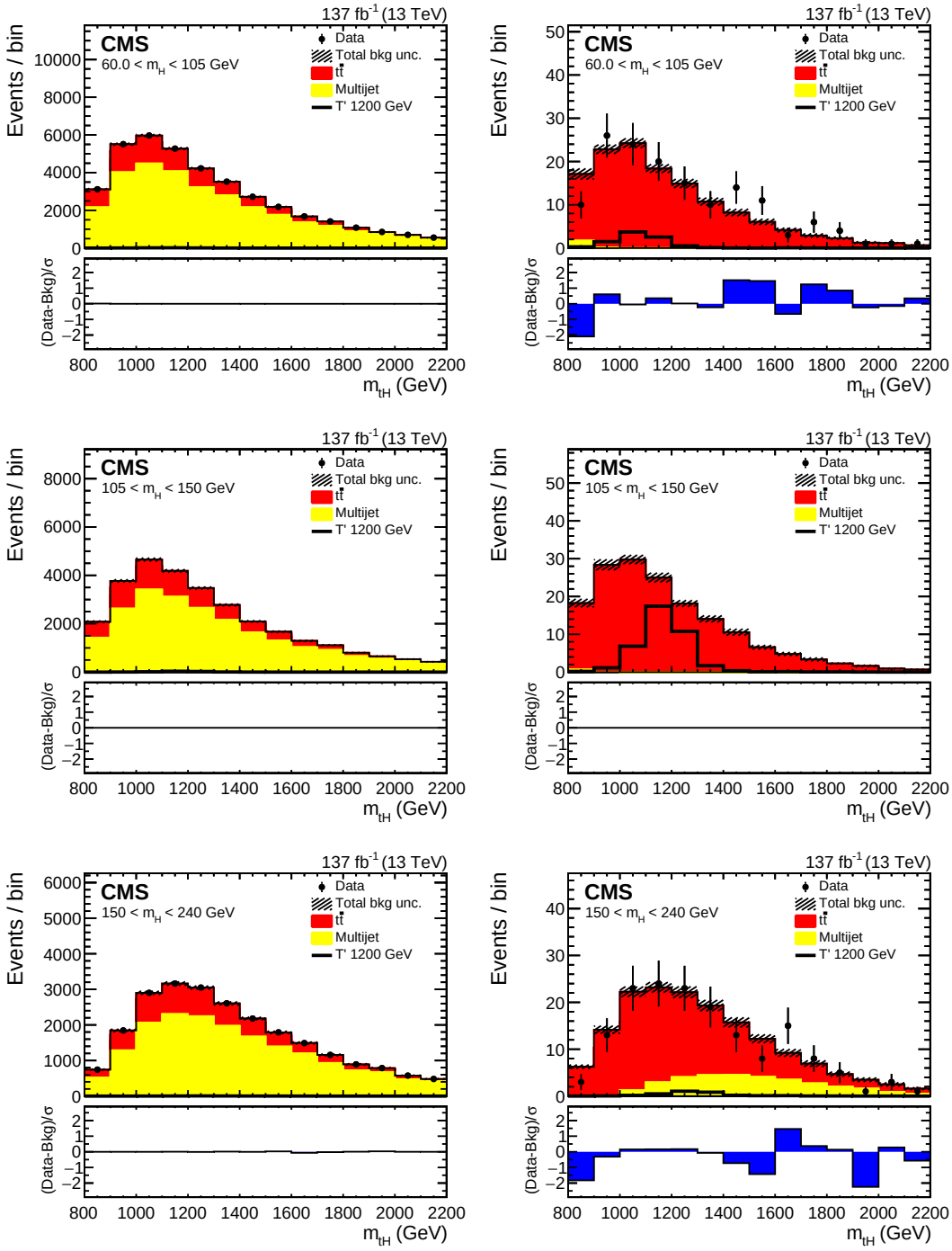

Figure 69: The m_{tH} mass distributions for the blinded background-only fit using the DeepAK8 tagger and a 2x2 $R_{P/F}$. A 1200 GeV T' signal is normalized to 0.1 pb and plotted with the backgrounds to show relative shapes and yields.

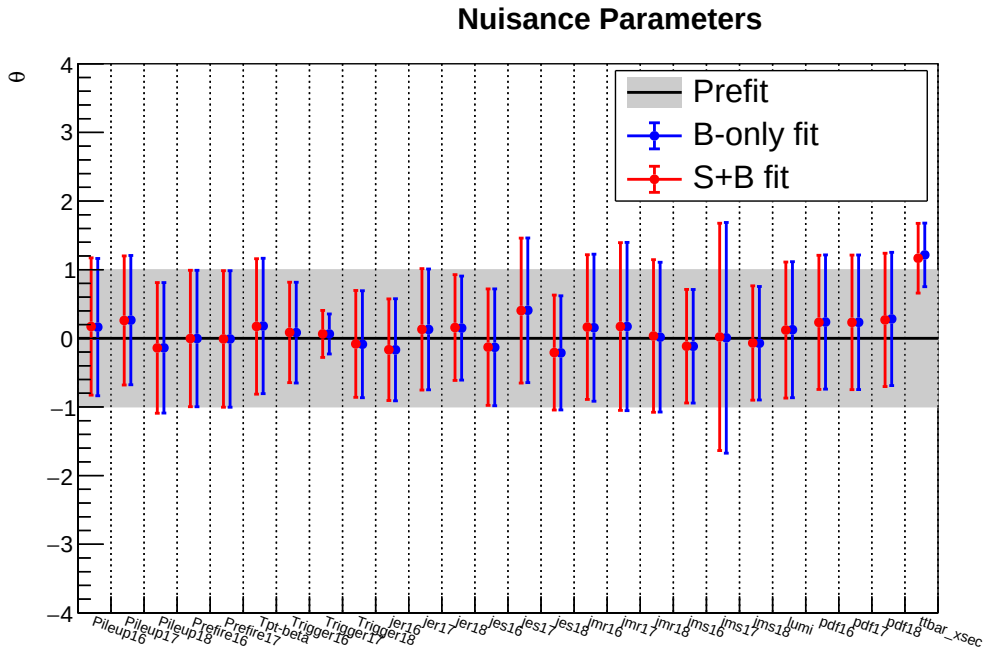

Figure 70: The nuisance parameter pulls for the blinded fits of the DeepAK8 based selection using a 2x2 $R_{P/F}$.

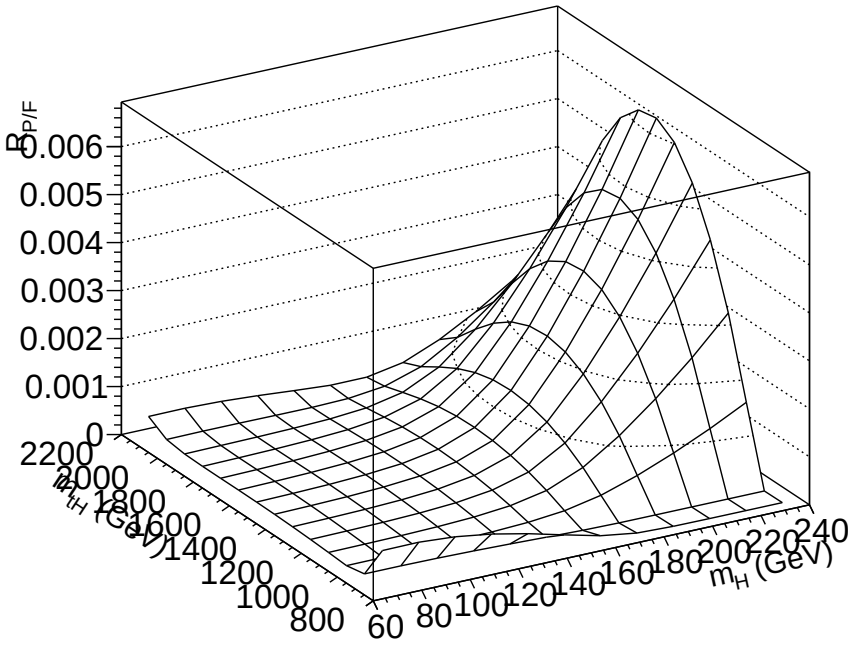

Figure 71: The post-fit $R_{P/F}$ for the blinded fits of the DeepAK8 based selection using a 2x2 $R_{P/F}$.

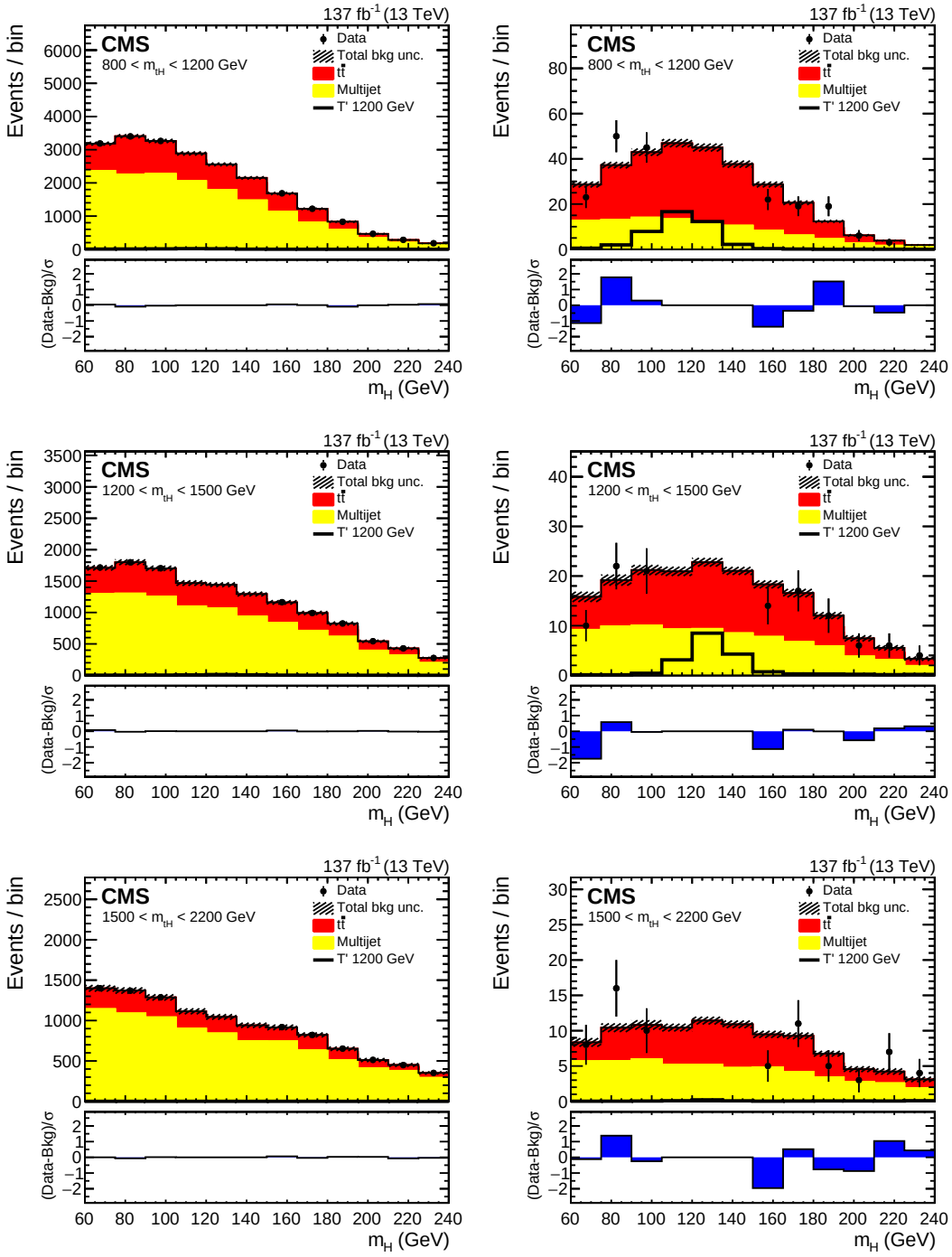

Figure 72: The m_H mass distributions for the blinded background-only fit using the ParticleNet tagger and a 2x2 $R_{P/F}$. A 1200 GeV T' signal is normalized to 0.1 pb and plotted with the backgrounds to show relative shapes and yields.

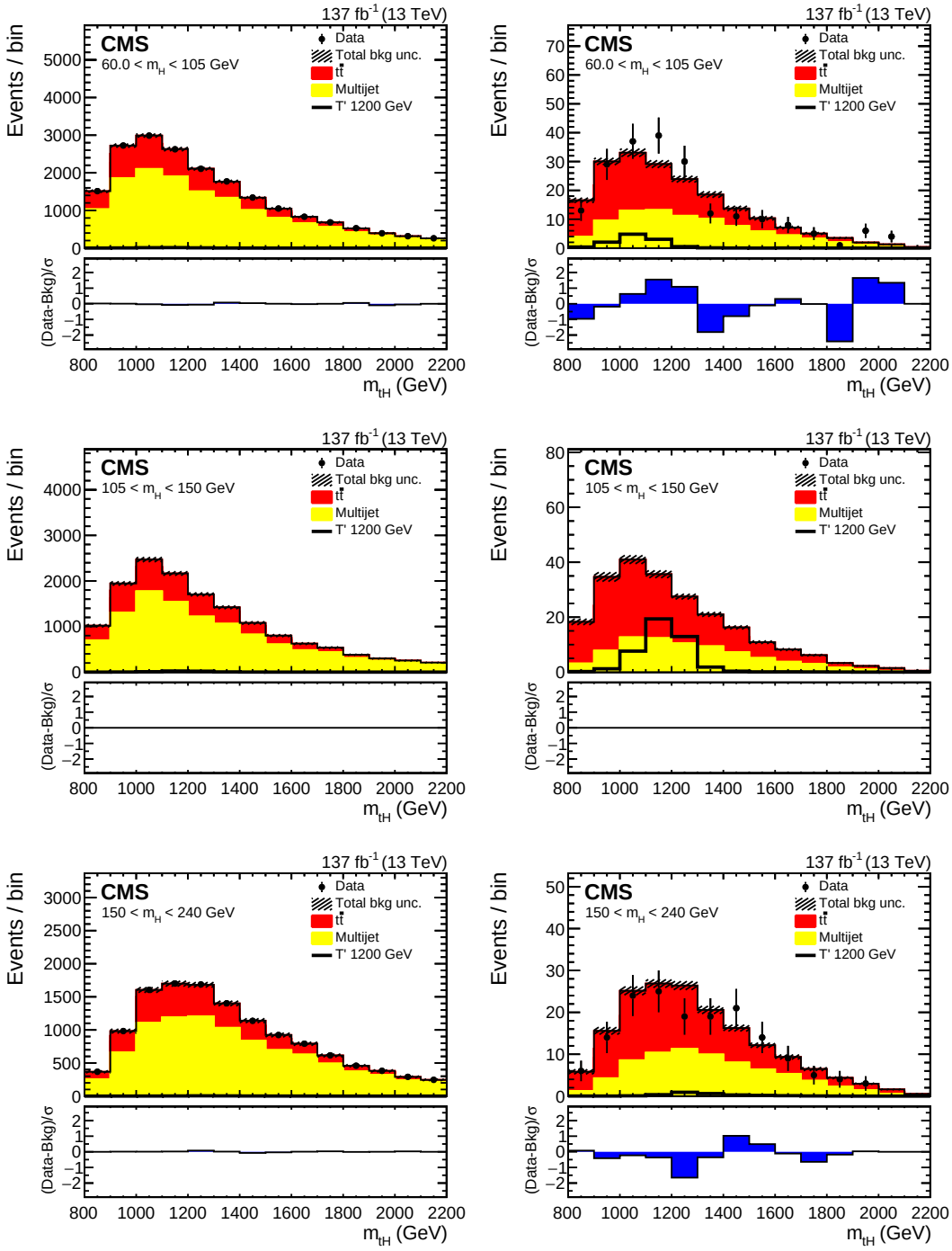

Figure 73: The m_{tH} mass distributions for the blinded background-only fit using the ParticleNet tagger and a 2x2 $R_{P/F}$. A 1200 GeV T' signal is normalized to 0.1 pb and plotted with the backgrounds to show relative shapes and yields.

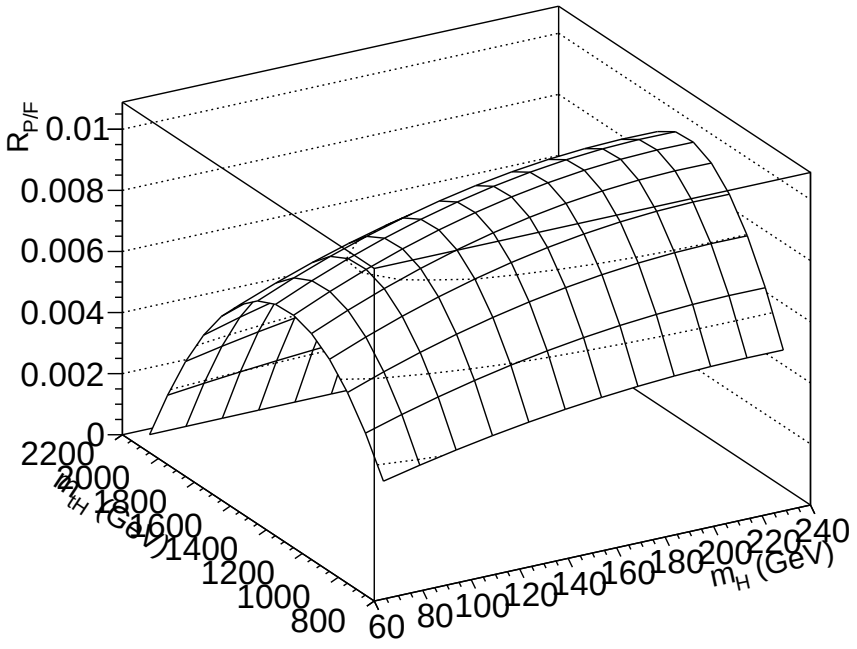

Figure 74: The post-fit $R_{P/F}$ for the blinded fits of the ParticleNet based selection using a 2x2 $R_{P/F}$.